République Algérienne Démocratique et Populaire

Ministère de l'enseignement Supérieure et de la recherche scientifique

Université Mohamed Khider – Biskra

Faculté des Sciences Exactes et des Sciences de la Nature et de la Vie

Département des Sciences de la Matière

THESE

En vue de l'obtention du diplôme de :

DOCTORAT EN SCIENCES

Option : Chimie Théorique

Structure électronique des clusters mixtes des groupes IIIA, IVA et VA

Présentée par

Farida Hakkar

Soutenue publiquement le : 19 / 01 / 2022, devant le jury composé de :

Mr. S. Belaidi	Prof	U. Biskra	Président
Mr. A. Chadli	MC.A	U. Biskra	Examinateur
Mr. A. Zaiter	MC.A	U. Oum el Bouaghi	Examinateur
Mr. B. Zouchoune	Prof	U. Oum el Bouaghi	Directeur de thèse

Acknowledgements

Firstly, I would like to express my sincere gratitude to my supervisor Mr. Zouchoune Bachir professor at Larbi Ben M'hidi University. Throughout this research work, he brought me a deeper understanding of the various aspects of the subject. I do not forget his continued guidance, motivation, advice, support and availability.

I would like to express my appreciation to all the thesis committee members for having accepted to be in my jury. My special thanks to Mr. S. Belaidi professor at Biskra University for having honored me by being the president of the jury. I warmly thank Mr. A. Chadli, and Mr. A. zaiter for agreeing to judge the work presented in this manuscript.

Finally, my particular gratitude is dedicated to my parents, sisters, and brother for their unconditional love and endless support throughout my studies.

Table of Contents

CHAPTER II

Structural stabilities and electronic properties of gallium-indium clusters

CHAPTER III

Structure and Bonding Nature of nH_2 (n = 1-6) interact on Al_3N Cluster

CHAPTER IV

Bonding and electronic structures in Nickel alkyne complexes

List of acronyms

Abbreviation	Description
ADF	Amsterdam Density Functional
AEA	Adiabatic electron affinity
AIP	Adiabatic Ionization Potentials
AO	Atomic Orbital
B3LYP	Becke -3 paramètres- Lee, Yang et Parr
BP86	Becke Perdew 86
DCD	Dewar - Chatt – Duncanson
DFT	Density Functional Theory
EA	electron affinity
EDA	Energy Decomposition Analysis
FMO	Frontier Molecular orbitals
GGA	Generalized Gradient Approximation
HF	Hartree Fock
HOMO	Highest Occupied Molecular Orbital
LDA	local density approximation
MVE	metal valence electrons
MO	Molecular Orbital
NBO	Natural Bond Orbital
STO	Slater-type orbital
VEA	Vertical electron affinity
VIP	Vertical Ionization Potentials
η	Chemical hardness
t-ButNC	Tertiobutyl isocyanid

List of Schemes

CHAPTER IV

List of figures

CHAPTER II

CHAPTER III

Chapter IV

Annexes

List of Tables

CHAPTER II

CHAPTER III

CHAPTER IV

Annexes

GENERAL INTRODUCTION

The term "cluster" was first used by F.A. Cotton in 1964 to refer specifically to compounds containing metal–metal bonds [1]. Later, the study of clusters has diversified greatly and the definition of the term cluster developed compared to that given by Cotton, and is defined as aggregates of atoms or molecules , generally intermediate in size, varying between three and a few thousand atoms. The clusters have very varied geometries: triangular, tetrahedral, octahedral, icosahedral or even more complex polyhedral structures. The properties of this finite system have attracted the interests of researchers coming from the chemical, physical and biological areas [2-4].

The great specificity of cluster compounds lies in their molecular character, which gives them very specific chemical reactivity and physical properties. The last decades have seen considerable development in the clusters chemistry field, due to the emergence of a new generation of high-technology materials. Therefore, the experimental studies have concentrated on determining the size dependence of the structural, electronic and magnetic properties of clusters to bridge the gap between atomic and bulk properties [5]. The small clusters, not only display behaviours of their own but also present new insights into the molecular origins of the properties of bulk matter [6, 7]

On the other hand, the theoretical study of small clusters according to their size attract more attention, which makes it possible to interpret and understand the existing experimental results. Detailed study of the physical and chemical nature of these small clusters is important for understanding the nucleation of thin films, as well as for predictive comprehension of metallic surfaces and heterogeneous catalysis.

The general objective of this thesis is to study theoretically the geometrical and electronic properties of variety of mixed clusters of IIIa and Va groups. As the formation of carbon-carbon bonds is at the basis of organic synthesis, we are therefore interested into nickel alkyne clusters, which are essential intermediates in a diversity of homogeneous catalytic processes.

During this study, we implemented the density functional theory (DFT) to examine the electronic properties of different small clusters studied in this thesis. Density functional theory is a very powerful and a reliable method in the study of electronic structures of molecules, where its electron density determines the energy of a system electron.

This thesis manuscript is divided into four chapters, which are the following:

Chapter one is devoted to the presentation of the theoretical foundations for density functional theory (DFT), the method that we used in this thesis.

In the second chapter, we will explored the lowest-energy structures of the mixed gallium-indium clusters Ga_mIn_{n-m} (n = 4, 6, 8 and m < n) and their electronic properties based HOMO-LUMO gaps, ionisation potential (IP), electron affinity (EA) and chemical hardness (η), in order to analyse the bonding and provide a detailed scheme of their electronic structures.

In chapter three, we will identify the structural and electronic properties of hydrogen interaction on stable Al_3N cluster, and explored the most probable sites of hydrogen molecules on Al_3N cluster, their bonding energies, vibrational frequencies, electronic properties based on MO analysis, HOMO-LUMO gaps, Hirschfeld Charge analysis. The energy decomposition of the studied compounds is envisaged in order to find their interaction types.

A series of clusters of general formula $NiL_2(RC{\equiv}CR)$ / (L = CO or t-BuNC) and (R = H, CH_3, Phenyl, CF_3, Cl, F or CN) will be studied in chapter four. The goal of the study is to examine the electronic structure of these complexes as well as the strength of the bond between NiL_2 and $RC{\equiv}CR$ the symmetrical substituted alkynes.

Bibliography

[1] Cotton, F. A. *"Metal atom clusters in oxide systems."* Inorg. Chem.3.9 (**1964**) 1217-1220.

[2] Haberland, H., ed. "*Clusters of atoms and molecules: theory, experiment, and clusters of atoms"*. Vol. 52. Springer Science and Business Media, **2013**.

[3] Alonso, J. A. "*Structure and properties of atomic nanoclusters*" World Scientific, **2012**.

[4] Pruett, J. G., Windischmann, H., Nicholas, M. L., & Lampard, P. S. *"Mass and Temperature Measurement in Pure Vapor Expansion of Metals and Semi-Metals"* Physics and Chemistry of Small Clusters. Springer, Boston, MA, (**1987**) 109-114.

[5] Rossi, G., & Ferrando, R. *"Structural properties of pure and binary nanoclusters investigated by computer simulations."* Nanomaterials: Design and Simulation (**2006**) 35-58.

[6] Lill, Th., Calaway, W. F., and Pellin, M. J. "*Sputtering of tin and gallium-tin clusters."* Nuclear Instruments and Methods in Physics Research Section B: Beam Interactions with Materials and Atoms 100.2-3 (**1995**) 361-365.

[7] Capek, I. *"Nanocomposite Structures and Dispersions-Science and Nanotechnology-Fundamental Principles and Colloidal Particles*" Nanotechnology and nanomaterials. (**2006**) 1-69.

CHAPTER I

Introduction to Density Functional Theory

We present in this Chapter a brief overview of Density Functional Theory (DFT), one of the most successful and widely applied approach in clusters, solids, organic and organometallic molecules, which provide reliable results for understanding the electronic structural and spectroscopic properties.

I. The Schrödinger equation

The ultimate objective of quantum chemistry is the approximate solution of the Schrödinger equation, which established by Erwin Schrödinger in 1925 [1], to describe the electronic structure of a system (atom, molecule, cluster or solid) with many nuclei and electrons.

For a system, which is composed of N electrons and M nuclei, the equation (time-independent), can is written as follow:

$$\hat{H}\Psi_i(x_1, x_2, \dots, x_N, R_1, R_2, \dots, R_M) = E_i\Psi_i(x_1, x_2, \dots, x_N, R_1, R_2, \dots, R_M) \quad (I.1)$$

Where: $\hat{H}$ represents the Hamiltonian operator and Ψ represents the wave function of the system associated to the energy level E, x_i and R_i are the spatial coordinates of the electron and nuclei respectively

The Hamiltonian operator can be decomposed as follows:

$$\hat{H} = -\frac{1}{2}\sum_{i}^{N}\nabla_i^2 - \sum_{I}^{M}\frac{1}{2M_I}\nabla_I^2 - \sum_{i,I}\frac{Z_I}{|r_i - R_i|} + \frac{1}{2}\sum_{i<j}\frac{1}{|r_i - r_j|} + \frac{1}{2}\sum_{I<J}\frac{Z_I Z_J}{|R_I - R_J|} \quad (I.2)$$

The first two terms of the Hamiltonian are respectively the kinetic energy operators of N electrons (indexed i) and of M atomic nuclei (indexed I). The other three terms represent the different potentials of electron-nucleus, electron-electron and nucleus-nucleus interaction.

II.The Born-Oppenheimer Approximation

For polyelectronic and polyatomic systems, the Schrödinger equation cannot be solved analytically. To overcome this issue, Max Born and Robert Oppenheimer proposed an approximation [2], which considers the position of atomic nuclei as fixed with respect to the electrons; their kinetic energy can therefore be neglected and the interaction term between nucleus considered to be constant (which we will note V_{NN}).

The operator can thus be rewritten as:

$$H = -\frac{1}{2}\sum_{i}^{N}\nabla_i^2 - \sum_{i,I}\frac{Z_I}{|r_i - R_i|} + \frac{1}{2}\sum_{i<j}\frac{1}{|r_i - r_j|} + V_{NN} \qquad (I.3)$$

To simplify the notations, we will represent by convention: the kinetic energy by T_e, the external potential by V_{ext} and the electron-electron interaction potential by V_{ee}.

The operator is therefore written in a more condensed form like:

$$\hat{H} = \hat{T}_e + \hat{V}_{ext} + \hat{V}_{ee} + \hat{V}_{NN} \qquad (I.4)$$

III. The density functional theory

DFT is a successful method to finding solutions to the fundamental equation that describes the quantum behavior of atoms and molecules at low energies. It is a theory that uses electron density as a fundamental function instead of the wave function as is the case in the Hartree and Hartree-Fock method [3].

The idea of using electron density originates from the Thomas-Fermi model which, from 1927 [4,5] expresses the total energy of an atomic or molecular system as a function of its electron density. Nevertheless, the precision obtained was lower than that of Hartree-Fock owing to the absence of the exchange-correlation term. Then completed by Dirac [6] who adds the functional exchange energy of electron density to it. However, the electronic correlation term was still absent in this new approach.

III.1. Hohenberg and Kohn theorems

The density functional theory as we know it today was born in 1964 with the appearance of the important paper of Hohenberg and Kohn [7]. In this paper, the authors stated two theorems represent the formalism of the DFT.

III.1.1. First Theorem

Hohenberg and Kohn showed that exists a one-to-one correspondence between the external potential and the electron density $\rho(r)$, allowing representing the first as a functional of the ground state of the second. Therefore**,** *the total energy of the system in the ground state is also a unique functional of the electron density*;

$$E = E[\rho(r)] \qquad (I.5)$$

This theorem differs from the Hartree-Fock method, in which the total energy of the system is the functional of the wave function. An immediate consequence of this theorem is that electron density uniquely determines the Hamiltonian operator of the system. Thus, by knowing the electron density, we can determine the Hamiltonian operator

III.1.2. Second Theorem

Kohn and Sham declared the second theorem resembling the variational principle, which stated that:

For a given potential V_{ext} *and number of electrons N, the total energy of the system reaches its minimum value when the density* $\rho(r)$ *corresponds to the exact density of the ground state* $\rho_0(r)$

$$E(\rho_0) = \min E(\rho) \qquad (I.6)$$

The total energy functional of the ground state is written as follows:

$$E[\rho(\vec{r})] = F[\rho(r)] + \int V_{ext}(r)\rho(r)d^3 r \qquad (I.7)$$

Where: $V_{ext}(r)$ represents the external potential acting on the particles and $F[\rho(r)]$ represents the universal functional *of Hohenberg and Kohn,* with:

$$F[\rho(\vec{r})] = \langle \Psi | \hat{T} + \hat{V} | \Psi \rangle \qquad (I.8)$$

Knowing this functional, allows determining the total energy and the electron density of the ground state for a given external potential. Unfortunately, *Hohenberg -Kohn* theorems give no indication of the form $F[\rho(r)]$.

III.2. Kohn - Sham Equation

Kohn and Sham [8] introduced a supplementary development that consists in replacing the real interactive system by a fictitious *non-interacting* system. This approach realizes an exact correspondence between the electron density, the energy of the ground state of a system consisting of non-interacting fermions placed in an effective potential, and the real system with several interacting electrons subjected to the real potential.

As a result, the electron density and energy of the real system are conserved in this fictitious system and the theorems of Hohenberg and Kohn apply.
The density functional $F[\rho(r)]$ for the interactive system can be expressed by the following expression:

$$\mathrm{F[\rho(r)] = T_0[\rho(r)] + E_H[\rho(r)] + E_{XC}[\rho(r)] + V_{ext}[\rho(r)]} \qquad \text{(I. 9)}$$

Where: $T_0[\rho(r)]$ is the kinetic energy of non-interacting electron gas; $\mathrm{E_H[\rho(r)]}$ designed the *Hartree* term (the classical Coulomb interaction between electrons described through their electron density); $\mathrm{E_{XC}[\rho(r)]}$ represents an additional functional that describes the interelectronic interaction called *exchange-correlation energy*; $\mathrm{V_{ext}[\rho(r)]}$ includes the Coulomb interaction of electrons with nuclei and that of nuclei with each other.

The Hartree term and kinetic energy are the most important terms in dealing with the interaction of electrons. The difference between the real kinetic energy and that of non-interacting electrons as well as the difference between the real interaction energy and that of Hartree are taken into account in the exchange and correlation energy $E_{XC}[\rho(r)]$.

The Schrödinger equation to be solved in the framework of the Kohn and Sham approach is of the following form

$$\left[-\frac{1}{2}\nabla_i^2 + \mathrm{V_{eff}(r)}\right]|\varphi_i(r)\rangle = \varepsilon_i|\varphi_i(r)\rangle\,, \qquad \mathrm{i = 1, \dots, N} \qquad \text{(I. 10)}$$

Where: the effective potential is of the form

$$\mathrm{\hat{V}_{eff}(r) = \hat{V}_{ext} + \int \frac{\rho(r)}{|r - r'|}\,dr + \hat{V}_{XC}} \qquad \text{(I. 11)}$$

The exchange and correlation potential is given by the derived functional:

$$\mathrm{\hat{V}_{XC}(r) = \frac{\delta E_{XC}[\rho(r)]}{\delta \rho(r)}} \qquad \text{(I. 12)}$$

Solving the Kohn and Sham equations requires the choice of a basis for the wave functions that can be taken as a linear combination of orbitals called Kohn-Sham orbitals (KS) written in following form

$$\rho(r) = \sum_{i=1}^{N} |\varphi_i(r)|^2 \qquad \text{(I. 13)}$$

Equation (I.10) correspond to the Kohn - Sham equation of and must be solved in a self-consistent manner, i.e. starting from a certain initial electron density, a potential $\hat{V}_{eff}(r)$ is obtained for which equation (I.9) is solved and a new electron density is then determined. From this new density, a new effective potential can be calculated. This process is repeated in a self-consistent fashion until convergence is achieved, i.e. until the new electron density is equal to or very close to the previous one (corresponding to the fixed convergence criterion).

III.3. The exchange-correlation functional

The development of the Kohn - Sham equation made it possible to highlight the fact that the only density functional that remains unknown in this formalism is the exchange-correlation functional $E_{XC}[\rho(r)]$. Thus, to solve the Kohn - Sham equation, various exchange-correlation functions have been considered.
The effects resulting from interactions between electrons are of three categories: the exchange, the dynamic correlation and non-dynamic correlation.

The exchange effect results from the antisymmetry of the total wave function to the exchange of electronic coordinates. It corresponds to Pauli principle, which states that two electrons of the same spin have a zero probability of being in the same place. This effect is independent of the electron charge and is taken into account in Hartree-Fock theory because of the antisymmetry of the Slater determinant representing the wave function.

The correlation effect refers to the correlation between electronic motions resulting from Coulomb interelectronic repulsion in $\frac{1}{(r-r')}$. It essentially corresponds to correlation effects for core electrons. Unlike the exchange effect, the correlation effect is owing to the electron charge but it is independent of the spin and is neglected by Hartree-Fock theory.

The third effect is that the electronic wave functions are formulated in terms of independent particles. This is the correction of ″ *self-interaction* ″, which should lead to correct counting of the electron pairs number.

The exchange-correlation functional must take into account, in addition to what has been stated, the difference in kinetic energy between the non-interactive fictitious system and the real system. Thus, the calculation of energy and exchange-correlation potential relies on a number of approximations.

III.3.1. The local density approximation (LDA)

LDA is the simplest approximation among all approximate exchange-correlation functionals. The principal idea of LDA is based on the assumption that electron density varies slowly throughout a molecule so that the local density can be treated as a uniform electron gas. This amounts to making the following two assumptions:

- ✓ The exchange-correlation effects are dominated by the density at the point ***r***
- ✓ The density $\rho(r)$ is a slowly varying function with respect to r

This approximation consists in considering that the contribution of $E_{XC}[\rho(r)]$ to the total energy of the system can be added cumulatively from each portion of the non-uniform gas as if it were locally uniform.

Exchange-correlation energy (LDA) can be written as:

$$\mathrm{E_{XC}^{LDA}}[\rho(\mathrm{r})] = \int \rho(\mathrm{r})\varepsilon_{\mathrm{XC}}^{\mathrm{LDA}}[\rho(\mathrm{r})]\mathrm{d}^3\mathrm{r} \qquad (\mathrm{I}.14)$$

Where: $\varepsilon_{\mathrm{XC}}^{\mathrm{LDA}}[\rho(\mathrm{r})]$ represents the exchange and correlation energy per electron in an electron gas, whose distribution is assumed to be uniform.

From $\varepsilon_{XC}^{LDA}[\rho(r)]$, the exchange-correlation potential $\mathrm{V_{XC}^{LDA}}(\mathrm{r})$ can be obtained in a variational way according to the equation:

$$\mathrm{V_{XC}^{LDA}}(\mathrm{r}) = \frac{\delta\left(\rho(\mathrm{r})\varepsilon_{\mathrm{XC}}^{\mathrm{LDA}}[\rho(\mathrm{r})]\right)}{\delta\rho(\mathrm{r})} \qquad (\mathrm{I}.15)$$

The LDA assumes that the functional $\varepsilon_{XC}[\rho(r)]$ is purely local. This energy is divided into two terms :

$$\varepsilon_{\mathrm{XC}}[\rho(\mathrm{r})] = \varepsilon_{\mathrm{X}}[\rho(\mathrm{r})] + \varepsilon_{\mathrm{C}}[\rho(\mathrm{r})] \qquad (\mathrm{I}.16)$$

Where: $\varepsilon_X[\rho(r)]$ is the exchange energy and $\varepsilon_C[\rho(r)]$ is the correlation energy.

The exchange energy for a uniform electron gas is given by the *Dirac-Fermi* formula and defined as follows:

$$\varepsilon_X^{LDA}[\rho(r)] = -\frac{0{,}4581}{r_s} \qquad (I.17)$$

With: $\rho = \left(\frac{4\pi r_s^3}{3}\right)^{-1}$

Where r_s is a parameter, which describes the radius of a sphere containing on average one electron in a homogeneous electronic system of density ρ

On the other hand, the correlation energy is not known exactly. It was first estimated by Wigner [9] :

$$\varepsilon_C^{LDA}[\rho(r)] = -\frac{0{,}44}{r_s + 7{,}8} \qquad (I.18)$$

Furthermore, the correlation energy of a free electron gas has been modeled by Ceperly and Alder [10] and has been given by Perdew and Zunger [11] by the following forms:

$$\varepsilon_C[\rho(r)] = \frac{-0{,}1423}{1 + 1{,}0529\sqrt{r_s} + 0{,}3334\, r_s} \qquad r_s > 1 \qquad (I.19)$$

$$\varepsilon_C[\rho(r)] = -0{,}048 + 0{,}031 \ln r_s - 0{,}0116\, r_s + 0{,}002\, r_s \ln r_s \qquad r_s < 1 \quad (I.20)$$

There are other parameterizations of the correlation energy functional have been developed (e.g., Kohn- Sham [12], Hedin-Lundqvist [13], Perdew -Wang(PW)[14] and Volko-Wilkes-Nusair (VWN)[15] the most commonly used.

III.3.2. The generalized gradient approximation (GGA)

The LDA approach hypothesizes a uniform distribution of electrons, which is quite far from the case of atomic and molecular systems. To take into account this inhomogeneity of the density, the idea is to introduce into the expression of the exchange-correlation energy not only the density $\rho(r)$ but also on its gradient $|\nabla\rho(r)|$. Thus, the functional $E_{XC}[\rho(r)]$ accounts the non-uniform nature of the electron gas.

In this case, the contribution of $E_{XC}[\rho(r)]$ to the total energy of the system can be added cumulatively from each portion of the non-uniform gas as if it were locally non-uniform. It is written in the following form:

$$E_{XC}^{GGA}[\rho(r)] = \int \rho(r)\varepsilon_{XC}[\rho(r).\nabla\rho(r)]d^3\, r \qquad (I.21)$$

Where $\varepsilon_{XC}[\rho(r).\nabla\rho(r)]$ represents the exchange-correlation energy per electron in a system of mutually interacting electrons of non-uniform density.

The use of GGA-type functionals significantly increases the precision of the calculations compared to the description provided by the LDA, in particular for the binding energy of molecules. This is the origin of the massive use of DFT by chemists in the 1990s. We find different parameterizations for the GGA including those of Perdew et al (1991) [16], Perdew et al (1996) [17] and the most used versions are those of Perdew and Wang [18] and Perdew [19].

III.3.3. Meta-GGA Functionals

The Meta-generalized gradient approximation (meta-GGA) exchange-correlation functionals [20] use the second derivative of the density $\nabla^2\rho(r)$ and/ or the kinetic energy density τ

$$\tau(\mathrm{r}) = \sum_{\mathrm{i}=1}^{\mathrm{N_{occ}}} \frac{1}{2}|\nabla\varphi_{\mathrm{i}}(\mathrm{r})|^2 \qquad \text{(I. 22)}$$

Some examples of this type of functionals are the exchange-correlation functionals B98 [21], TPSS [22], VSXC [23] and the correlation functional KCIS [24, 25].
In gas phase studies of molecular properties, Meta-GGAs such as the TPSS [26] functional have been shown to offer improved performance over LDAs and GGAs [22, 27-29].

III.3.4. Hybrid Functionals

The GGA approach is not always sufficient for a correct description of various chemical properties of compounds. To keep up with the search for a more accurate exchange correlation functional, another approach have been developed, which is considering the exchange part of E_{xc} as a combination between the Hartree-Fock exchange energy and exchange density functional [30]. The exchange-correlation functionals based on this strategy are commonly known as hybrid functionals.

We can cite as an example the *Becke 3 parameter functional* (*B3*), the most famous hybrid functionals developed by Becke, which employs three parameters, a_{1-3} (determined through fitting to experiment) to control the mixing of the HF exchange and density functional exchange and correlation.
For this functional, the expression for the exchange-correlation is given by:

$$E_{XC}^{B3} = a_1 E_X^{HF} + (1 - a_1) E_X^{LDA} + a_2 \Delta E_X^{B88} + E_C^{LDA} + a_3 \Delta E_C^{PW91} \qquad (I.23)$$

The substitution of the correlation terms in this B3 functional (I.23) by the correlation functional LYP was proposed by Stevens et al. [31] and gave the appearance of the widely known B3LYP functional, which stands for "Becke, 3-parameter, Lee–Yang–Parr".

$$E_{XC}^{B3LYP} = a_1 E_X^{HF} + (1 - a_1) E_X^{LDA} + a_2 \Delta E_X^{B88} + a_3 E_C^{LYP} + (1 - a_3) E_C^{VWN} \qquad (I.24)$$

Bibliography

[1] Schrödinger, E. "*An undulatory theory of the mechanics of atoms and molecules.*" Phys. Rev. 28.6 **(1926**) 1049-1070

[2] Born, M., and Oppenheimer, R. *"Zur quantentheorie der molekeln."* Annalen der physik 389.20 (**1927**) 457-484.

[3] (a) Hartree, D. R. *"The Wave Mechanics of an Atom with a Non-Coulomb Central Field. Part I. Theory and Methods."* Mathematical Proceedings of the Cambridge Philosophical Society. Vol. 24. N°. 1. Cambridge University Press, **1928**. p. 89-110. (b) Fock, V. *"Selfconsistent field "mit Austausch für Natrium." Zeitschrift für Physik* 62.11 (**1930**) 795-805.

[4] Thomas, L. H. *"Inhomogeneous electron gas"* Proc. Cambridge Phil. Roy. Soc. 23 (**1927**) 542-548.

[5] FERMI, E. *"Statistical method to determine some properties of atoms"* Rend. Accad. Naz. Lincei 6. 602-607 (**1927)** 5.

[6] Dirac, P.A.M. *"Note on exchange phenomena in the Thomas atom."* Proc. Cambridge Phil. Roy. Soc.26 (**1930**) 376-385

[7] Hohenberg, P. and Kohn, W. J. P. R. *"Density functional theory (DFT)."* Phys. Rev. 136 (**1964**) B864.

[8] Kohn, W. and Sham, L. J. *"Self-consistent equations including exchange and correlation effects."* Phys. Rev. 140.4A (**1965**) A1133.

[9] Wigner, E. *"Effects of the electron interaction on the energy levels of electrons in metals."* Transactions of the Faraday Society 34 (**1938**) 678-685.

[10] Ceperley, D. M., and Alder, B. J. *"The ground state of the electron gas by a stochastic method."* Phys. Rev. Lett. *4*45.7 (**1980**) 566-569.

[11] Perdew, J. P., and Zunger, A. *"Self-interaction correction to density-functional approximations for many-electron systems."* Phys. Rev. *B* 23.10 (**1981)** 5048-5079

[12] Fermi, E. *"Eine statistische Methode zur Bestimmung einiger Eigenschaften des Atoms und ihre Anwendung auf die Theorie des periodischen Systems der Elemente."* Zeitschrift für Physik 48.1-2 (**1928**) 73-79.

[13] Hedin, L. and Lundqvist, B. I. *"Explicit local exchange-correlation potentials."* Journal of Physics C: Solid state physics 4.14 (**1971**) 2064-2083

[14] Perdew, J. P. and Wang, Y. *"Accurate and simple analytic representation of the electron-gas correlation energy."* Phys. Rev. B 45.23 (**1992**) 13244.

[15] Vosko, S. H., Wilk, L. and Nusair, M. *"Accurate spin-dependent electron liquid correlation energies for local spin density calculations: a critical analysis."* Can. J. Phys. 58.8 (**1980**) 1200-1211.

[16] Perdew, J. P., Chevary, J. A., Vosko, S. H., Jackson, K. A., Pederson, M. R., Singh, D. J., and Fiolhais, C. *"Atoms, molecules, solids, and surfaces: Applications of the generalized gradient approximation for exchange and correlation."* Phys. Rev. B 46.11 (**1992**) 6671- 6687

[17] Perdew, J. P., Burke, K. and Ernzerhof, M. *"Generalized gradient approximation made simple."* Phys. Rev. Lett. 77.18 (**1996**) 3865-3868.

[18] Perdew, J. P., and Wang Y. *"Accurate and simple density functional for the electronic exchange energy: Generalized gradient approximation."* Physical review B 33.12 (**1986**) 8800-8802

[19] Perdew, J. P. *"Electronic Structure of Solids '91*" edited by P. Ziesche and H." *Eschrig (Akademie Verlag, Berlin, 1991)* (**1991**).

[20] Perdew, J. P., Kurth, S., Zupan, A., and Blaha, P. *"Accurate density functional with correct formal properties: A step beyond the generalized gradient approximation.*" Phys. Rev. Lett. 82.12 (**1999**) 2544-2547.

[21] Schmider, Hartmut L., and Axel D. Becke. *"Optimized density functionals from the extended G2 test set."* J. Chem. Phys. 108.23 (**1998**) 9624-9631.

[22] Tao, J., Perdew, J. P., Staroverov, V. N., and Scuseria, G. E. *"Climbing the density functional ladder: Nonempirical meta–generalized gradient approximation designed for molecules and solids."* Phys. Rev. Lett. 91. 14 (**2003**) 146401-146401

[23] Van Voorhis, T., and Scuseria, G. E. "*A novel form for the exchange-correlation energy functional."* J. Chem. Phys. 109.2 (**1998**) 400-410

[24] Rey, J., and Savin, A. *"Virtual space level shifting and correlation energies."* Int. J. Quantum Chem. 69.4 (**1998**) 581-590.

[25] Toulouse, J., Andreas, S. and Adamo, C. *"Validation and assessment of an accurate approach to the correlation problem in density functional theory: The Kriger–Chen–Iafrate–Savin model."* J. Chem. Phys. 117.23 (**2002**) 10465-10473.

[26] Csonka, G. I., Perdew, J. P., Ruzsinszky, A., Philipsen, P. H., Lebègue, S., Paier, J. and Ángyán, J. G. *"Assessing the performance of recent density functionals for bulk solids."* Phys. Rev. B 79.15 (**2009**) 155107- 155107

[27] Staroverov, V. N., Scuseria, G. E., Tao, J., and Perdew, J. P. *"Comparative assessment of a new nonempirical density functional: Molecules and hydrogen-bonded complexes."* J. Chem. Phys.119.23 **(2003**) 12129-12137.

[28] Zhao, Y. and Truhlar, D. G. "*Benchmark databases for nonbonded interactions and their use to test density functional theory."* J. Chem. Theo. Comput. 1.3 (**2005**) 415-432.

[29] Zhao, Y. and Truhlar, D. G. "*Design of density functionals that are broadly accurate for thermochemistry, thermochemical kinetics, and nonbonded interactions."* J. Phys. Chem. A 109.25 (**2005**) 5656-5667.

[30] Becke, A. D. "*Molecular excitation energies to high-lying bound states from time-dependent density-functional response theory: Characterization and correction of the time-dependent local density approximation ionization threshold."* J. Chem. Phys. 98 **(1993**) 5648-5652.

[31] Stephens, P. J., Devlin, F. J., Chabalowski, C. F., and Frisch, M. J. *"Ab initio calculation of vibrational absorption and circular dichroism spectra using density functional force fields»* J. Phys. Chem. 98.45 (**1994**) 11623-11627.

CHAPTER II

Structural stabilities and electronic properties of Gallium-Indium clusters

I. Introduction

The determination of the geometric and electronic structures of metal clusters and their chemical and physical properties has become an interesting field of research and grows significantly in importance [1]. Experimental and theoretical studies of small clusters formed by 13 group elements have been carried out during the past several decades because of their fundamental interest and potential application in nano-science.

Gallium and Indium as 13 group elements are of great importance in physics and chemistry of nanoclusters and thin film deposition.

I.1. Gallium Clusters

Small gallium clusters have been extensively studied in order to provide an in-depth look into these clusters. There are several studies performed in both theoretical [2-16] and experimental [17-19] fields. Song and Cao [10] have theoretically investigated the geometrical parameters and electronic structures of Ga_n (n = 2-26) clusters, using the generalized gradient approximation for the exchange correlation potential to the DFT. It turned out that gallium clusters tend to adopt compact structures with increasing cluster size. Figure 1 shows the most stable structures for the Ga_n (n = 3-8) clusters according to previous studies [3, 4, 10].

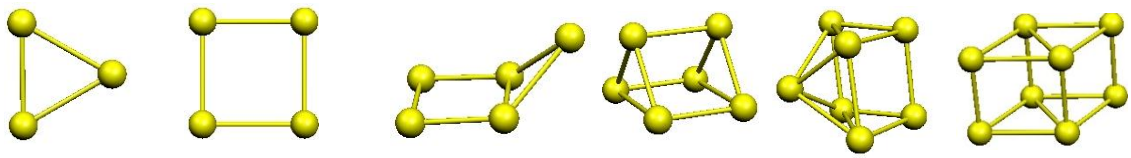

Figure 1. Lower- energy structure of Ga_n (n = 3-8) Clusters [3, 4, 10]

I.2. Indium Clusters

Indium clusters have been studied experimentally [20-25], as well as theoretically [2, 27-30]. Zhang et al. [30] have systematically investigated the lowest-energy structures and electronic properties of indium In_n (n = 1-16) ones using DFT, showing the tendency towards compact structures with increasing cluster size.

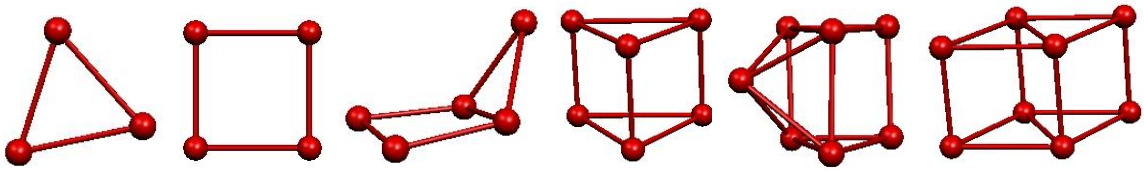

In_3 In_4 In_5 In_6 In_7 In_8

Figure 2. Lower- energy structure of In_n (n =3-8) Clusters [30]

We also have calculated the total energy for different structures of Ga_n and In_n (n =3-8) clusters. We have found almost the same results for the most stable structures. The only exception is for n = 4, of which we found that lowest-energy structures for Ga_4 and In_4 is butterfly-shaped as shown in Figure 3 and not a square shaped as in previous studies (see Figures 1 and 2) .

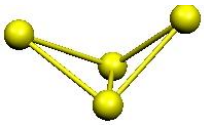

Figure 3. Lower- energy structure of Ga_4 (or In_4) cluster according to our work

I.3. Gallium-Indium Clusters

For the composition of mixed gallium-indium clusters, experimental studies have been done. Lill et al. [31, 32] have produced neutral and positively charged clusters by 4 keV Ar+ ion bombardment of a liquid gallium indium eutectic alloy and then they studied it by time-of-flight mass spectrometry coupled with single photon. The figure 4 shows the Mass spectra of sputtered neutral gallium-indium Ga_mIn_{n-m} (n = 4- 8 and m < n) clusters, as Lill et al have found it.

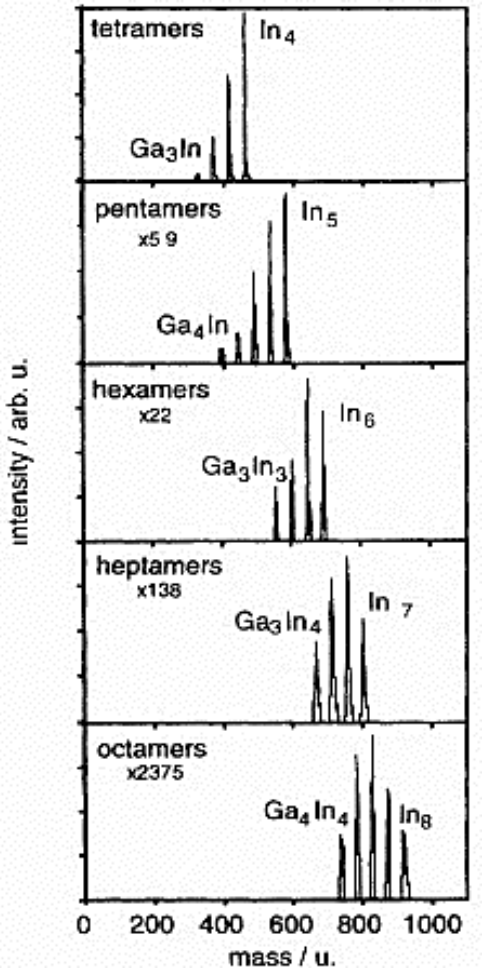

Figure 4. Mass spectra of sputtered neutral Ga_mIn_{n-m} (n = 4- 8 and m < n) clusters [31]

To gain a deep understanding of gallium-indium clusters, calculations have been carried out of small gallium-indium Ga_mIn_{n-m} (n = 4, 6, 8 and m < n) clusters, based on the DFT method at the B3LYP/TZP level.

II. Results and discussion

II-1. Geometries and stability of isomers

We have explored the Ga_mIn_{n-m} (n = 4, 6, 8 and m < n) clusters in order to found their lowest-energy structures. Indeed, full geometry optimizations of Ga_mIn_{4-m} (m<4), Ga_mIn_{6-m} (m < 6) and Ga_mIn_{8-m} (m < 8) showed a variety of singlet spin state structures which are

found as energy minimum much lower in energy than those of triplet state ones (Figures. 5-7). The different isomers are designated by ma_n, mb_n, mc_n, where m and (n – m) are the gallium and indium atom numbers, respectively. For the studied structures, the calculated values of relative energies between isomers, HOMO-LUMO energy gaps and the Ga-In, In-In and Ga-Ga bond distances are gathered in Tables 1, 2, 3, 1A, 2A.

In order to predict the relative stabilities and electronic properties of gallium-indium Ga_mIn_{n-m} (n = 4, 6, 8 and m < n) clusters, we have calculated the bonding energy, IPs, EAs, and the chemical hardness (η).

II.1.1. Four vertex Ga_mIn_{4-m} (m < 4) clusters.

The most stable structure for the $GaIn_3$ clusters corresponds to the $1a_4$ bent of C_s symmetry one as shown in Figure 5. Two other $1b_4$ and $1c_4$ isomers keeping the gallium atom between indium ones are higher in energy than the most stable one by 1.6 and 2.7 kcal/mol, respectively. The Ga atom binds to In ones with the bond lengths of 2.553 Å, while the In-In bond distances are of 3.369 Å, in accordance with the Ga and In radii. The $1a_4$ structure global minimum exhibits a significant HOMO-LUMO gap of 1.15 eV synonymous of good thermodynamic stability.

The Y-shaped $1g_4$ isomer with C_{2v} symmetry in which the gallium atom is at the apex position is the seventh low-lying isomer. It is important to note that the less stable isomers correspond to the linear geometry featuring a maximum of In-In bonds.

For the Ga_2In_2 clusters, the $2a_4$ bent structure characterized by rhombus geometry with C_{2v} symmetry is found as the global minimum presenting only Ga-Ga and Ga-In bonds, in which the gallium atoms are adjacent. This global minimum possesses one Ga-Ga bond with a length of 2.346 Å and four Ga-In bonds with an averaged bond distance of 3.085 Å. The computed HOMO-LUMO gap of 1.32 eV is large and predicting the possibility of the existence of this cluster. Energetically, the second isomer $2b_4$ corresponds to a planar geometry with D_{2h} symmetry, which lies 3.5 kcal/mol above the global minimum isomer and exhibiting a large HOMO-LUMO gap of 1.35 eV with comparable Ga-Ga and Ga-In bond lengths than those obtained for $2a_4$ structure.

These results emphasize that the Ga-Ga bond acts as a stabilizing effect, contrarily to the In-In one. The different $2i_4$, $2j_4$ and $2k_4$ linear structures lie high in energy than the global minimum as shown in Figure 5 and Table 1.

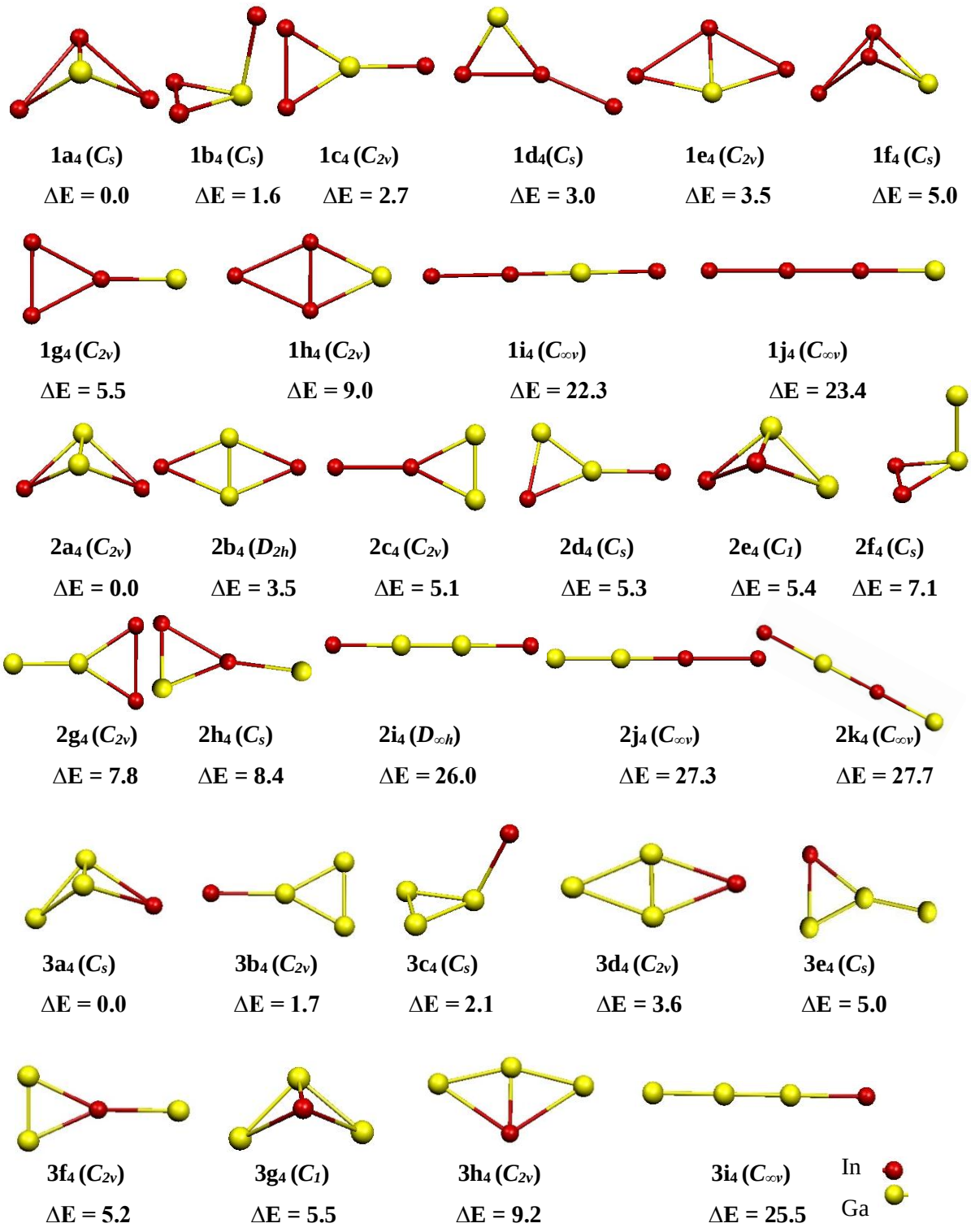

Figure 5. Ground state structures of Ga_mIn_{4-m} (m < 4) clusters. Relative energies ΔE between the isomers are given in kcal/mol.

Table 1. Relative energies (kcal/mol), HOMO-LUMO gap (eV), Ga-Ga, In-In and Ga-In bond lengths (Å) and the lowest and highest vibrational frequencies (LVF and HVF (cm^{-1})) for Ga_mIn_{4-m} ($m < 4$)

Cluster	Isomer	Sym	Relative energy	HOMO-LUMO gap	Ga-Ga	In-In	Ga-In	LVF (cm^{-1})	HVF (cm^{-1})
$GaIn_3$	$1a_4$	C_s	0.0	1.15	-	3.369	2.553	29	194
	$1b_4$	C_s	1.6	0.99	-	3.107	2.746	8	162
	$1c_4$	C_{2v}	2.7	1.11	-	2.922	2.780	15	196
	$1d_4$	C_s	3.0	1.13	-	3.000	2.652	22	174
	$1e_4$	C_{2v}	3.5	1,14	-	3.404	2.523	20	215
	$1f_4$	C_s	5.0	1.11	-	2.743	3.117	31	158
	$1g_4$	C_{2v}	5.5	1.11	-	2.871	2.907	23	168
	$1h_4$	C_{2v}	9.0	1.07	-	2.703	3.127	20	177
	$1i_4$	$C_{\infty v}$	22.3	0.89	-	306.1	2.707	72	217
	$1j_4$	$C_{\infty v}$	23.4	0.84	-	2.877	2.885	78	189
Ga_2In_2	$2a_4$	C_{2v}	0.0	1.32	2.346	-	3.085	31	244
	$2b_4$	D_{2h}	3.5	1.35	2.333	-	3.093	21	259
	$2c_4$	C_{2v}	5.1	1.27	2.434	3.093	2.801	24	205
	$2d_4$	C_s	5.3	1.81	2.559	-	2.685	18	210
	$2e_4$	C_1	5.4	1.15	2.816	3.416	2.545	32	198
	$2f_4$	C_s	7.1	1.04	2.702	3.058	2.751	19	174
	$2g_4$	C_{2v}	7.8	1.14	2.703	2.904	2.782	9	208
	$2h_4$	C_s	8.4	1.15	-	2.992	2.657	24	180
	$2i_4$	$D_{\infty h}$	26.0	0.8	2.517	-	2.884	3	248
	$2j_4$	$C_{\infty v}$	27.3	0.91	2.687	3.060	2.696	83	228
	$2k_4$	$C_{\infty v}$	27.7	0.90	-	-	2.701	80	220
Ga_3In	$3a_4$	C_s	0.0	1.35	2.339	-	3,107	35	247
	$3b_4$	C_{2v}	1.7	1.38	2.459	-	2.908	23	223
	$3c_4$	C_s	2.1	1.33	2.501	-	2.869	9	208
	$3d_4$	C_{2v}	3.6	1.37	2.322	-	3.107	24	264
	$3e_4$	C_s	5.0	1.20	2.560	-	2.685	18	219
	$3f_4$	C_{2v}	5.2	1.31	2.434	-	2.802	26	205
	$3g_4$	C_1	5.5	1.17	2.849	-	2.540	37	199
	$3h_4$	C_{2v}	9.2	1.13	2.810	-	2.512	25	219
	$3i_4$	$C_{\infty v}$	25.5	0.98	2.511	-	2.889	86	257

Three energetically close structures are found for Ga_3In species. The most stable corresponds to the $3a_4$ bent C_s structure with the indium atom occupying a peripheral position, while the three Ga atoms occupy the three vertices of the same triangle.

The Ga-Ga and Ga-In bond distances are of 2.339 and 3.107 Å, in agreement with short and long bonds, respectively. The $3a_4$ global minimum structure displays a significant HOMO-LUMO gap of 1.35 eV, suggesting a thermodynamically stable species. The planar $3b_4$

structure, where the indium atom is connected to one Ga atom of the triangular Ga_3, constructing a Y-like structure lies only 1.7 kcal/mol above the most stable $3a_4$ isomer. The three dimensional $3c_4$ structure with C_s symmetry is among the low-lying isomer found 2.1 kcal/mol above the global minimum, keeping the indium atom between the gallium ones and does not provide Ga_3In clusters as more stable structures. It is clear that Ga_3In clusters prefer structures containing Ga_3 triangle with a maximum of Ga-Ga bonds.

II.1.2. Six vertex Ga_mIn_{6-m} (m < 6) clusters

The lowest-energy structure for $GaIn_5$ clusters corresponds to the $1a_6$ trigonal prismatic one having C_s symmetry (Figure 6), in which the In-Ga-In valence angle is of 82°. The $1b_6$ lies only 2.6 kcal/mol above the lowest one corresponding. The third isomer $1c_6$ is also corresponds to a distorted trigonal prismatic geometry in which the gallium atom form an angle of 56° within the $GaIn_2$ triangle, lying 2.9 kcal/mol above the global minimum (Table 2).

For Ga_2In_4 clusters, fourteen structures were found as energy minimum (Figure 6, Table 2 and Figure A1, Table A1 of the Annex). The $2a_6$ structure with C_{2v} symmetry (Figure 6), is obtained by gallium insertion in the apex of one triangular base of $GaIn_5$, forming a direct Ga-Ga bond. Other positions of gallium atoms of trigonal prism structure corresponding to $2b_6$, $2c_6$, $2e_6$, $2f_6$ and $2g_6$ isomers are less stable than the global minimum by $2a_6$ by 3.0, 3.8, 3.9, 6.0 and 6.3 kcal/mol, respectively. It is obvious that the planar geometry (Figure A1) gives rise to the less stable isomers, thus, the absence of Ga-Ga bond induces loss of energies.

As shown in Figure A1, sixteen isomers are found as energy minimum of Ga_3In_3 clusters within the range of 14.4 kcal/mol. The most stable $3a_6$ structure corresponds to a distorted triangle prism obtained without symmetry constraints (Figure 6), which can be obtained by substituting one gallium atom for one indium atom from the most stable Ga_2In_4.

The replacement of In by Ga atoms in the same lateral face of trigonal prismatic structure of the Ga_3In_3, gives rise to the Ga_4In_2 clusters, where the $4a_6$ isomer has been obtained as the lowest-energy structure and slightly more stable than the $4b_6$ and $4c_6$ ones only by 0.4 and 0.6 kcal/mol, respectively.

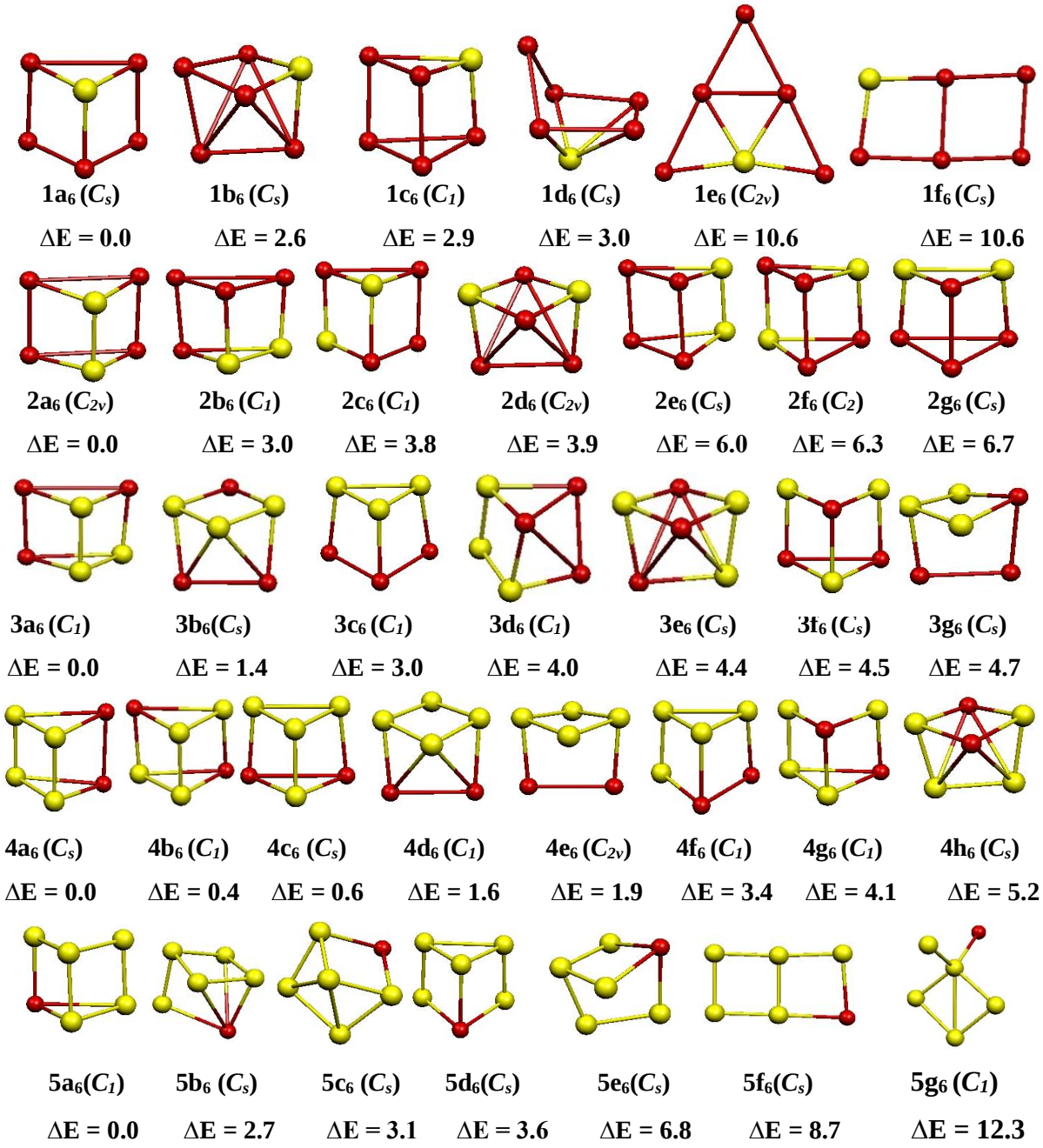

Figure 6. Ground state structures of Ga_mIn_{6-m} (m < 6) clusters. Relative energies ΔE between the isomers are given in kcal/mol.

In the case of Ga_5In, the most stable structure corresponds to a trigonal prismatic geometry with one Ga-Ga bond breaking as sketched in Figure 6 is obtained without any symmetry constraints. The other low-lying structure, $5d_6$ with the lower C_s symmetry is also displaying a distorted trigonal prismatic geometry, in which Indium atom form an angle of

56.2° and lies only 2.7 kcal/mol higher in energy than the $5a_6$ global minimum. Twelve other isomers exhibiting various geometries are sketched in Figure A1 of the Annex

Table 2. Relative Energies (kcal/mol), HOMO-LUMO Gaps (eV), Ga–Ga, In-In, and Ga–In Bond Lengths (Å), the lowest and highest vibrational frequencies (LVF and HVF (cm^{-1})) for Ga_mIn_{6-m} ($m < 6$) Clusters

Cluster	Isomer	Sym	Relative energy	HOMO-LUMO gap	Ga-Ga	In-In	Ga-In	LVF (cm^{-1})	HVF (cm^{-1})
$GaIn_5$	$1a_6$	C_s	0.0	1.52	-	2.976	2.762	19	155
	$1b_6$	C_s	2.6	1.35	-	2.966	2.766	16	151
	$1c_6$	C_1	2.9	1.35	-	2.955	2.755	21	160
	$1d_6$	C_s	3.0	1.49	-	3.021	2.703	11	171
	$1e_6$	C_{2v}	10.6	1.27	-	2.971	2.825	8	177
	$1f_6$	C_s	10.6	1.32	-	2.879	2.697	12	182
Ga_2In_4	$2a_6$	C_{2v}	0.0	1.65	2.547	3.002	2.771	23	178
	$2b_6$	C_1	3.0	1.50	2.541	2.966	2.773	23	189
	$2c_6$	C_1	3.8	1.47	-	2.978	2.761	23	158
	$2d_6$	C_{2v}	3.9	1.40	-	3.128	2.770	4	157
	$2e_6$	C_s	6.0	1.36	2.550	2.970	2.776	24	185
	$2f_6$	C_2	6.3	1.34	-	2.998	2.749	30	162
	$2g_6$	C_s	6.7	1.35	-	2.982	2.767	31	162
Ga_3In_3	$3a_6$	C_1	0.0	1.66	2.550	3.091	2.766	25	188
	$3b_6$	C_s	1.4	1.63	2.514	3.129	2.822	16	203
	$3c_6$	C_1	3.0	1.55	2.546	3.000	2.792	25	193
	$3d_6$	C_1	4.0	1.46	2.552	3.088	2.739	37	185
	$3e_6$	C_s	4.4	1.38	2.567	3.608	2.771	13	178
	$3f_6$	C_s	4.5	1.47	-	3.565	2.778	30	160
	$3g_6$	C_s	4.7	1.48	2.566	2.997	2.767	30	180
Ga_4In_2	$4a_6$	C_s	0.0	1.68	2.570	3.025	2.771	26	191
	$4b_6$	C_1	0.4	1.65	2.546	-	2.794	32	192
	$4c_6$	C_s	0.6	1.67	2.559	3.758	2.789	30	189
	$4d_6$	C_1	1.6	1.63	2.530	3.150	2.811	17	193
	$4e_6$	C_{2v}	1.9	1.56	2.758	3.139	2.791	27	182
	$4f_6$	C_1	3.4	1.52	2.541	2.992	2.778	27	192
	$4g_6$	C_1	4.1	1.46	2.567	-	2.779	33	185
	$4h_6$	C_s	5.2	1.33	2.609	-	2.789	12	179
Ga_5In	$5a_6$	C_1	0.0	1.69	2.551	-	2.792	32	192
	$5b_6$	C_s	2.7	1.56	2.566	-	2.815	30	188
	$5c_6$	C_s	3.1	1.59	2.504	-	2.840	9	206
	$5d_6$	C_s	3.6	1.56	2.553	-	2.790	37	195
	$5e_6$	C_s	6.8	1.42	2.559	-	2.785	40	185
	$5f_6$	C_s	8.7	1.61	2.533	-	2.774	16	235
	$5g_6$	C_1	12.3	2.13	2.501	-	2.747	15	214

II.1.3. Eight vertex Ga_mIn_{8-m} (m < 8) clusters.

For the $GaIn_7$ clusters, two isomers are found as energy minimum featured by a rhombic prismatic geometry with C_s symmetry differing by the symmetry plane disposition as shown in Figure 7 and Table 3. The lowest $1a_8$ structure, presenting four Ga-In bonds exhibits a large HOMO-LUMO gap of 1.62 eV and characterized by In-In and Ga-In bond distances of 2.913 and 2.724 Å as gathered in Table III, respectively. The second $1b_8$ isomer lies 1.5 kcal/mol above the lowest one, in which the gallium atom occupying a peripheral position and forms three bonds with indium ones. We can see that the number of In-In bonds of $1a_8$ structure the most stable isomer is less than that of the $1b_8$ one. The $1a_8$ global minimum structure lies only 1.5 kcal/mol below the $1b_8$ structure, where this weak difference arises chiefly from the difference concerning the number of Ga-In contacts, which are four in the latter and three in the former.

Five energetically close structures are found as the energy minimum for the Ga_2In6 clusters (Figure 7), which can be generated by substituting one indium atom by equivalent gallium one from the most stable $GaIn_7$ structure adopting the rhombic prismatic geometry. The lowest-energy $2a_8$ C_{2v} structure is computed to be slightly more stable than the $2b_8$ isomer (by 0.8 kcal/mol), which is not significant at the considered level of theory.

For the Ga_3In_5 clusters, the most stable $3a_8$ structure corresponds to a distorted rhombic prismatic geometry of the Cs symmetry. The Ga atoms are bound to each other forming two short Ga–Ga bonds of 2.565 A, while there are seven Ga–In bonds with an average length of 2.711 A, thus reducing the In–In direct contact to only two bonds of 2.947 A. The computed HOMO-LUMO gap is 1.71 eV. Note that the reduction of Ga–Ga and Ga–In contacts induces energy loss. The other isomer can be generated by substituting one gallium atom for one indium atom at the equatorial position stemming the most stable Ga_2In_6.

In the case of Ga_4In_4 clusters, most stable $4a_8$ adopts the rhombic prismatic geometry with the D_{2h} symmetry, where gallium atoms occupy the equatorial positions, forming a Ga_4 rhombus. Fourteen distorted rhombic prisms with gallium atoms substituting different positions of a rhombic prism are obtained within the range of 5.5 kcal/mol (Figure 7, Table III and Figure A2, Table A2 of the Annex). For the $4o_8$ D_{2h} structure, indium atoms occupy the equatorial positions of a rhombic prismand form a In_4 rhombus, unlike most stable $4a_8$

forming a Ga_4 rhombus. These results mean that the Ga–Ga bond is stronger than the In–In one and produces a stabilizing effect.

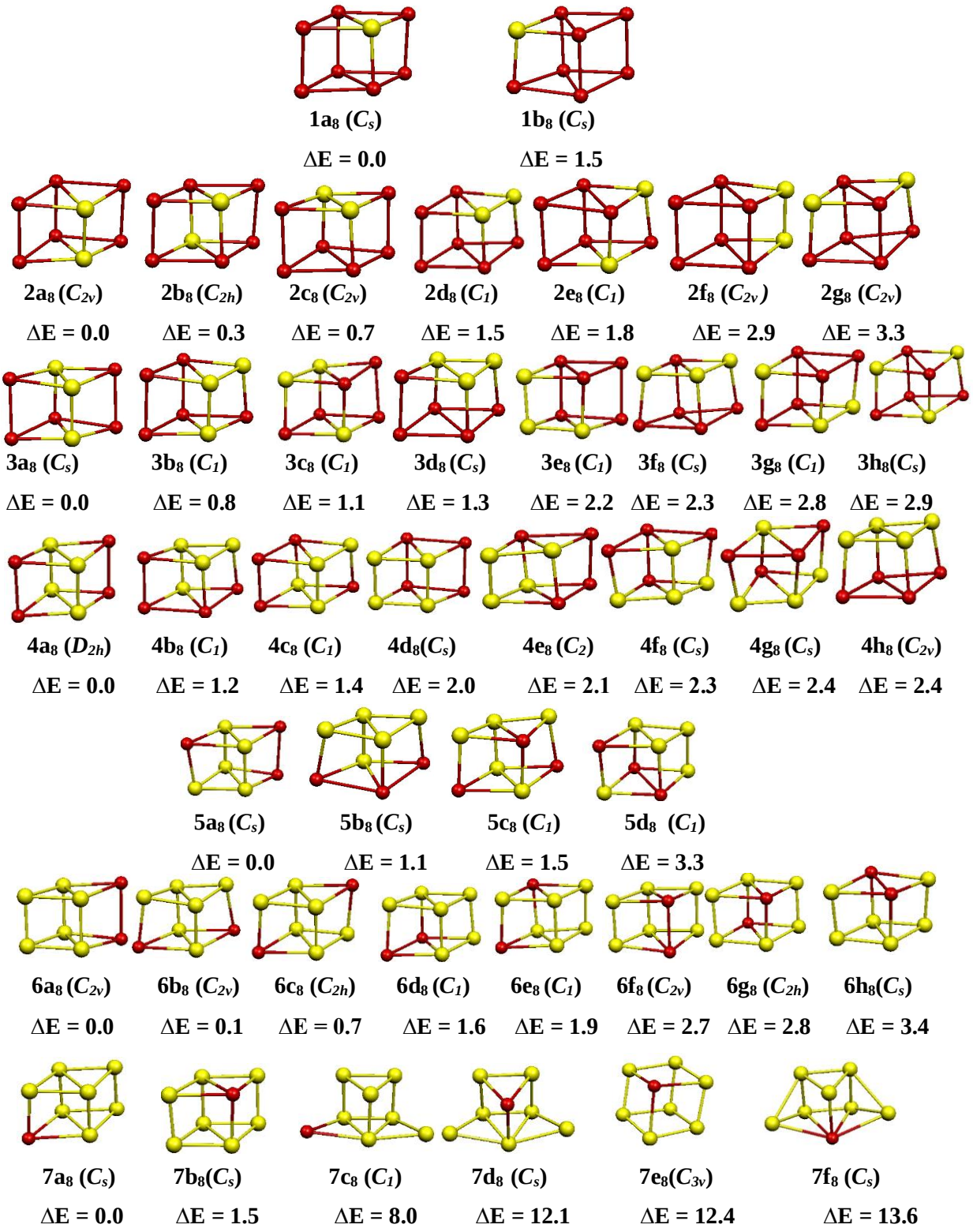

Figure 7. Ground state structures of Ga_mIn_{8-m} (m < 8) Clusters. The relative energies ΔE between isomers are given in (kcal/mol).

Table 3. Relative Energies (kcal/mol), HOMO–LUMO Gaps (eV), Ga–Ga, In–In, and Ga–In Bond Lengths (Å) for Ga_mIn_{8-m} (m < 8) Clusters

Cluster	Isomer	Sym	relative energies	HOMO-LUMO gap	Ga-Ga	In-In	Ga-In
$GaIn_7$	$1a_8$	C_s	0.0	1.62	-	2.913	2.724
	$1b_8$	C_s	1.5	1.66	-	2.926	2.742
Ga_2In_6	$2a_8$	C_{2v}	0.0	1.66	2.517	2.940	2.907
	$2b_8$	C_{2h}	0.3	1.65	-	2.938	2.722
	$2c_8$	C_{2v}	0.7	1.68	2.730	2.945	2.715
	$2d_8$	C_1	1.5	1.63	2.671	2.918	2.730
	$2e_8$	C_1	1.8	1.64	-	2.949	2.729
	$2f_8$	C_{2v}	2.9	1.61	2.533	2.930	2.936
	$2g_8$	C_{2v}	3.3	1.66	-	2.926	2.745
Ga_3In_5	$3a_8$	C_s	0.0	1.71	2.508	2.947	2.711
	$3b_8$	C_1	0.8	1.68	2.520	2.913	2.744
	$3c_8$	C_1	1.1	1.67	2.669	2.948	2.725
	$3d_8$	C_s	1.3	1.69	2.712	2.943	2.722
	$3e_8$	C_1	2.2	1.64	2.528	2.925	2.738
	$3f_8$	C_s	2.3	1.67	2.664	2.927	2.737
	$3g_8$	C_1	2.8	1.70	2.686	2.924	2.736
	$3h_8$	C_s	2.9	1.69	-	2.917	2.739
Ga_4In_4	$4a_8$	D_{2h}	0.0	1.79	2.505	2.944	2.934
	$4b_8$	C_1	1.2	1.73	2.514	2.955	2.718
	$4c_8$	C_1	1.4	1.72	2.522	2.963	2.727
	$4d_8$	C_s	2.0	1.69	2.526	2.918	2.922
	$4e_8$	C_2	2.1	1.68	2.524	2.950	2.734
	$4f_8$	C_s	2.3	1.72	2.529	2.914	2.752
	$4g_8$	C_s	2,4	1.70	2.655	3.201	2.728
	$4h_8$	C_{2v}	2.4	1.73	2.693	3.157	2.726
Ga_5In_3	$5a_8$	C_s	0.0	1.81	2.508	2.959	2.749
	$5b_8$	C_s	1.1	1.78	2.521	3.242	2.727
	$5c_8$	C_1	1.5	1.77	2.529	-	2.728
	$5d_8$	C_1	3.3	1.75	2.540	3.212	2.732
$Ga_6I\ n_2$	$6a_8$	C_{2v}	0.0	1.81	2.530	2.959	2.955
	$6b_8$	C_{2v}	0.1	1.86	2.517	-	2.758
	$6c_8$	C_{2h}	0.7	1.87	2.513	-	2.756
	$6d_8$	C_1	1.6	1.81	2.527	3.219	2.727
	$6e_8$	C_1	1.9	1.80	2.524	-	2.759
	$6f_8$	C_{2v}	2.7	1.80	2.543	2.928	2.991
Ga_7In	$7a_8$	C_s	0.0	1.88	2.523	-	2.757
	$7b_8$	C_s	1.5	1.85	2.539	-	2.733
	$7c_8$	C_1	8.0	1.72	2.514	-	2.852
	$7d_8$	C_s	12.1	1.99	2.513	-	2.689
	$7e_8$	C_{3v}	12.4	1.52	2.570	-	3.012
	$7f_8$	C_s	13.6	1.90	2.510	-	2.686

For the Ga_5In_3 clusters, the most stable structure $5a_8$ is also a distorted rhombic prism with C_s symmetry, which can be obtained by substituting one indium atom by one gallium atom from the most stable Ga_4In_4 isomer. The remaining low-lying isomers are within the range of 3.3 kcal/mol.

In the case of Ga_6In_2 clusters, eight structures were found as energy minimum as displayed in Figure A2 (see Annex II). The global minimum $3a_8$ structure adopts a distorted rhombic prism having C_s symmetry, which the indium atoms occupying peripheral positions, is lower in energy than $6b_8$, $6c_8$ and $6d_8$ by 0.1, 0.7 and 1.6 kcal/mol, respectively, and displays a large HOMO-LUMO gap of 1.81 eV and short Ga-Ga, Ga-In and In-In bond distance of 2.530, 2.955 and 2.959.

Nine lowest-energy structures are found for the Ga_7In clusters with various geometries as displayed in Figure A2 and Table A2. As presented in Figure 7, the 7a8 isomer exhibiting rhombus prismatic or *cubane*-like structure is computed as the global minimum displaying a large HOMO-LUMO gap of 1.88 eV and short Ga-Ga and Ga-In bond distance of 2.523 and 2.757. The second most stable isomer corresponds to the $7b_8$ one with same rhombus prismatic geometry lies only 1.5 kcal/mol, while the less stable $7i_8$ one with a planar geometry is found 21.4 kcal/mol above the global minimum.

III.2. The substitution effects on the Ga_8 and In_8 cage

Seen the existence of $Ga_8(C_{13}H_9)_8^{2-}$ cluster [33], it seemed appropriate to us to investigate the substituted and the bare Ga_8 and In_8 cage, in order to give a deeper understanding of the substitution effects on the cluster cage (Figure 8). For the substituted Ga_8H_8 species, each gallium atom engages one electron among three to form Ga-H bond, thus, requires more connections with its neighbouring gallium atoms to counter in this electronic deficiency. Consistent with this electron consideration, it was turned out that the square antiprismatic structure is obtained as energy minimum, whereas that the rhombic prismatic Ga_8H_8 structure it is not obtained as energy minimum exhibiting large imaginary frequencies.

Likewise to Ga_mIn_{8-n} clusters, the bare Ga_8 adopts a *cubane*-like geometry with tri-connected Ga atoms involving three electrons in the cluster cage rather than the substituted species adopting the square antiprismatic one with tetra-connected Ga atoms engaging only two electrons in the cluster cage.

The calculations have been carried out on the bare Ga_8^{2-} and the substituted $Ga_8H_8^{2-}$ prismatic species showing the existence of large imaginary frequencies for the latter, thus, these dianionic rhombic prismatic clusters is not found as energy minimum, while the $Ga_8H_8^{2-}$ square antiprismatic structure is authenticated as energy minimum describing the experimental one with short Ga-Ga bond distances in the range 2-561-2.723 Å compared to those of the neutral Ga_8H_8 one ranging from 2.654 to 2.877 Å.

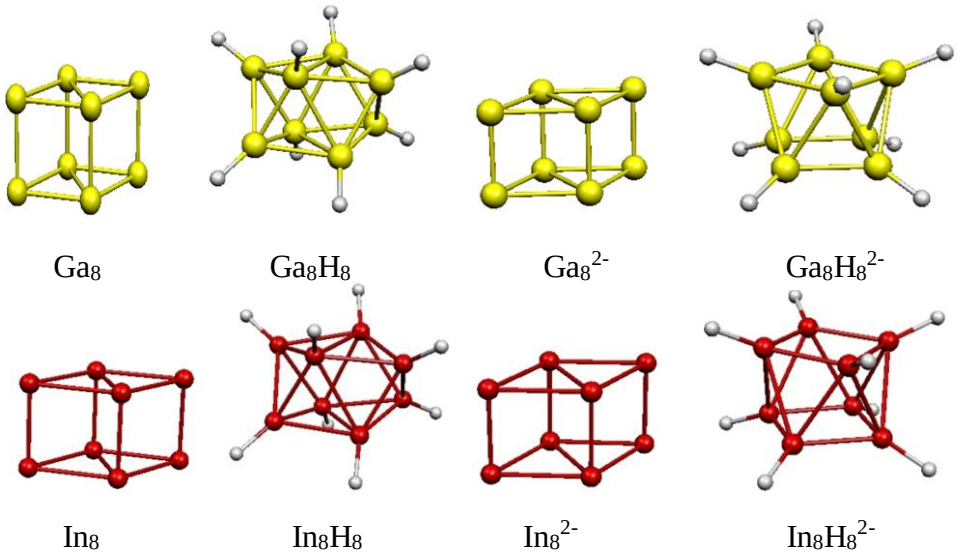

Figure 8. Optimized molecular structures of the M_8, M_8H_8, M_8^{2-} and $M_8H_8^{2-}$ (M = Ga, In) isomers of lowest energy.

The Ga-Ga bond distances obtained for the dianionic $Ga_8H_8^{2-}$ species are comparable to those found in recent theoretical work for the protonated Ga_8H_{10} [34]. It is worthwhile noting that rhombic prismatic structures display comparable bond distances ranging from 2.534 to 2.810 Å.

The same tendencies are obtained for the In_8H_8 and In_8, where the bare cluster adopt the rhombic prismatic structure exhibiting short In-In bond distances within the large range 2.153-3.092 Å; however, the substituted species adopts the square antiprismatic one, with In-In bond distances within the narrow range 2.993-3.262 Å. It is important to note that the bond In-In bond distances in the dianionic $In_8H_8^{2-}$ and In_8^{2-} species undergo somewhat lengthening compared to those of the neutral $In_8H_8^{2-}$ and In_8^{2-} ones.

II.3. Bonding energy per atom

The bonding energies E_{Ga} and E_{In} of Ga or In atom of each of the most stable Ga_mIn_{n-m} (n = 4, 6, 8 and m = 1, 2.., n–1) clusters are calculated by the following expressions, respectively:

$$E_{Ga} = [E(Ga_mIn_{n-m}) - (E(Ga_{m-1}In_{n-m}) + E(Ga))]$$

$$E_{In} = [E(Ga_mIn_{n-m}) - (E(Ga_mIn_{n-m-1}) + E(In))],$$

Where: E(Ga) and E(In) are the energies of isolated gallium and indium atoms, respectively, while the $E(Ga_{m-1}In_{n-m})$ and $E(Ga_mIn_{n-m-1})$ are the energies of fragments.

The values of bonding energies of Ga or In atom calculated by the above formula are gathered in Table IV. The relationship between E_{Ga} or E_{In} and the m number of gallium or Indium atoms of the cluster is shown in Figure 9.

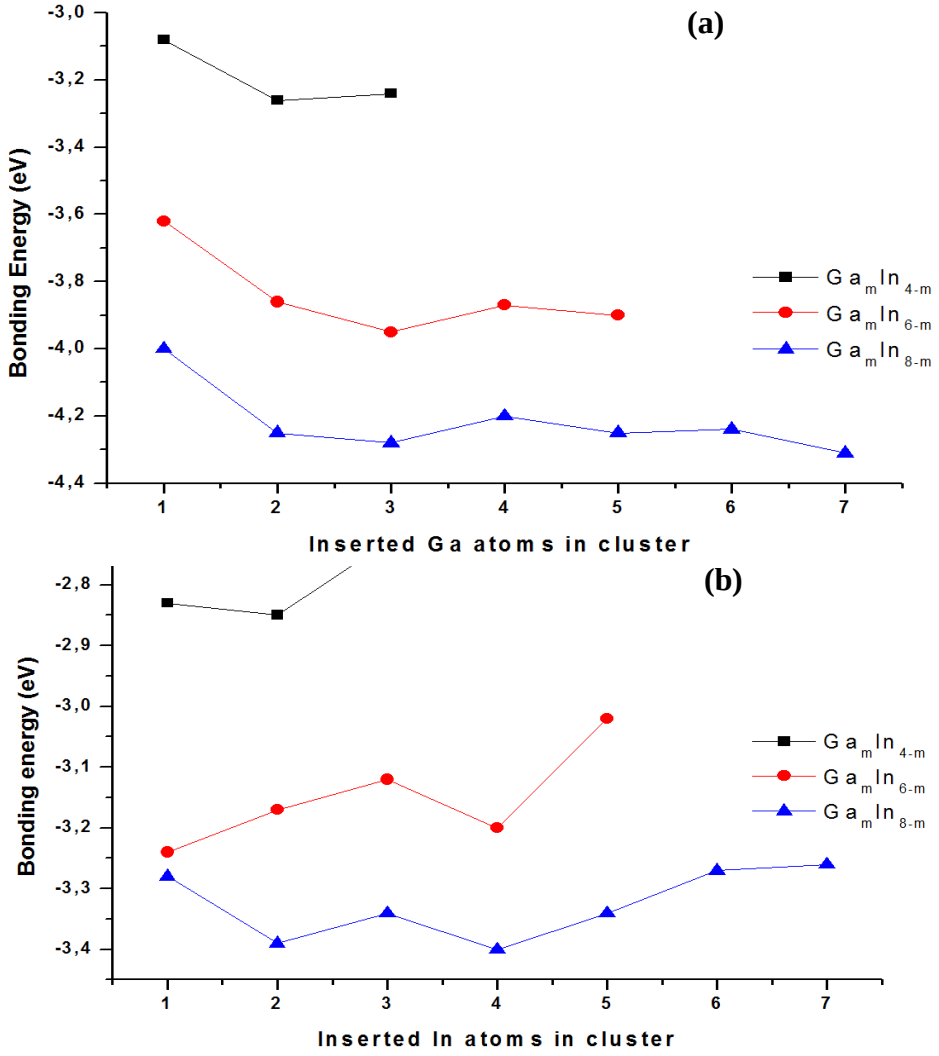

Figure 9. The bonding energy as a function of inserted Ga (a) and In (b) atoms in various Ga_mIn_{n-m} (n = 4, 6, 8 and m < n) clusters

It is clear from the three curves (Figure 9) that E_{Ga} increases gradually as m increases. Furthermore, one can observe that the cluster becomes more compact with enlarging cluster size, as found by the previous works on Al element clusters [35].

For Ga_mIn_{n-m} clusters with the same total number n, the bonding energies E_{Ga} of Ga_mIn_{n-m} ($m < 4$) are the smallest ones. This result indicates that Ga bonds are very important for the stability of Ga_mIn_{n-m} clusters. It further shows that the Ga-rich clusters are more stable than the In-rich ones with the same total number of atoms. Overall, according to the bonding energies per atom, it can be concluded that the most stable clusters correspond to those with the maximum of Ga atoms, while the less stable clusters correspond to those with the minimum of Ga atoms.

Table 4. Bonding energy of Ga or In atoms E_{Ga} and E_{In}, vertical ionization potential (VIP), adiabatic ionization potential (AIP), vertical electron affinity (VEA), adiabatic electron affinity (AEA) and chemical hardness (η) of the most stable Ga_mIn_{n-m} (n = 4, 6, 8 and m < n) clusters are given in eV.

Cluster	E_{Ga}	E_{In}	E_{HOMO}	E_{LUMO}	VIP	AIP	VEA	AEA	η
$GaIn_3$	-3.08	-2.73	-4.20	-3.08	5.80	5.76	1.64	1,82	2.08
Ga_2In_2	-3.26	-2.85	-4.36	-3.04	5.94	5.89	1.53	1.65	2.21
Ga_3In	-3.24	-2.83	-4.44	-3.09	6.02	5.83	1.52	1.63	2.25
$GaIn_5$	-3.62	-3.02	-4.59	-3.08	6.03	5.90	1.77	2.04	2.13
Ga_2In_4	-3.86	-3.20	-4.69	-3.04	6.12	6.00	1.69	1.96	2.21
Ga_3In_3	-3.95	-3.12	-4.75	-3.09	6.18	6.04	1.70	1.98	2.24
Ga_4In_2	-3.87	-3.17	-4.84	-3.17	6.26	6.10	1.71	2.00	2.28
Ga_5In	-3.90	-3.24	-4.91	-3.23	6.35	6.18	1.71	2.01	2.32
In_8			-4.74	-3.15	6.09	5.93	1.96	1.96	2.06
$GaIn_7$	-4.00	-3.26	-4.79	-3.17	6.14	5,97	1.94	1.99	2.10
Ga_2In_6	-4.25	-3.27	-4.82	-3.16	6.16	6,01	1.90	1.91	2.13
Ga_3In_5	-4.28	-3.34	-4.90	-3.19	6.23	6,05	1.89	1.94	2.17
Ga_4In_4	-4.20	-3.40	-4.98	-3.19	6.30	6,12	1.86	1.86	2.22
Ga_5In_3	-4.25	-3.34	-5.03	-3.22	6.32	6,13	1.84	1.90	2.24
Ga_6In_2	-4.24	-3.39	-5.10	-3.29	6.37	6,22	1.90	1.87	2.26
Ga_7In	-4.31	-3.28	-5.20	-3.31	6.47	6,23	1.84	1.88	2.32
Ga_8			-5.32	-3.40	6.58	6.34	1.84	1.85	2.37

II.4. HOMO-LUMO energy gaps

The HOMO-LUMO gap is among the useful parameters evaluating the stability and the chemical reaction ability of the clusters. A system with a large energy gap is chemically less reactive, therefore, could be more stable. From the Tables 1, 2, 3, it is interesting to mention that the calculated values of HOMO-LUMO gaps for the most stable Ga_mIn_{n-m} (n = 4, 6, 8 and m<n) clusters are in the range 1.15-1.88 eV (Figure 10), which are synonymous of good thermodynamic stability of the studied clusters. Cleary from the curves displayed in Figure 10, there is an apparent increase according to the increase of the m number of gallium. Moreover, one can see that the HOMO-LUMO gaps increase according the following order: $Ga_mIn_{4-m} < Ga_mIn_{6-m} < Ga_mIn_{8-m}$ and consistent with the bonding energy results. The largest HOMO-LUMO gap of 1.88 eV corresponds to the Ga_7In, indicating that this cluster is the less reactive system and relatively the most stable one due essentially to the stabilization of the HOMO, while the LUMO remains almost at the same energy compared to those of small and less Ga-rich clusters.

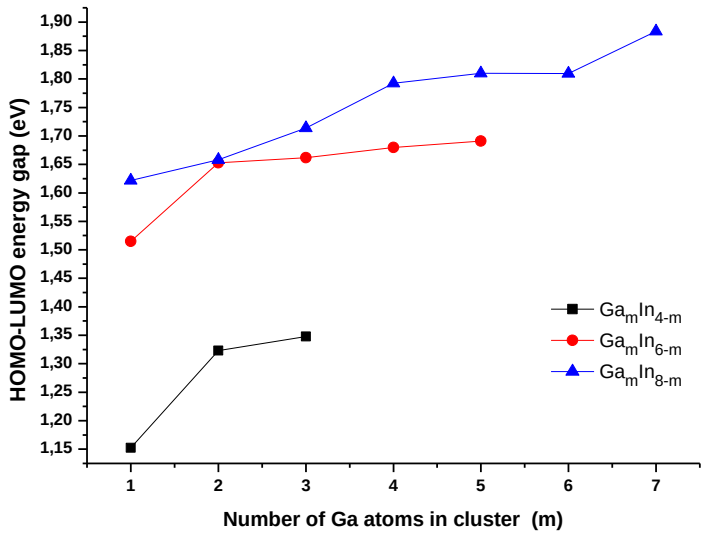

Figure 10. Variation of HOMO-LUMO energy gaps as a function of m number of Ga atoms calculated for the most stable structures of Ga_mIn_{n-m} (n = 4, 6, 8 and m < n) clusters.

II.5. Ionization potential and electron affinity

The ionization potential (IP) and electron affinity (EA) are used as important properties to probe the electronic structure modifications with respect to the cluster size. The ionization potential (AIP, VIP) and electron affinity (AEA, VEA) were calculated for each

most stable isomers clusters related to the Ga_mIn_{n-m} (n = 4, 6, 8 and m < n) clusters as shown in Figure 11 and Table 4.

VIP is defined as the energy difference between cationic and neutral clusters, when both are at the optimized geometry of the neutral cluster. AIP is defined similarly, but with both clusters at their respective optimized geometries.

VEA is defined as the energy difference between neutral and anionic clusters, when both are at the optimized geometry of the neutral cluster. AEA is the energy difference between neutral and anionic clusters, both at their respective optimized geometries.

The calculated VIP and AIP values of the lowest-energy of Ga_mIn_{n-m} (n = 4, 6, 8 and m < n) structures are summarized in Table IV and plotted in Figure 11, where the energy needed for removal of an electron from the cluster yields valuable information on the electronic structure.

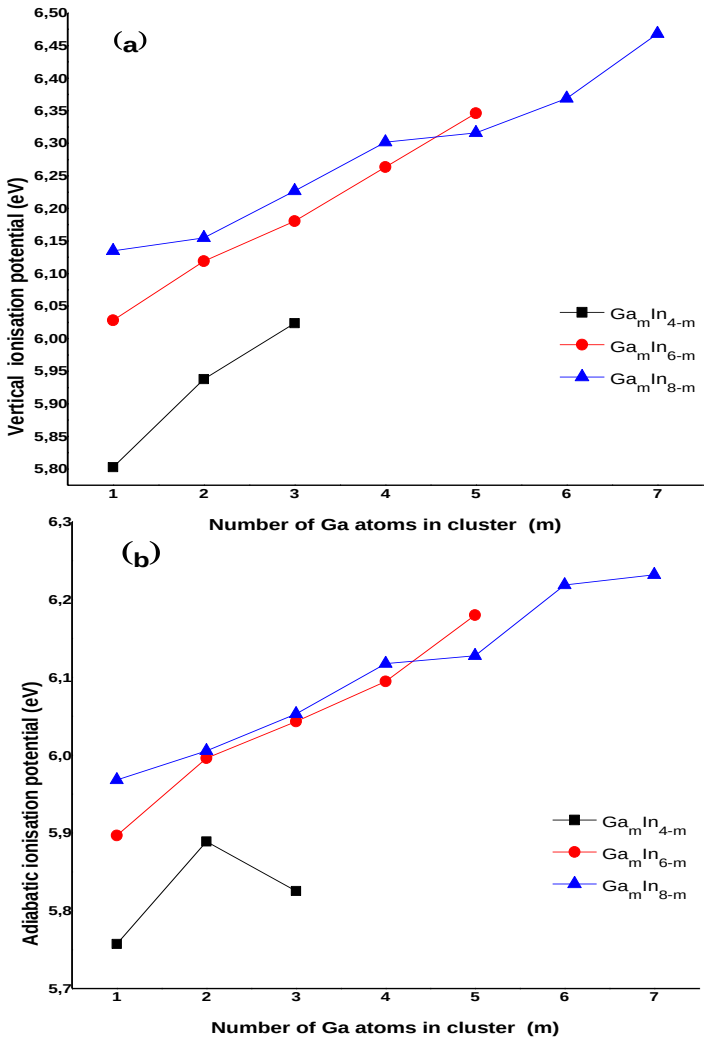

Figure 11. VIPs (a), and AIPs (b) for the most stable structures of Ga_mIn_{n-m} (n = 4, 6, 8 and m<n) clusters as a function of m number of Ga atoms

The calculated VIP values are larger than the AIP ones and the energy difference between them is an indication of the energy gain due to structural relaxation. As can be seen from Figure 11, the Ga_mIn_{n-m} clusters with the same total number n of atoms, the VIP and AIP of Ga_mIn_{n-m} (m = 1) are the smallest ones. For all the three curves, Ga_mIn_{n-m} clusters with the same total number n, VIP and AIP increase as function of the m number of gallium atoms increasing, showing the same behavior as compared to that of the bonding energy per atom E(Ga). Therefore, this result indicates that the Ga-rich clusters are more stable than In-rich ones. The smallest VIP value (5.80 eV) shows that the $GaIn_3$ cluster is more readily ionized than the large and Ga-rich clusters.

The Ga_mIn_{3-m} clusters have the lowest VIPs (5.80-6.02 eV) and AIPs (5.76-5.89 eV), therefore, they are the most easily oxidizable species, contrarily to the Ga_mIn_{8-m} clusters with the highest VIPs (6.30-6.47 eV) and AIPs (6.12-6.23 eV), thus, they are the most difficult to oxidize, in accordance with their HOMO energies, where the one electron removing from a deep orbital requires more energy, this corresponds to the largest IP, contrarily to those related to the high HOMO energies.

The AIP, VIP and E_{HOMO} values summarized in Table 4 show clearly that the decreasing of HOMO energies correlated to the enhancement of AIP and VIP values. The comparison of IP's between Ga_mIn_{n-m} shows a progressive rise in presence of more Ga atoms and for large cluster size, in accordance with the relatively high Ga electronegativity compared to that of In one. This upward trend of the ionization potential as a function of the cluster size has been highlighted for the small Al-Si_{n-1} clusters [36].
Thus reduction in IP can be explained by the increase of the HOMO energies, thus, Ga-rich species are more stable than the In-rich.

Contrarily to the potential ionization, the AEA values are larger than those of VEA ones as given in Figure 12 and Table 4. For the same total number n, one can notice the downward of the energy's trend led by the increasing of Ga atoms. The smallest VAE (1.52 eV) and AEA (1.63 eV) are obtained for the Ga_3In cluster indicating its ease to be reduced, whereas, the largest VAE (1.94 eV) and AEA (1.99 eV) are obtained for the $GaIn_7$ containing the minimum of Ga, corresponding to the most difficult species to be reduced.

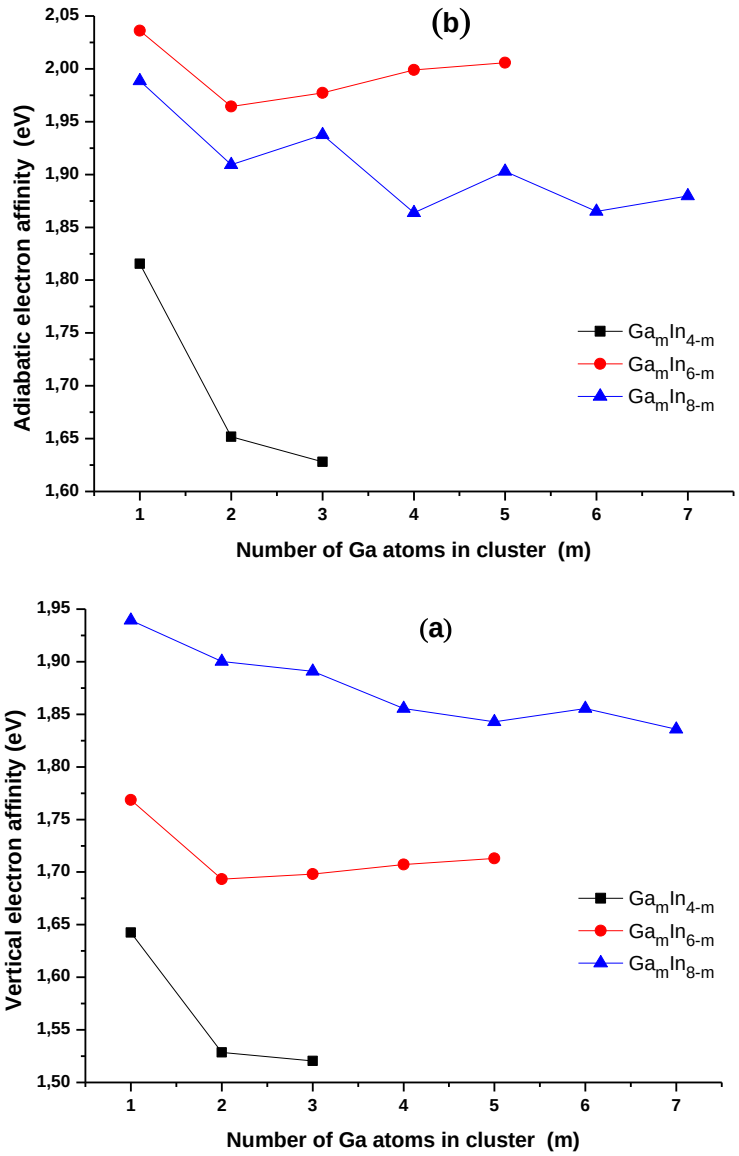

Figure 12. VEA (a) and AEA (b), calculated for the most stable structures of Ga_mIn_{n-m} (n = 4, 6, 8 and m < n) clusters as a function of m number of Ga atoms.

II.6. Chemical hardness

Chemical hardness (η) given below is an electronic quantity characterizing the relative stability of clusters. The chemical hardness (η) [37, 38] is a measure of the resistance of a chemical entity to change in the number of electrons, which is given by the following formula: η = 1/2(VIP - VEA), where VIP and VEA represent the vertical ionization and

vertical electron affinity, respectively. The computed values of chemical hardness (η) for the studied lowest-energy clusters are summarized in Table 4 and plotted in Figure 13.

From the curves, one can observe that for the Ga_mIn_{n-m} clusters with the same total number n, the chemical hardness (η) increases as the number m of gallium atoms increases, showing the same behaviour compared to those of the binding energy per atom E_B, energy gaps and IPs. The largest hardness values are obtained for the Ga_7In (2.34 eV) and Ga_8 (2.36 eV) isomers (Figure 13), which has the largest HOMO–LUMO energy gap, hence having minimum tendency to exchange electrons (minimum reactivity), whereas, the smallest hardness values are obtained for In_8 (2.06 eV) and GaI_3 (2.08 eV) predicting the maximum tendency to exchange electrons (maximum reactivity).

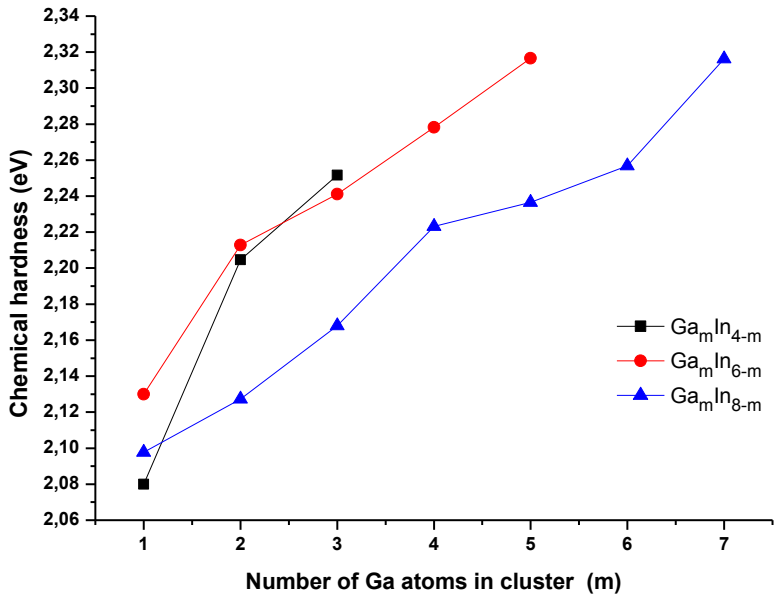

Figure 13. Chemical hardness as a function of m number of Ga atoms obtained for the most stable structures of Ga_mIn_{n-m} (n = 4, 6, 8 and m < n) clusters.

III.Conclusions

In this work, a detailed study has been provided of structural parameters, relative stabilities and electronic properties of gallium–indium Ga_mIn_{n-m} clusters (n = 4, 6, 8 and m < n). The obtained clusters prefer to adopt three-dimensional (3D) structures, the trigonal prism and rhombic prism configurations are favored energetically when n = 6 and 8, respectively.

Substituting of In atom(s) with Ga atom(s) keeps the geometry unchanged, but induces some important variations concerning the bonding energy per atom, the HOMO-LUMO gaps, the ionization potential, the electron affinity and the chemical hardness. Indeed, the bonding energy evolution, and the electronic properties including HOMO-LUMO gap, ionization potential (IP), electron affinity (EA) and chemical hardness (η) show that the Ga-rich clusters are more stable than those of In-rich ones with the same number of the total atoms. It is found that the studied properties strongly depend on the cluster size as well as the Ga and In contributions. The Ga-Ga bond is stronger than the Ga-In bond and the latter is stronger than the In-In one. Therefore, Ga_7In cluster is relatively, the most stable structure. Thus, the stability increases with the Ga-Ga bonds increasing.

Bibliography

[1] Johnston, R. L. *"The development of metallic behaviour in clusters"* Phil. Trans and R. Soc. Lond. A356 (**1998**) 211-230.

[2] Balasubramanian, K. and Feng, P.Y. "*The Electronic States of Ga_3"*. Chem. Phys. Lett. 146 (**1988**) 155-161

[3] Gong, X.G. and Tosatti, E. *"Structure of small gallium clusters"*. Phys. Lett. A 166 (**1992**) 369-372.

[4] Jones, R.O. "*Simulated annealing study of neutral and charged clusters: Al_n and Ga_n*" J. Chem. Phys. 99 (**1993**) 1194-1206.

[5] Yi, J.Y. "*Stability, structural transformation, and reactivity of Ga13 clusters"*. Phys. Rev. B 61 (**2000**) 7277-7279

[6] Song, B., Cao, P. L., and Li, B. X. *"Theoretical study of the structure of a Ga6N6 cluster".* Phys. Lett. A 315 (**2003**) 308-312

[7] BelBruno, J .J. *"Bonding and energetics in small clusters of gallium and arsenic." Heteroat*. Chem. 14 (**2003**) 189-196.

[8] Zhao, Y., Xu, W., Li, Q., Xie, Y., and Schaefer, H. F. *"Gallium Clusters Ga_n (n = 1−6): Structures, Thermochemistry, and Electron Affinities."* J. Phys. Chem. A 108 (**2004**) 7448-7459.

[9] Chacko, S., Joshi, K., Kanhere, D. G., & Blundell, S. A. "*Why Do Gallium Clusters Have a Higher Melting Point than the Bulk"* Phys. Rev. Lett. 92, (**2004**) 135506_1-135506_4.

[10] Song, B. and Cao, P.L. *"Evolution of the geometrical and electronic structures of Ga_n (n = 2-26) clusters: a density-functional theory study"* J. Chem. Phys. 123 (**2005**) 144312_1-144312_8.

[11] Krishnamurty, S., Joshi, K., Zorriasatein, S., & Kanhere, D. G. *"Density functional analysis of the structural evolution of Ga_n (n=30–55) (n=30–55) clusters and its influence on the melting characteristics"* J. Chem. Phys. 127 (**2007**) 054308_1-054308_7.

[12] Gaston, N., and Parker, A. J. *"On the bonding of Ga_2, structures of Ga_n clusters and the relation to the bulk structure of gallium."* Chem. Phys. Lett. 501, 4-6 (**2011**) 375-378.

[13] Schnöckel, H. *"Structures and properties of metalloid Al and Ga clusters open our eyes to the diversity and complexity of fundamental chemical and physical*

processes during formation and dissolution of metals". Chem. Rev, 110.7 **(2010**). 4125-4163.

[14] Drebov, N., Weigend, F., and Ahlrichs, R. "*Structures and properties of neutral gallium clusters: a theoretical investigation."* J. Chem. Phys. 135 (**2011**) 044314_1-044314_7

[15] Núñez, S., López, J. M., and Aguado, A. "*Neutral and charged gallium clusters: structures, physical properties and implications for the melting features."* Nanoscale. 4 (**2012**) 6481-6492.

[16] Steenbergen, K. G., and Gaston, N. *First-principles melting of gallium clusters down to nine atoms: structural and electronic contributions to melting*".Phys.Chem. Chem. Phys. 15 (**2013**) 15325-15332.

[17] Cha, C. Y., Ganteför, G., and Eberhardt, W. *"The development of the 3 p and 4 p valence band of small aluminum and gallium clusters"* J. Chem. Phys., 100.2 (**1994**) 995-1010.

[18] Schnepf, A., and Schnöckel, H. "*Metalloid aluminum and gallium clusters: element modifications on the molecular scale".* Angew. Chem. Int. Ed. 41, 19 (**2002**) 3532-3554.

[19] Xan, X., & Dagdigian, P. J. *"Electronic spectrum of the gallium dimer".* J. Phys. Chem. A 107.15 (**2003**) 2642-2649.

[20] Himmel, H. J., and Gaertner, B. "*Characterization of Isolated Ga_2 Molecules by Resonance Raman Spectroscopy and Variations of Ga-Ga Bonding*." Chem. Eur. J. 10.23 (**2004**) 5936-5941.

[21] Van Harlingen, D. J., Heidel, D. F., & Garland, J. C. *"Experimental study of thermoelectricity in superconducting indium"*. Phys. Rev. B, 21.5 (**1980**) 1842-1857.

[22] Rayane, D., Melinon, P., Cabaud, B., Hoareau, A., Tribollet, B., and Broyer, M. Electronic properties and fragmentation processes for singly and doubly charged indium clusters. J. Chem. Phys. 90 **(1989**) 3295-3299.

[23] Schriver, K. E., Persson, J. L., Honea, E. C., and Whetten, R. L., *"Electronic shell structure of group-IIIA metal atomic clusters."* Phys. Rev. Lett. 64.21 (**1990**) 2539-2542

[24] Magaud, L., Khanna, S. N., & Jena, P. *"Limitation on the success of the jellium model for metal clusters. "*Chem. Phys. Lett., 183.5 (**1991**) 333-336.

[25] Wucher, A., Ma, Z., Calaway, W. F., and Pellin, M. J. *"Yields of sputtered metal clusters: the influence of surface structure."* Surf. Sci., 304.1-2 (**1994**) L439-L444.

[26] Staudt, C., and Wucher, A. "Generation of large indium clusters by sputtering." Phys. Rev. B.66 (**2002**) 075419_1-075419_12

[27] Onwuagba, B. N. (1993). *"Electronic and chemical properties of barium and indium clusters."* Phys. Stat. Sol. 180 (**1993**) 391-399

[28] Sin'ko, G. V., and Smirnov, N. A. *"Structural transitions in indium under high pressure: Ab initio electronic structure calculations."* Phys. Rev. B. 74 **(2006**) 134113_1-134113_8.

[29] Gao, L., Shi, D., Zhao, J., Wang, B., and Jia, J. *"Structural and Electronic Properties of In_n (n= 2–13) Clusters by Density Functional Theory."*.J. Comput. Theor. Nanosci. 4.1 (**2007**) 152-157.

[30] Zhang, W. Q., Zhao, G. F., Sun, J. M., Zhi, L. L., and Gu, Y. Z. "*First-principles study of the geometrical and electronic structures of Inn (n= 2–16) clusters"* Chem. Phys. 361. 44 (**2009**) 44-48

[31] Lill, T. B., Callaway, W. F., Pellin, M. J., and Gruen, D. M. *"Abundance and depth of origin of neutral and ionic clusters sputtered from a liquid gallium-indium eutectic alloy"* Phys. Rev. Lett. 73.12 (**1994**) 1719-1722

[32] Lill, T.B., Callaway, Ma, W.F. Z. and Pellin, M. J. *"Sputtering of Group-IIIa elements. Properties of the metal cluster formation mechanism*" Surf. Sci. 322.1-3 (**1995**) 361-372

[33] Schnepf, A., StoÈûer, G., and SchnoÈckel, H. *"Der erste molekulare quadratisch-antiprismatische Ga8-Cluster mit closo-Struktur."* Z. Anorg. Allg. Chem, 626 (**2000**) 1676-1680.

[34] Maatallah, M., Cherqaoui, D., Jarid, A., and Liebman, J. F. *"Large gallanes and the PSEPT theory: a theoretical study of Ga n H n+ 2 clusters (n= 7–9)"* J. Mol. Model. 18.7 (**2012**) 3321-3328.

[35] Akola, J., H. Häkkinen, and M. Manninen. *"Ionization potential of aluminum clusters."* Physical Review B 58.7 (**1998**) 3601- 3604.

[36] Chiranjib, M. and Kulshreshtha, S. K. "*Influence of Al substitution on the atomic and electronic structure of Si clusters by density functional theory and molecular dynamics simulations."* Phys. Rev. B 69 **(2004**) 115432_1-115432_8

[37] Pearson, R. G. "*Recent advances in the concept of hard and soft acids and bases"* J. Chem. Ed. 64.7 (**1987**) 561-567

[38] Parr, R. G., and Yang, W. "*Density-Functional Theory of Atoms and Molecules"* New York: Oxford Univ. (**1989**)142-197

CHAPTER III

Structure and Bonding Nature of nH_2 (n = 1-6) interact on Al_3N Cluster

I-Introduction

It is known that molecular hydrogen is one of the clean energy sources for the future, due to its efficiency, abundance, and its respect for the environment [1]. However, the manner of storing hydrogen under ambient conditions becomes a difficult problem for the development of hydrogen technologies [2]. Continuous efforts have been focused on the storage of hydrogen in solid-state materials, and an increasing interest in the search for suitable materials such as carbon nanotube, Boron nitride and aluminium nitride has arisen in the recent decades [3-14]

At the same time as hydrogen was used to modify the physical properties of aluminium nitride films, and controlling their crystalline quality [14-17], computational methods have been of great importance in the search of usage of AlN nanomaterials in hydrogen storage field [18-26]. An analysis of the published studies shows that H_2 dissociation on AlN nanotubes is thermodynamically favorable [20] and atomic H selects to be adsorbed on an N atom and liberate an energy of 0.22 eV [22]. In addition, hydrogen can remain in its molecular form in the $Al_{12}N_{12}$ cage [19]

Understanding hydrogen interaction with AlN clusters or other materials, could lead to suitable materials for storage of hydrogen [27]. However, there is still a lack of detailed knowledge about the mechanism of hudrogen interaction on Aluminium nitride clusters

The objective of this chapter is to identify the structural and electronic properties of hydrogen interaction on stable Al_3N cluster. We have explored the most probable sites of hydrogen molecules on Al_3N cluster, and their bonding energies, vibrational frequencies, electronic properties based on MO analysis, HOMO-LUMO gaps, NBO and Hirschfeld Charge analysis in order to provide a detailed scheme of their electronic structures. Moreover, the energy decomposition of the studied compounds is envisaged in order to find their interaction types.

II. Results and discussion

II.1.Optimized geometry and electronic structure of Al_3N

Initially, we have optimized a number of low-lying isomers and determined the lowest-energy structure for Al_3N cluster which have been detected experimentally, when laser-ablated aluminium atoms react with dinitrogen gas on condensation at 10 K [27].

In Figure 1(A), only the most stable structure is shown. The global minimum of Al_3N was found that N atom is bound to the three Al atoms to form a triangular structure. This geometry is the same as the previous theoretical study [28-37]. Geometry parameters of the Al_3N cluster with BP86-D and PW91 are shown in Table 1.

Charge analysis (Table 1) shows that the localised charge density of Al_3N cluster is mainly seen around nitrogen atom. Owing to the electronegativity difference between Al and N atoms, electrons are transferred from Al to N.

II.2. Interaction between H_2 molecules and Al_3N

To study the hydrogen molecules storage capacity and their effects on Al_3N cluster, we investigated the hydrogenation of Al_3N cluster with different number of hydrogen molecules, which were added arbitrarily to Al_3N cluster from various sites, directions and distances, in order to examine the preferential position of H_2 on Al_3N cluster.
During the overall geometry optimizations, Hydrogen molecules were added one at a time to the Al_3N cluster, and no symmetry constraint was imposed.

All the optimised structures of the Al_3N cluster interacting with one to six H_2 molecules are presented in Figures1, 2. Geometrical parameters, and Atomics Charges calculated for different Al_3NH_n (n = 2, 4, 6) and Al_3N-nNH_2 (n =1-6) are presented in Figure 8 and Table 1

In order to evaluate the stability of Al_3N-nH_2 clusters and measure the interaction strength between the Al_3N cluster and hydrogen molecules, E_B the bonding energy between Al_3N and nH_2, and the bonding energy (E_{H2}) of H_2 on Al_3N-$(n-1)H_2$ were calculated by BP86-D and PW91 methods according to the following equations:

$Al_3N + nH_2 \rightarrow Al_3N\text{-}nH_2$

$$\mathbf{E_B = (E_{Al3N\text{-}nH2} - E_{Al3N} - nE_{H2})} \qquad (1)$$

$Al_3N\text{-}(n\text{-}1)H_2 + H_2 \rightarrow Al_3N\text{-}nH_2$

$$\mathbf{E_{H2} = E_{Al3N\text{-}nH2} - E_{Al3N\text{-}(n\text{-}1)H2} - E_{H2}} \qquad (2)$$

Where $E_{Al3N\text{-}nH2}$ and $E_{Al3N\text{-}(n\text{-}1)H2}$ stand for total energy of the Al_3N-nH_2 and Al_3N-$(n-1)H_2$ systems, E_{Al3N} denotes total energy of Al_3N, while E_{H2} stands for total energy of H_2 molecule.

II.2.1. Al_3N-H_2 complex

First, one H_2 introduced into the Al_3N system may either be in dissociative form (Figure 1.B), or remain in molecular form (Figure 2. 1A).

For the dissociative form, we have placed the H_2 molecule at 1.8 Å distance to Al atom, and after DFT geometry optimization, the H_2 molecule is re-oriented such that the H_2 molecule dissociate and bind on top of the Al atom to form a covalent bond (see Figure 1.B) with a bonding energy of -158.28 and -160.48 kcal/mole for BP86-D and PW91 respectively. The equilibrium Al-H distance is found to be 1.595 Å (BP86-D), or 1.593 Å (PW91), which is in accordance with previous studies [9,18, 20] close to the experimental value 1.648 [38], and different as the Al–H bond distance of the AlH_6 octahedra in α-AlH_3 [39]. The computed Al_1-N distances change slightly from 1.860 Å and 1.854 Å for Al_3N to 1.822 Å and 1.814 Å for Al_3NH_2 with, BP86-D and PW91 respectively

As can be seen in Table 1, that when one hydrogen is added to the Al_3N, the Al_1-Al_2 bond length is just slightly changed from 3.220 Å to 3.117 Å at BP86-D level. Furthermore, The hydrogen atomic natural charge of -0.360 and -0.160, obtained by hirshfeld and Natural Bond Orbital (NBO) analysis respectively reflects the electronic transfer from the Al_3N to the H_2 as shown in Table 1, and confirm that H_2 strongly binds to Al_3N.

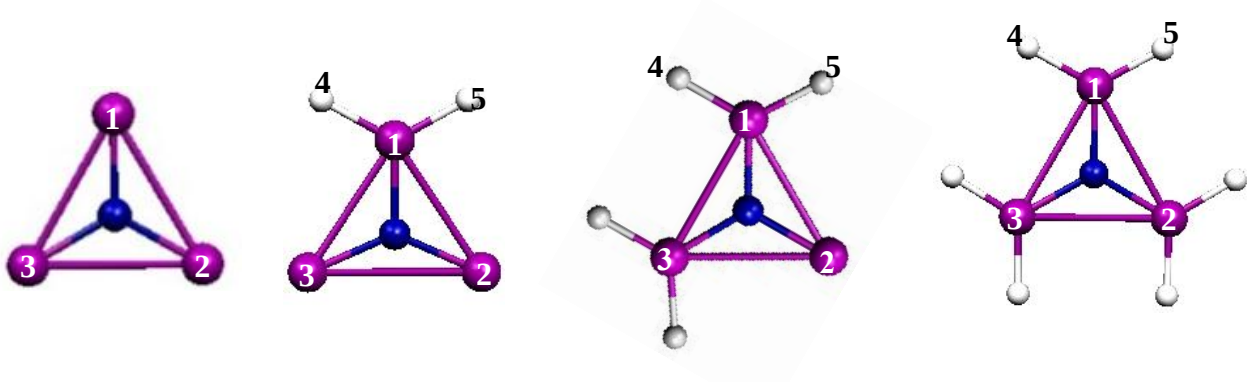

A (D_{3h}) **B (C_{2v})** **C(C_{2v})** ***D(D_{3h})***

Figure 1. Optimized geometries of Al_3N and Al_3NH_n (n = 2, 4, 6)

For the molecular form, we placed hydrogen molecule in different positions and orientations to Al_3N at 4.78 Å distance. After DFT geometry optimization, the H_2 molecule is re-oriented such that the H_2 is parallel to the Al-Al bond (see Figure 2.1A), with a calculated bonding energy of -2.20 Kcal/mol (BP86-D) or -1.98 Kcal/mol (PW91).

Table 1. Selected geometrical and energetic parameters calculated for Al_3NH_n (n =2, 4, 6). Bond distances, bonding energy (E_B) homo-lumo gap are given in Å, Kcal/mol and eV respectively

	Al_3N (A)		Al_3NH_2 (B)		Al_3NH_4 (C)		Al_3NH_6 (D)	
	BP86-D	PW91	BP86-D	PW91	BP86-D	PW91	BP86-D	PW91
E_{H2}	-	-	-158.28	-160.48	-156.28	-158.32	-154.12	-155.89
homo-lumo gap	2.55	2.52	2.71	2.69	3.41	3.33	4.92	4.85
Al_1-N	1.860	1.854	1.822	1.814	1.856	1.845	1.825	1.818
Al_2-N	1.860	1.854	1.856	1.844	1.820	1.812	1.825	1.818
Al_1-Al_2	3.220	3.210	3.117	3.090	3.169	3.138	3.160	3.148
Al_2-Al_3	3.220	3.210	3.339	3.334	3.180	3.193	3.160	3.148
Al_1-H_4	-	-	1.595	1.593	1.596	1.597	1.591	1.592
Al_1-H_5	-	-	1.595	1.593	1.590	1.590	1.591	1.592
Al_1-N-Al_2	120°	120°	115.9°	115.3°	119.1°	118.2°	120°	120°
Al_3-N-Al_2	120°	120°	128.2°	129.4°	121.8°	123.6°	120°	120°
Charges								
Al_1	0.807[a] 0.170[b]	0.809 0.171	1.349 0.436	1.340 0.435	1.399 0.216	1.397 0.214	1.418 0.474	1.415 0.473
Al_2	0.807 0.170	0.809 0.171	0.833 0.193	0.835 0.193	0.848 0.457	0.848 0.457	1.418 0.474	1.415 0.473
Al_3	0.807 0.170	0.809 0.171	0.833 0.193	0.835 0.193	1.399 0.216	1.397 0.214	1.418 0.474	1.415 0.473
N	-2.423 -0.509	-2.429 -0.512	-2.297 -0.502	-2.230 -0.503	-2.182 -0.493	-2.185 -0.494	-2.058 -0.479	-2.060 -0.481
H_4	-	-	-0.359 -0.160	-0.355 -0.159	-0.360 -0.155	-0.357 -0.155	-0.366 -0.157	-0.364 -0.156
H_5	-	-	-0.359 -0.160	-0.355 -0.159	-0.372 -0.164	-0.370 -0.163	-0.366 -0.157	-0.364 -0.156

a: Natural charges (NBO) b: Hirschfeld charges

As expected, low E_B -bonding energy between Al_3N and nH_2- values lead to a significant distance between aluminium and hydrogen ($d_{Al\text{-}H}$ = 2.670 Å (BP86-D), or 2.653 Å (PW91). The calculations based on the BP86-D (Figure 3) show that the Al-Al length nearest to the hydrogen atoms elongate from 3.222 to 3.231 Å, while the two others Al-Al lengths are shortens to 3.202 Å.

II.2.2. Al_3N-nH_2 (n = 2-6) complex

When added two hydrogen molecules at 1.7 Å distance to Al atoms, and after DFT geometry optimization, we found that the hydrogen molecules dissociate and bind on top of the Al atom to form a covalent bond (Fig.1.C) with a bonding energy of -156.28 and -158.32 Kcal/mole for BP86-D and PW91 respectively. Where the optimized Al-H bond lengths is found to be 1.59 Å for the two functionals, in good accordance with other results [40].

Similarly, the addition of three hydrogen molecules at 1.6 Å distance to Aluminium atoms, gives covalent bonds (as shown in Figure 1.D).

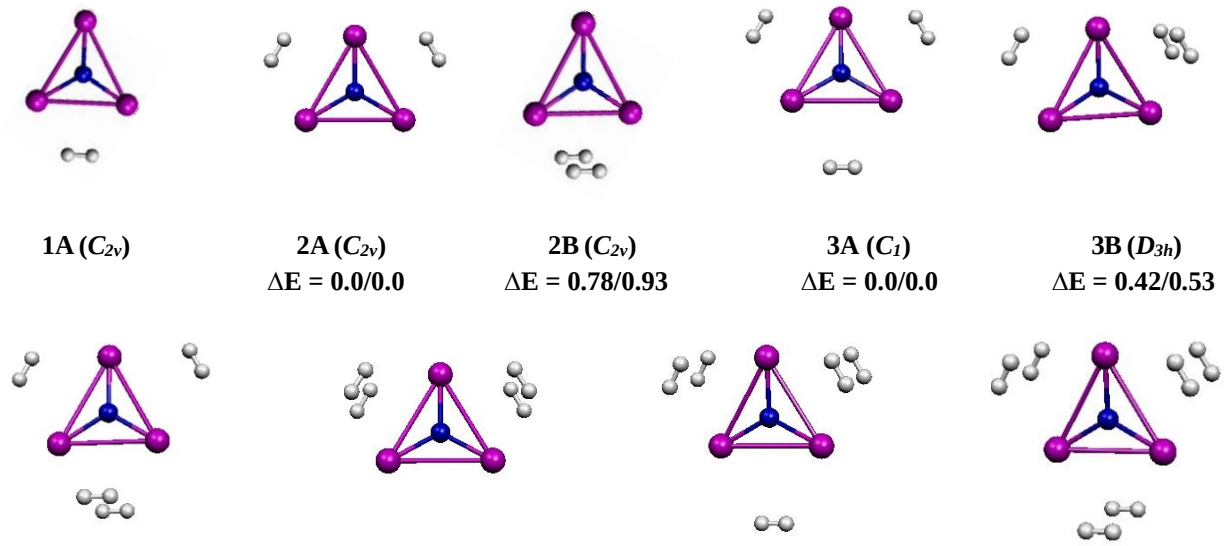

Figure 2. Optimized geometries of Al_3N-nH_2 (n = 1–6). The relative energies ΔE between isomers are given in kcal/mol, obtained by BP86-D and PW91, respectively .

We then studied the interaction of Al_3N with two to six hydrogen molecules. We found that all the successive H_2 molecules added to the Al_3N-nH_2 complexes (n = 2–6) at 4.78 Å distance to Al_3N remain in the form of hydrogen molecules (Figure 2) with H–H bond lengths ranging from 0.765 to 0.758 Å (BP86-D) or 0.766 to 0.754 Å (PW91), thus slightly larger compared to 0.751Å and 0.750 Å the calculated equilibrium distance of isolate H_2 molecule for BP86-D and PW91 functionals respectively (experimental value [38] is 0.74 Å) .

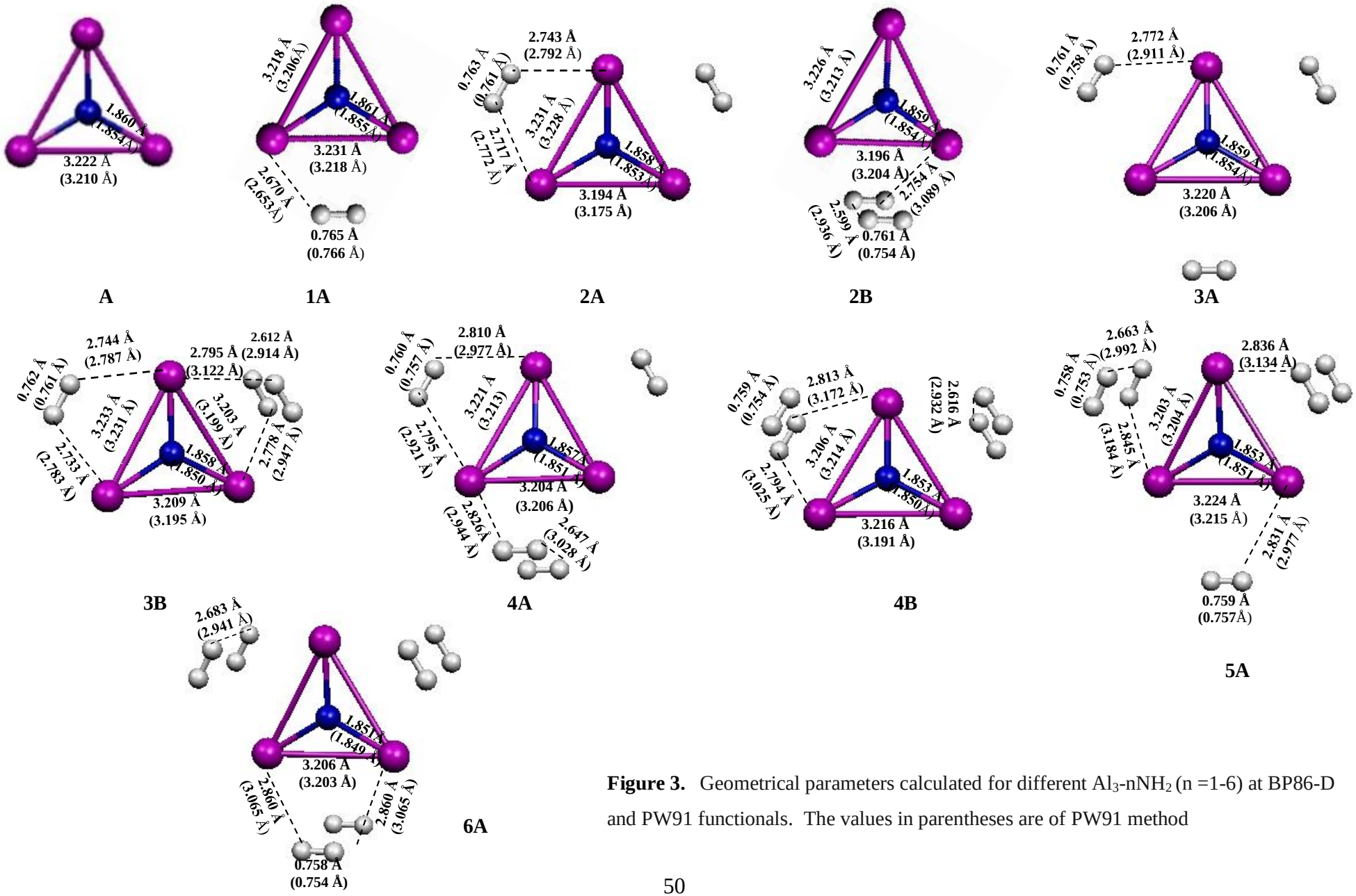

Figure 3. Geometrical parameters calculated for different Al_3-nNH_2 (n =1-6) at BP86-D and PW91 functionals. The values in parentheses are of PW91 method

When more hydrogen molecules are interacted with Al_3N, the strength of Al_3N-nH_2 interaction is somewhat weakened (As shown in Table 2 and Figure 4).

For n = 2, the average bonding energy decreases to -1.89 Kcal/mol /H_2 (BP86-D), and the Al-H distance and H-H bond length are found to be 2.730 and 0.761 Å, respectively.

Table 2. Bonding Energy E_B and E_{H2} (Kcal/mol) of Al_3N-nH_2 (n = 1-6) Clusters

	BP86-D		PW91	
	E_B	E_{H2}	E_B	E_{H2}
Al_3N-H_2 (1A)	-2.20	-2.20	-1.98	-1.98
Al_3N-$2H_2$ (2A)	-4.03	-1.89	-3.44	-1.61
Al_3N-$2H_2$ (2B)	-4.06	-1.53	-2.31	-1.22
Al_3N-$3H_2$ (3A)	-5.34	-1.43	-4.52	-1.32
Al_3N-$3H_2$ (3B)	-5.80	-1.56	-3.97	-1.14
Al_3N-$4H_2$ (4A)	-6.88	-1.30	-5.04	-0.85
Al_3N-$4H_2$ (4B)	-7.44	-1.48	-4.39	-1.14
Al_3N-$5H_2$ (5A)	-8.37	-1.20	-5.60	-1.05
Al_3N-$6H_2$ (6A)	-9.67	-1.09	-6.35	-1.03

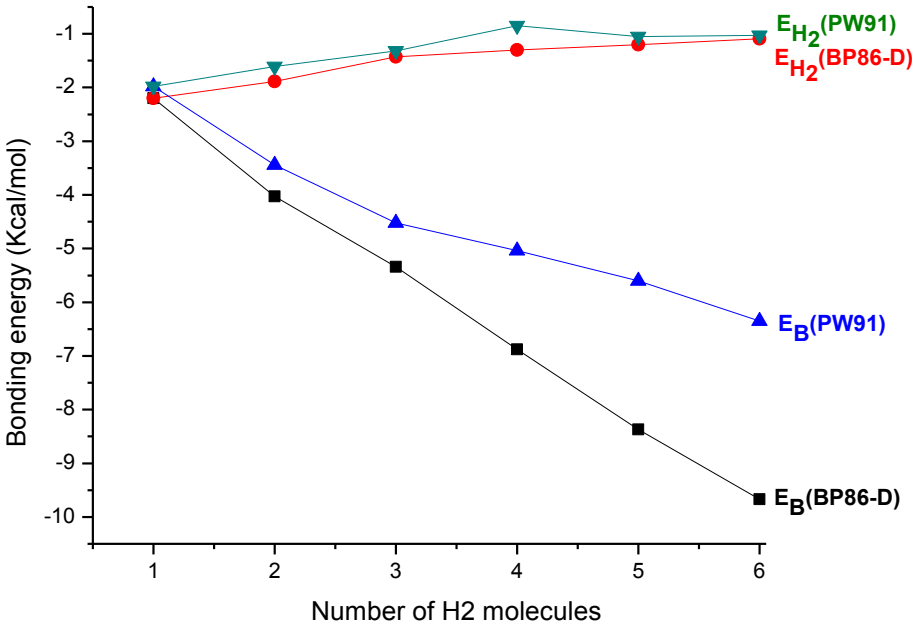

Figure 4. Bonding energy of the Al_3N-nH_2 (n=1-6) system as a function of the number of H_2 molecules bound

When six H_2 molecules are bound to Al_3N, the average bonding energy decreases to -1.09 Kcal/mol (BP86-D) or -1.03 Kcal/mol (PW91). Consequently, the H–H distance is elongated to 0.758 Å and 0.754 Å and Al–H distance enlarged to 2.86 Å and 3.065 Å, with BP86-D and PW91 respectively.

Using the calculations based on the BP86-D and PW91, the relation between H-H bond length and Al-H distance in the Al_3N-nH_2 system and the number of H_2 units bound is shown in Figure 5. It is clear from the two curves (Figures 5a, 5b) that H-H bond length decreases gradually as the number of H_2 increases, while the Al-H distance increases with the increasing of hydrogen number

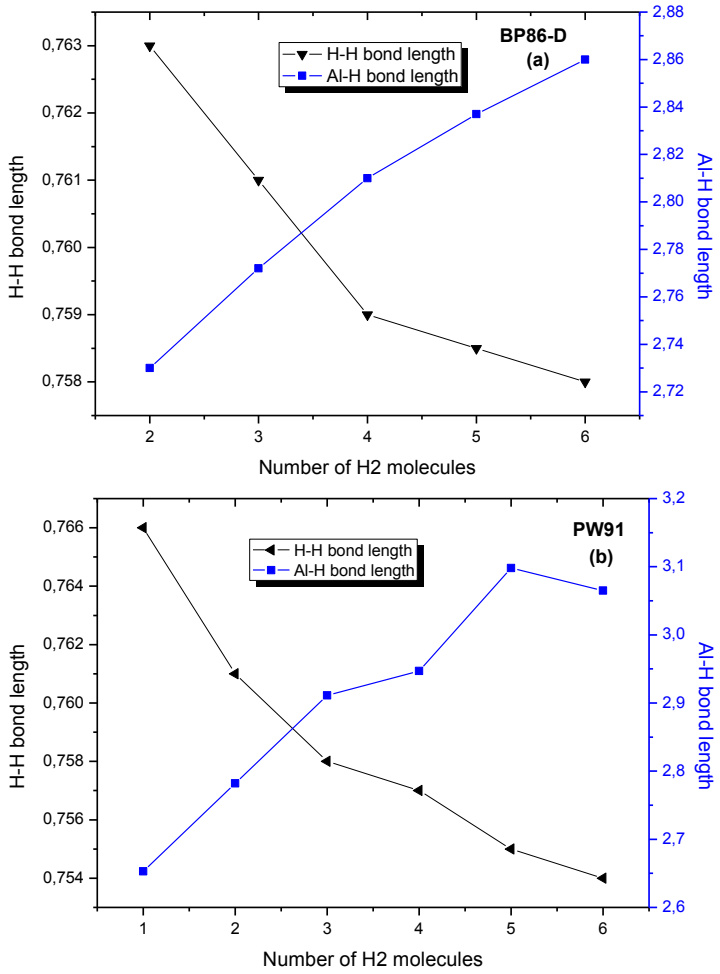

Figure 5. H-H and Al-H distances of the Al_3N-nH_2 system as a function of the number of H_2 molecules bound

In order to gain in-depth information regarding the interaction behavior between Al_3N and H_2, it is imperative to further optimize Al_3N-$7H_2$. Geometry optimization with BP86-D functional shows that the seven H_2 deviates away from the Al_3N cluster, leading to a very low bonding energy of -0.01 kcal /mol and a large Al–H distance of 8.66 Å.
The seven hydrogen molecule in the optimized structure have a bond distance of 0.751 Å, which is the same as that obtained for isolated molecular hydrogen optimized. This reflects the absence of any interaction between the Al_3N and the seven hydrogen molecule. For this reason, we conclude that the Al_3N cluster can take up to six H_2 molecules.

II.3. Molecular Orbital Analysis.

The fragment analysis in ADF [41] present a particular interest, it can determine the percentage contribution of molecular orbitals of Al_3N and H_2 fragments to molecular orbitals of the Al_3N-H_2 system. In order to give a deep insight into the bonding within the Al_3N-nH_2 (n = 1-6) structures, the results of BP86-D functional were used; the bonding is described in terms of interaction diagram in Fig. 5 and Fig.A3. On the left side are the frontier molecular orbitals of Al_3N and on the right are the Molecular orbitals for hydrogen ligands. The highest occupied molecular orbital (HOMO) and the lowest unoccupied molecular orbital (LUMO) energies, energy gaps, representation of the molecular orbitals and the quantitative contributions (in percentages) of H_2 ligands in the molecular orbitals are also shown in Figures 6, 7, 8 .

For all compounds Al_3N-nH_2, their HOMOs are largely localized on Al_3N molecular orbitals with small contributions from H_2 ligands, except the Al_3N-H_2, where its HOMO is localized on Al_3N molecular orbital. While the LUMOs are mainly delocalized over the whole molecules.

Taking Al_3N-H_2 diagram (Fig. 5. 1A) as an example, the HOMO is destabilized from -5.13 eV to -5.09 eV while the LUMO is stabilized to -2.65 eV and then a lower band gap (2.44 eV) is found, compared to Al_3N band gap. The molecular orbital diagram clearly state that the ligand fragment H_2 contributes about 3.80 ٪ towards the HOMO-1.
It can be seen from diagrams Figure 6.2A and (3A, 4A, 5A and 6A) in Figure 7 and Figure 8, that more H_2 ligands introduced on Al_3N, can remarkably stabilize the HOMO energies and destabilize the LUMO energies, and then lead to a bigger HOMO-LUMO gap. The

energy gap values rise from 2.55 eV for Al_3N to 2.44, 2.73, 3.23, 3.04, 3.04 and 3.21 eV for Al_3N-$2H_2$,

Al_3N-$3H_2$, Al_3N-$4H_2$, Al_3N-$5H_2$ and Al_3N-$6H_2$ respectively, which are synonymous of good thermodynamic stability of the studied systems.

As shown in Figures 6-8, interaction diagrams are quite similar to the Dewar-Chatt-Duncanson model [42, 43] and that of kubas [44, 45]. All diagrams show the two interactions, which are a donation from H_2 to Al_3N and a back-donation from Al_3N to H_2. The liante interaction between the vacant anti-bonding orbitals LUMO and LUMO+1 of Al_3N and bonding orbitals HOMOs of nH_2 is stabilized and leads to electron transfer of about 0.07 e, 0.12 e, 0.16 e, 0.18 e, 0.22 e and 0.27 e from H_2, $2H_2$, $3H_2$, $4H_2$, $5H_2$, and $6H_2$ ligands to Al_3N respectively. Therefore, it is a donation.

On the other hand, the bonding interaction between the vacant anti-bonding orbitals LUMO and LUMO+1 of H_2 and bonding orbitals HOMO and HOMO-1 of Al_3N is stabilized and leads to electron transfer of about 0.08 e, 0.14 e, 0.18 e, 0.21 e, 0.23 e and 0.26 e from Al_3N to the H_2, $2H_2$, $3H_2$, $4H_2$, $5H_2$, and $6H_2$ ligands respectively. Therefore, it is a back-donation.

The H_2 play a role of an electron acceptor through its vacant orbital. The back-donation tends to weaken the H-H bond and enhances the attraction Al_3N.... H_2. In Al_3N-H_2 (Figure 9. 1A), the charge transfer is confirmed by a significant elongated of H-H bond length by 0.015 Å from 0.75 Å to 0.765 Å. One can see the elongation of the H-H bond and Al-H distance in the other studied systems (Figure 5). As can be seen, that the back-donation was dominate such that the partial charge on the Aluminium atoms metal increased.

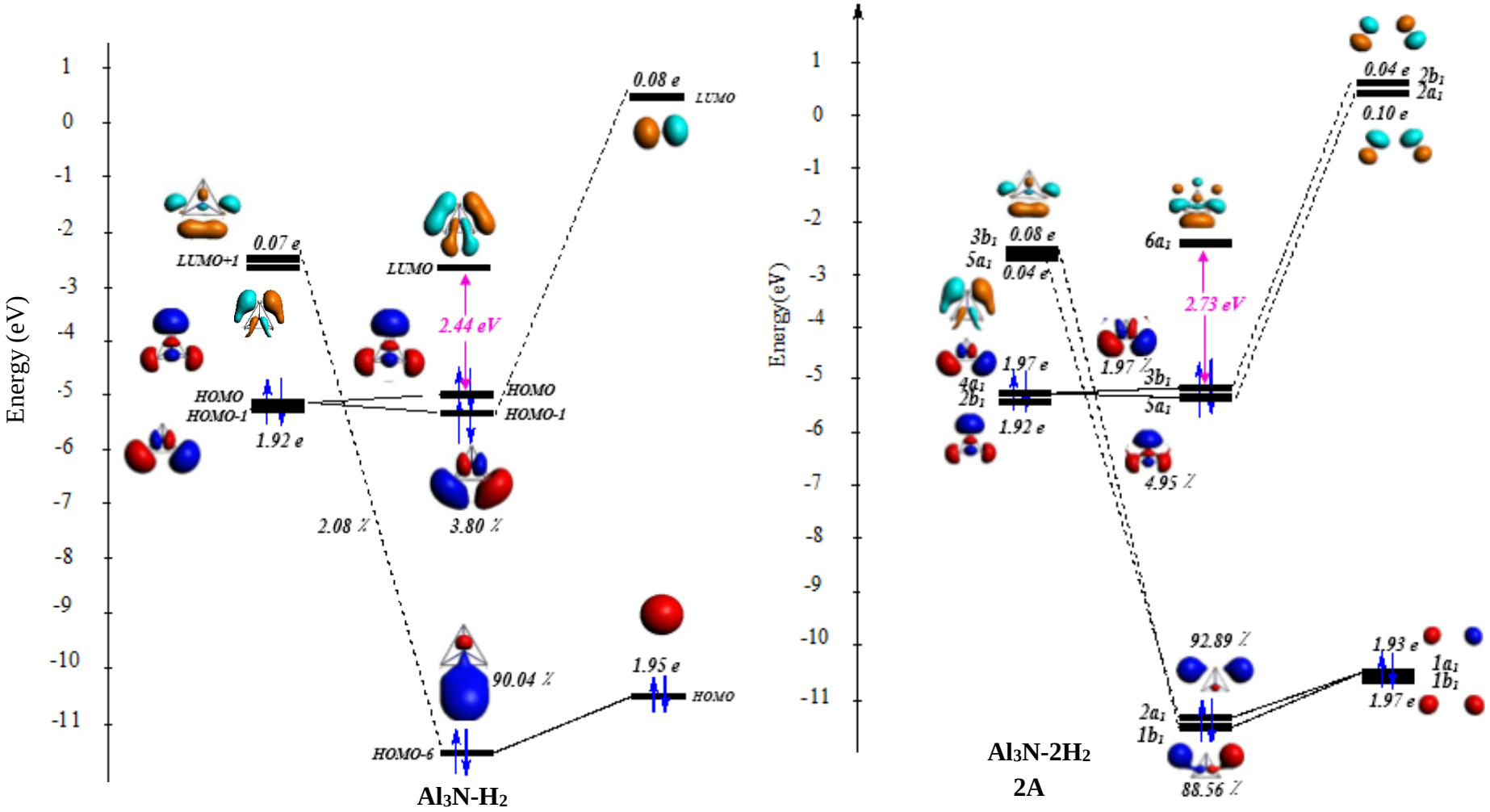

Figure 6. Tracing the interactions of molecular orbitals of Al_3N with those of nH_2 ligands (n = 1, 2). The MO contributions ratio of H_2 ligands and occupations orbitals are given. The isosurfaces are plotted at the 0.03 isovalues

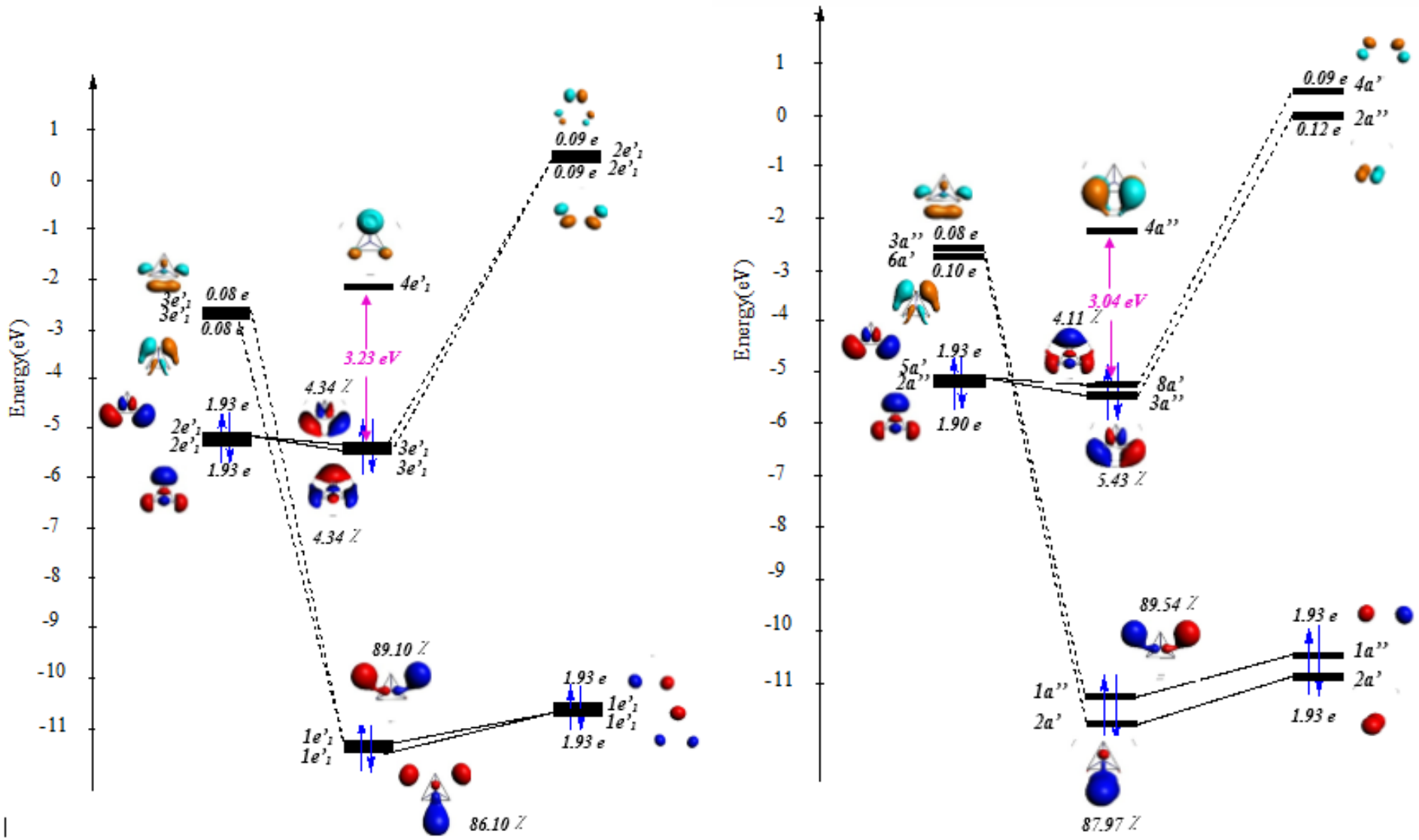

Figure 7. Tracing the interactions of molecular orbitals of Al_3N with those of nH_2 ligands (n = 3-4). The MO contributions ratio of H_2 ligands and occupations orbitals are given. The isosurfaces are plotted at the 0.03 isovalues

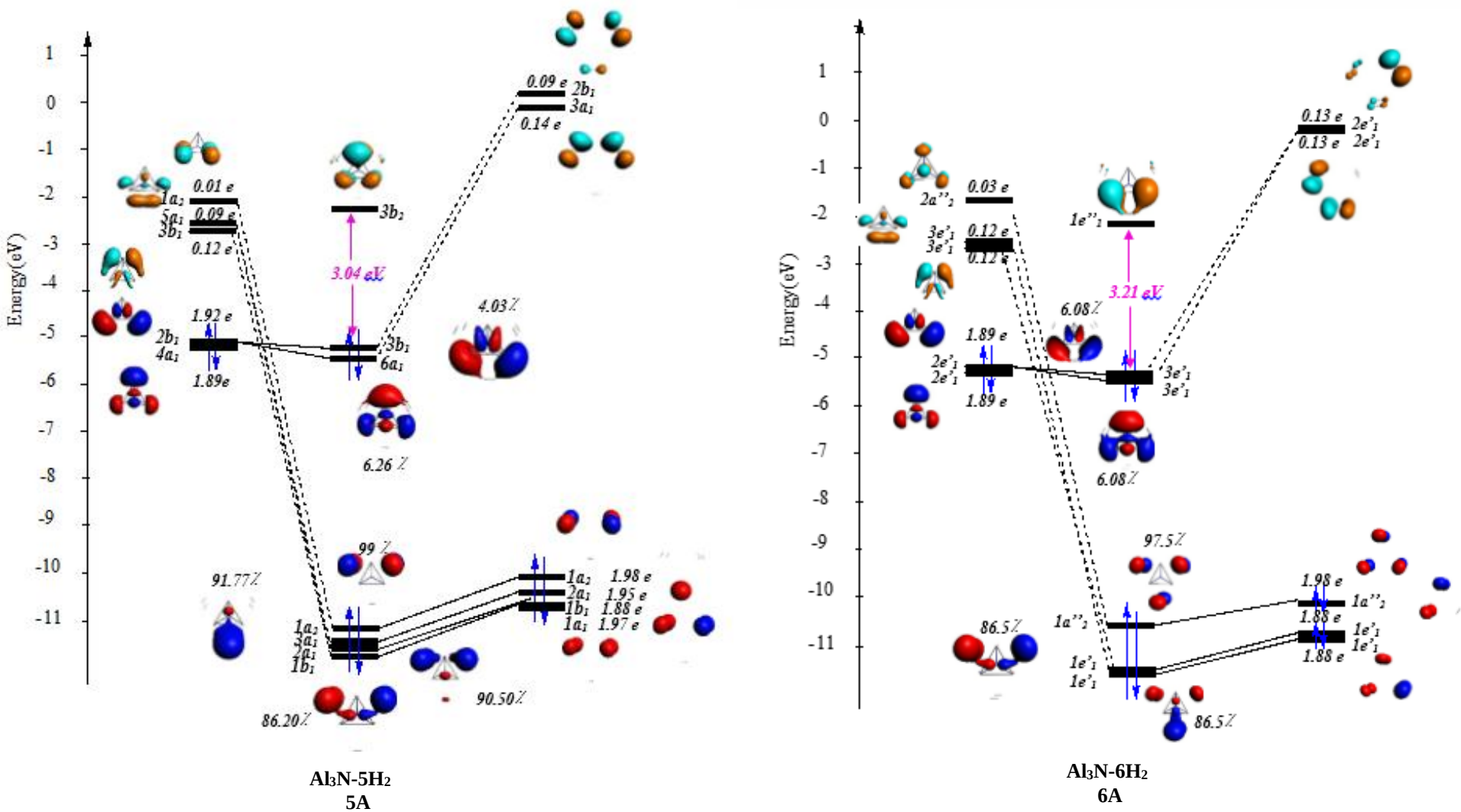

Al_3N-$5H_2$ **Al_3N-$6H_2$**
5A **6A**

Figure 8. Tracing the interactions of molecular orbitals of Al_3N with those of nH_2 ligands (n = 5-6). The MO contributions ratio of H_2 ligands and occupations orbitals are given. The isosurfaces are plotted at the 0.03 isovalues

II.4. Vibrational frequencies

The stability of the Al_3N-nH_2 (n=1-6) clusters were further tested by normal mode analysis. There are no imaginary frequencies to Al_3N-nH_2 clusters for the two functionals BP86-D and PW91, indicating the structures are quantum mechanically stable. Vibrational frequency analysis was also employed to elucidate the influence of the hydrogen molecules on Al_3N. The vibrational frequencies of H-H bonds in Al_3N-nH_2 clusters are listed in Table S1. we note that the H_2 stretching mode in Al_3N-nH_2 clusters is found to increase from Al_3N-H_2 to Al_3N-$6H_2$, in the range of 4016-4153 cm^{-1} and 3995-4283 cm^{-1} for BP86-D and PW91 respectively, which is quite smaller than that of the free H_2 molecule (4160 cm^{-1}) in the gas phase [46]. The H_2 stretching mode for free H_2 molecule, according to our computations, it is found around 4291 cm^{-1} (BP86-D) or 4308 cm^{-1} (PW91), which are higher than the experimental frequency of a free H2 molecule.

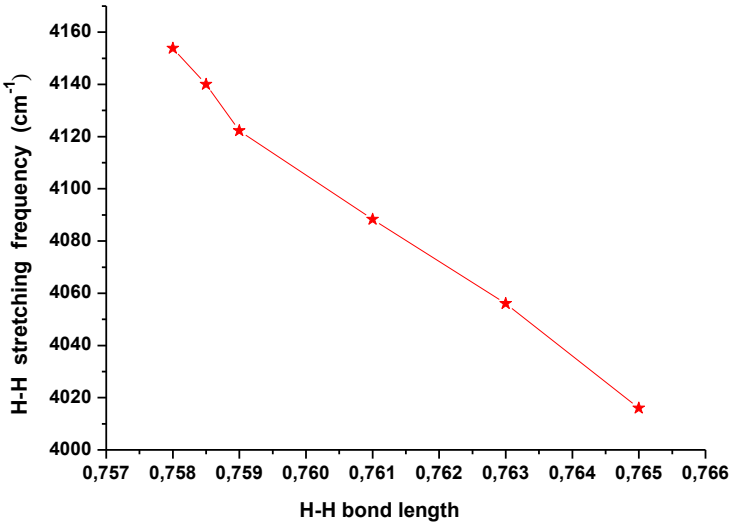

Figure 9. H-H stretching frequency as a function of H-H bond length obtained for Al_3N-nH_2 clusters at BP86-D level

It is noteworthy that when more electrons are transferred from Al_3N orbital to anti-bonding orbitals of H_2 molecules (electron donation), suggesting significant Al_3N….H_2 interaction and hence weakening the H-H bond which leads to the decrease of H–H stretching frequency. In all of the computational models upon binding to the Al_3N cluster, the H–H bond is seen to lengthen, its stretching frequency is shown to reduce (Figure 9). Al_3N-H_2 system have a smaller H–H stretching frequency of 4016 cm^{-1} (BP86-D), or 3995 cm^{-1} (PW91), which confirm the higher interaction between Al_3N cluster and H_2 molecule

among other systems Al_3N-nH_2 (n = 2-6), showing the same behaviour compared to those of the bonding energy.

II.5. Charge Analysis

The influence of the hydrogen molecules on Al_3N, can be further clarified from the natural bond orbital (NBO) charges [47] and Hirschfeld Charge analysis [48]. To examine the electronic structure of Al_3N-nH_2 (n = 1-6), calculated charge distribution in Al_3N-nH_2 clusters based on Hirschfeld population analysis and NBO are indicated in Figure 10.

Hydrogen interaction with Al_3N increase the positive charge on Al atoms. These quantities are raised by successive addition of hydrogen molecules to the system, which can be a reflection of charge transfers, as reported in Figure 10 and discussed in Molecular Orbital Analysis above.

In the case of Al_3N-H_2 cluster, Al atoms have positive charges and its neighbouring H atoms have negative charges, which show that for BP86-D method, the charge transfer with 0.013 e (NBO) or 0.012 e (hirshfeld) has occurred from Al_3N to H atom. As show in Figure 10, from Al_3N-$2H_2$ to Al_3N-$6H_2$ clusters, the charge values of H atoms are all negative.

It is also found that the capability of the receiving electrons decrease slightly for each hydrogen with the increase of the hydrogen molecules number added to Al_3N. For more clarification, the partial charge on the Al, N and H atom of the Al_3N-nH_2 system as a function of the number of H_2 molecules bound are plotted in Figure 11 in both cases hirshfeld and NBO charges with BP86-D results.

Cleary from the curves displayed in Figure 11, the partial charge on the N atom decreases slightly with successive addition of H_2 molecules on Al_3N. It reduced from -0.508 (hirshfeld) with no H_2 molecules bound down to -0.494 (hirshfeld) with six bound H_2 molecules (Figure 11.a). One can see that the all atomic charges for Al_3N-nH_2 atoms show that the charge is transferred to the hydrogen atoms from the nitrogen and the aluminium atoms nearest neighbour to hydrogen. According to the increase of the n number of hydrogen molecules, charge transfer from Al_3N to H_2 makes the Al atoms more positive as shown in Figure 11.b.

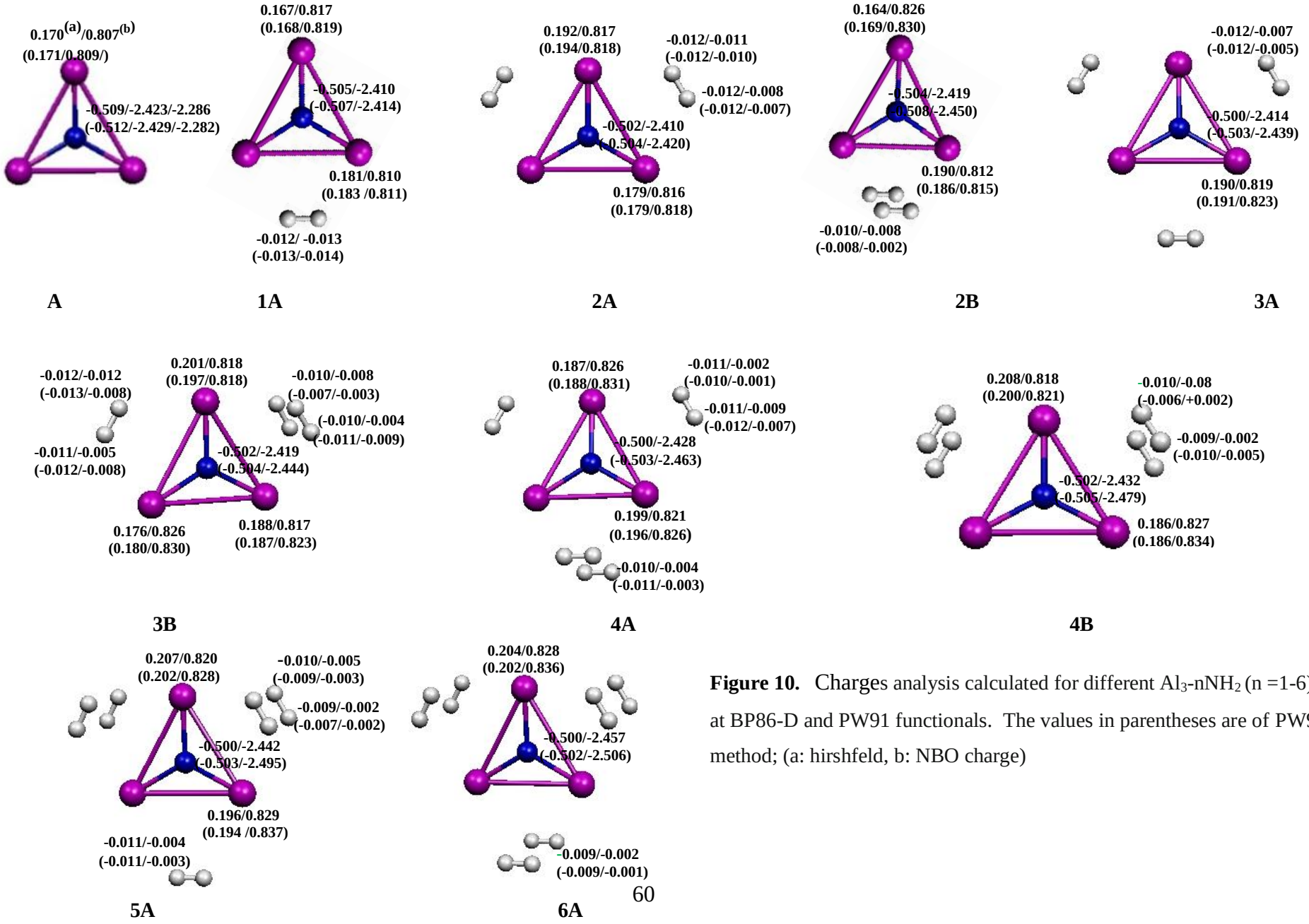

Figure 10. Charges analysis calculated for different Al_3-nNH_2 (n =1-6) at BP86-D and PW91 functionals. The values in parentheses are of PW91 method; (a: hirshfeld, b: NBO charge)

The reduction in partial charge of N and Al atoms suggests that the interaction is overall an electron donation from the Al_3N cluster to the Hydrogen molecules, consistent with the increase in H–H bond length (Figure 11.c) and reduction in stretching frequency (Figure 9 and Table 3A), as electron density is removed from the Al_3N bonding orbital to antibonding orbitals of H_2 molecules

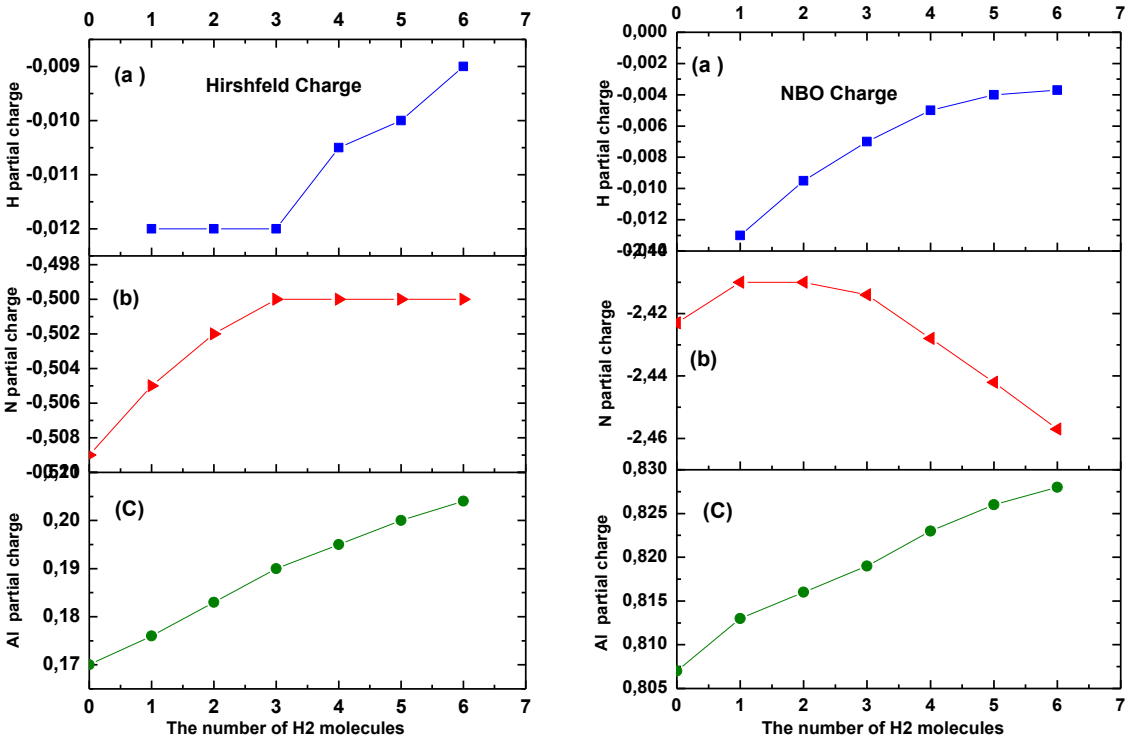

Figure 11. The hirshfeld and NBO charge on the Al, N and H atoms of the Al_3N-nH_2 system as a function of the number of H_2 molecules bound at BP86-D

II.6. Energy decomposition

In order to gain a deeper understanding into the interaction between the Al_3N-(n-1)H_2 and the H_2 fragments by means of the ADF program, the total interaction energy ΔE_{int} for Al_3N-nH_2 compounds was partitioned through the energy decomposition analyses (EDA) in the framework of Morokuma–Ziegler scheme [49,50]. The total energy ΔE_{int} is composed of three major components as follows: $\Delta E_{int} = \Delta E_{pauli} + \Delta E_{elstat} + \Delta E_{orb}$, where the ΔE_{elstat} term is the electrostatic interaction energy between the fragments. The ΔE_{orb} accounts for the covalent character of the fragment-fragment interaction, and the term ΔE_{Pauli} refers to the repulsive interactions between the fragments due to the fact that two electrons with same spin cannot occupy the same region in space. It has been suggested that the relative values of the two attractive terms ΔE_{elstat} and ΔE_{orb} are used to characterize the nature of the chemical bonding [51, 52]. The energy decomposition data using BP86-D and PW91 exchange-correlation functional with a TZP basis set are summarized in Table 3.

The values of ΔE_{elstat} and ΔE_{orb}, calculated with the BP86-D method which lies between (-3.76, -2.64 Kcal/mole) and (-6.14, -3.57 kcal/mol) respectively, show that there is a significant orbital overlapping between Al_3N-(n-1)H_2 and H_2 fragments, whereas the corresponding PW91 values indicating that there is a weak interaction between Al_3N-(n-1)H_2 and H_2 fragments.

The Table 3 shows that the covalent contributions rather than electrostatic ones dominate the interactions. For the Al_3N-H_2 compound, 62 % of the attractive interaction energy are due to covalent contributions, 38 % are from electrostatic ones.

It is interesting to observe that the smaller distance between Al_3N-(n-1)H_2 and H_2 fragments results in a sizable increase in the ΔE_{pauli} and ΔE_{orb}. For BP86-D results, the smaller Al-H distance is 2.67 Å in Al_3N-H_2 correspond to higher repulsion energy ΔE_{pauli} = 9.52 kcal/mol and Orbital energy ΔE_{orb} -6.14 kcal/mol.

The BP86-D results shows for a distance of Al-H = 2.65 Å, that the interactions are dominated by the electrostatic contributions rather than covalent ones.

Table 3. Energy decomposition in (kcal/mol) obtained between Al_3N-(n-1)H_2 and H_2 fragments

	BP86-D			PW91		
Compound	ΔE_{Pauli}	ΔE_{elstat}	ΔE_{orb}	ΔE_{Pauli}	ΔE_{elstat}	ΔE_{orb}
Al_3N-H_2 (1A)	9.52	-3.76 (37.98)[a]	-6.14 (62.02)[b]	9.24	-4.27 (38.06)[a]	-6.95 (61.94)[b]
Al_3NH_2-H_2 (2A)	8.55	-3.40 (39.26)	-5.26 (60.74)	6.12	-3.10 (40.10)	-4.63 (59.90)
Al_3NH_2-H_2(2B)	7.05	-2.69 (41.38)	-3.81 (58.62)	2.34	-1.54 (43.26)	-2.02 (56.74)
Al_3NH_4-H_2(3A)	8.25	-3.24 (40.75)	-4.71 (59.25)	3.14	-1.83 (42.66)	-2.46 (57.34)
Al_3NH_4-H_2(3B)	8.49	-3.34 (41.49)	-5.14 (58.51)	4.47	-2.46 (42.49)	-3.33 (57.51)
Al_3NH_6-H_2(4A)	7.74	-2.93 (41.27)	-4.17 (58.73)	2.38	-1.52 (43.18)	-2.00 (56.82)
Al_3NH_6-H_2(4B)	7.78	-3.04 (41.19)	-4.34 (58.81)	4.00	-2.27 (42.83)	-3.03 (57.17)
Al_3NH_8-H_2(5A)	7.37	-2.87 (41.78)	-4.00 (58.22)	3.63	-2.13 (43.03)	-2.82 (56.97)
Al_3NH_{10}-H_2(6A)	7.10	-2.64 (42.51)	-3.57 (57.49)	2.80	-1.69 (44.13)	-2.14 (55.87)

a Electrostatic energy ΔE_{elstat} contribution to the total attractive energy ($\Delta E_{elstat} + \Delta E_{orb)}$

b Orbital energy ΔE_{orb} contribution to the total attractive energy ($\Delta E_{elstat} + \Delta E_{orb}$)

III. Conclusion

In this work, we have performed density functional calculations at the BP86-D and PW91 functionals for the interaction of molecular hydrogen on Al_3N cluster. A detailed study has been provided of structural parameters and electronic properties of Al_3N-nH_2.

Firstly we investigated on the all possible positions of H_2 molecules on Al_3N cluster. Moreover we also discuss the dissociative and non-dissociative interaction on Al_3N. The results show that the hydrogen molecules can bond strongly to the Al_3N and form a covalent bond Al-H with average bonding energy of -158.28 kcal/mol and of -160.40 kcal/mol for BP86-D and PW91 respectively. Hydrogen can also bind to the Al_3N cluster and remain in their molecular form, and the average bonding energies of H_2 lying in the range of -2.20 kcal/mol /H_2, for which it was shown that decrease with the increasing of number of hydrogen molecules.

The capacity of Al_3N to store hydrogen molecule is also studied, we have shown that Al_3N can bind up to six H_2 molecules amounting to a gravimetric density of 11.8 wt %. Employing fragment analysis, it was shown that the electron donation and back-donation is the mechanism of bonding that occurs between Al_3N and H_2 molecules. The electron donation interaction tends to weaken the H-H bond and enhances the attraction Al_3N- H_2. The energy decomposition analysis show that the interaction between Al_3N-$(n-1)H_2$ and hydrogen molecule has a predominant covalent character than electrostatic one.

Bibliography

[1] Crabtree, G.W., Dresselhaus, M. S. and Buchanan M.V. *"The hydrogen economy."* Physics today 57.12 (**2004**) 39-44.

[2] Wang, G., Yuan, H., Kuang, A., Hu, W., Zhang, G., & Chen, H. *"High-capacity hydrogen storage in Li-decorated (AlN) n (n= 12, 24, 36) nanocages."* International journal of hydrogen energy 39.8 (**2014**) 3780-3789.

[3] Wang, Q., Sun, Q., Jena, P., & Kawazoe, Y. "*Potential of AlN nanostructures as hydrogen storage materials*." ACS nano 3.3 (**2009**) 621-626.

[4] Lochan, R. C. and Head-Gordon, M. *"Computational studies of molecular hydrogen binding affinities: the role of dispersion forces, electrostatics, and orbital interactions."* Physical Chemistry Chemical Physics 8.12 (**2006**): 1357-1370.

[5] Dillon, A., Jones, K. M., Bekkedahl, T. A., Kiang, C. H., Bethune, D. S. and Heben, M. J.*"Storage of hydrogen in single-walled carbon nanotubes."* Nature 386.6623 (**1997**) 377-379.

[6] Chambers, A., Park, C., Baker, R. T. K., & Rodriguez, N. M. "*Hydrogen storage in graphite nanofibers*." The journal of physical chemistry B 102.22 (**1998**) 4253-4256.

[7] Liu, C., Fan, Y. Y., Liu, M., Cong, H. T., Cheng, H. M., & Dresselhaus, M. S."*Hydrogen storage in single-walled carbon nanotubes at room temperature."* Science 286.5442 (**1999**) 1127-1129.

[8] Ye, Y., Ahn, C. C., Witham, C., Fultz, B., Liu, J., Rinzler, A. G., ... & Smalley, R. E. *"Hydrogen adsorption and cohesive energy of single-walled carbon nanotubes."* Applied physics letters 74.16 (**1999**) 2307-2309.

[9] Yang, R. T. "*Hydrogen storage by alkali-doped carbon nanotubes–revisited."* Carbon 38.4 (**2000**) 623-626.

[10] Hirscher, M., Becher, M., Haluska, M., Dettlaff-Weglikowska, U., Quintel, et al. *"Hydrogen storage in sonicated carbon materials".* Applied Physics A, 72.2 (**2001**) 129-132.

[11] Ma, R., Bando, Y., Zhu, H., Sato, T., Xu, C., & Wu, D. *"Hydrogen uptake in boron nitride nanotubes at room temperature."* Journal of the American Chemical Society 124.26 (2002): 7672-7673.

[12] Ruffieux, P., Gröning, O., Bielmann, M., Mauron, P., Schlapbach, L., & Gröning, P. *"Hydrogen adsorption on sp 2-bonded carbon: Influence of the local curvature"* Physical Review B, 66.24 (**2002**) 245416_1-245416_8

[13] Meregalli, V., & Parrinello, M. *"Review of theoretical calculations of hydrogen storage in carbon-based materials"*. Applied Physics A, 72.2 (**2001**) 143-146.

[14] McAfee, J. L., & Poirier, B. *"Quantum dynamics of hydrogen interacting with single-walled carbon nanotubes."* J. Chem. Phys. 130.6 (**2009**) 064701_1-064701_16

[15] Qiu, N. X., Tian, Z. Y., Guo, Y., Zhang, C. H., Luo, Y. P., & Xue, Y "*A first-principle study of calcium-decorated BC2N sheet doped by boron or carbon for high hydrogen storage"*. International journal of hydrogen energy, 39.17 (**2014**) 9307-9320.

[16] Han, S. S., Lee, S. H., Kang, J. K., & Lee, H. M. High coverage of hydrogen on a (10, 0) single-walled boron nitride nanotube. Physical Review B, 72.11 (**2005**) 113402_1-113402_4

[17] Shevlin, S. A., & Guo, Z. X. *"Transition-metal-doping-enhanced hydrogen storage in boron nitride systems."* Applied physics letters, 89.15 (**2006**) 153104.

[18] Cheng, J., Ding, R., Liu, Y., Ding, Z., & Zhang, L. "*Computer simulation of hydrogen physisorption in single-walled boron nitride nanotube arrays"* Computational materials science, 40.3 (**2007**). 341-344.

[19] Lim, S. H., & Lin, J. "*Ab initio study of the hydrogen chemisorption of single-walled aluminum nitride nanotubes*." Chemical Physics Letters, 466.4-6 (**2008**) 197-204.

[20] Beheshtian, J., Soleymanabadi, H., Kamfiroozi, M., & Ahmadi, A. (2012). *The H_2 dissociation on the BN, AlN, BP and AlP nanotubes: a comparative study"*. Journal of molecular modeling, 18.6 (**2012**) 2343-2348.

[21] Li, Y., Zhou, Z., Shen, P., Zhang, S. B., & Chen, Z. "*Computational studies on hydrogen storage in aluminum nitride nanowires/tubes*." Nanotechnology, 20.21 (**2009**) 215701_1-215701_8

[22] Moradi, M., & Naderi, N. "*First principle study of hydrogen storage on the graphene-like aluminum nitride nanosheet"* Structural Chemistry, 25. 4 (2014) 1289-1296.

[23] Zhang, Y., Zheng, X., Zhang, S., Huang, S., Wang, P., & Tian, H. *"Bare and Ni decorated $Al_{12}N_{12}$ cage for hydrogen storage: a first-principles study."* International journal of hydrogen energy, 37. 17 (**2012**) 12411-12419.

[24] Rad, A. S., & Ayub, K. "*Coordination of nickel atoms with Al12X12 (X= N, P) nanocages enhances H_2 adsorption: a surface study by DFT*." Vacuum, 133 (**2016**) 70-80.

[25] Sayhan, S., & Kinal, A. *"Computational investigation and comparison of hydrogen storage properties of $B_{24}N_{24}$ and $Al_{24}N_{24}$ nanocages*". International Journal of Hydrogen Energy, 42(20 (**2017**) 14166-14180.

[26] Zhang, C. W., & Yan, S. S. "*First-principles study of ferromagnetism in two-dimensional silicene with hydrogenation."* The Journal of Physical Chemistry C, 116. 6 (**2012**) 4163-4166.

[27] L. Guo, H.S.Wu, Z.H. Jin, Appl Surf Sci. 24 (**2005**) 288.

[28] Zhang, C. W., & Zheng, F. B. "*First-principles prediction on electronic and magnetic properties of hydrogenated AlN nanosheets*" Journal of computational chemistry, 32.14 (**2011**) 3122-3128.

[29] Kawamura, H., Kumar, V., Sun, Q., & Kawazoe, Y. Magic behavior and bonding nature in hydrogenated aluminum clusters. Physical Review B, 65.4 (**2001**) 045406_1-045406_11

[30] Andrews, L., Zhou, M., Chertihin, G. V., Bare, W. D., & Hannachi, Y. "*Reactions of laser-ablated aluminum atoms with nitrogen atoms and molecules. Infrared spectra and density functional calculations for the AlN_2, Al_2N, Al_2N_2, AlN_3, and Al_3N molecule*s." The Journal of Physical Chemistry A, 104.8 (**2000**) 1656-1661.

[31] Curotto, V. F., & Diez, R. P. "*Density functional study on the geometric features and growing pattern of Al_nN_m clusters ($n= 1–4$, $m= 1–4$, $n+ m \leqslant 5$)."* Computational Materials Science, 50.12 (***2011***) 3390-3396.

[32] Nayak, S. K., Khanna, S. N., & Jena, P. *"Evolution of bonding in Al n N clusters: A transition from nonmetallic to metallic character."* Physical Review B, 57.7 (**1998**) 3787-3790

[33] Boo, B. H., & Liu, Z. "*Ab initio investigation of structures and energies of low-lying electronic states of AlN_3, Al_3N, and Al_2N_2*." The Journal of Physical Chemistry A, 103.9 (**1999**) 1250-1254.

[34] BelBruno, J. J. "*The structure of AlnNn (n= 2–4) clusters: a DFT study*." Chemical physics letters, 313.5-6 (**1999**) 795-804.

[35] Curotto, V. F., & Diez, R. P. "*Density functional study on the geometric features and growing pattern of Al_nN_m clusters (n= 1–4, m= 1–4, n+ m⩽5).*" Computational Materials Science, 50.12 **(2011**) 3390-3396.

[36] Jiang, Z. Y., Ma, W. J., Wu, H. S., & Jin, Z. H. "*The structure, electronic state and stability of nitrogen-doped aluminum clusters*." Journal of Molecular Structure: THEOCHEM, 678. 1-3 (**2004**) 123-127.

[37] Leskiw, B. D., Castleman Jr, A. W., Ashman, C., & Khanna, S. N. *"Reactivity and electronic structure of aluminum clusters: the aluminum–nitrogen system*." The Journal of Chemical Physics, 114.3 (**2001**). 1165-1169.

[38] Wang, B., Zhao, J., Shi, D., Chen, X., & Wang, G. "*Density-functional study of structural and electronic properties of Al_nN (n= 2–12) clusters."* Phys. Rev. A, 72. 2 (**2005**) 023204_1-023204_5

[39] Averkiev, B. B., Boldyrev, A. I., Li, X., & Wang, L. S. *"Planar nitrogen-doped aluminum clusters Al x N−(x= 3–5)."* The Journal of chemical physics, 125.12 (**2006**) 124305.

[40] Lide, D.R. CRC Handbook of Chemistry and Physics, 88th ed., CRC Press, Boca Raton, FL, **2007–2008**.

[41] Graetz, J., Chaudhuri, S., Lee, Y., Vogt, T., Muckerman, J. T., & Reilly, J. J. *"Pressure-induced structural and electronic changes in α− AlH_3."* Phys. Rev. B, 74.21 **(2006**) 214114.

[42] Dewar, J. S. *"A review of the pi-complex theory."* Bull Soc. Chim. Fr.18.3-4 (**1951**) C71-C79.

[43] J. Chatt, L.A. Duncanson, J. Chem. Soc. (**1953**) 2929

[44] Kubas, G. J., Ryan, R. R., Swanson, B. I., Vergamini, P. J., & Wasserman, H. J. "*Characterization of the first examples of isolable molecular hydrogen complexes, $M(CO)_3(PR_3)_2(H_2)$(M = molybdenum or tungsten; R = Cy or isopropyl). Evidence for a side-on bonded dihydrogen ligand*." Journal of the American Chemical Society, 106. 2 (**1984**) 451-452.

[45] Kubas, G. J. *"Metal Dihydrogen and s-Bond Complexes: Structure, Theory, and Reactivity".* Springer Science & Business Media, **2001.**

[46] Stoicheff, B. P."High resolution Raman spectroscopy of gases: IX. Spectra of H_2, HD, and D_2." Canadian Journal of Physics, 35.6 **(1957**) 730-741.

[47] Weinhold, F., & Landis, C. R. "*Valency and bonding: a natural bond orbital donor-acceptor perspective"*. Cambridge University Press **2005.**

[48] Hirshfeld, F. L. *"Bonded-atom fragments for describing molecular charge densities"* Theoretica chimica acta, 44.2 (**1977**) 129-138.

[49] Kitaura, K., & Morokuma, K. *"A new energy decomposition scheme for molecular interactions within the Hartree-Fock approximation."* International Journal of Quantum Chemistry, 10.2 (**1976**) 325-340.

[50] Ziegler, T., & Rauk, A. "*On the calculation of bonding energies by the Hartree Fock Slater method"*. Theoretica chimica acta, 46.1 (**1977**) 1-10.

[51] K.B. Lipkowitz, D.B. Boyd (Eds.), Wiley-VCH, New York, 15 (**2000**) 1.

[52] Ehlers, A. W., Dapprich, S., Vyboishchikov, S. F., & Frenking, G. *"Structure and Bonding of the Transition-Metal Carbonyl Complexes M (CO) 5L (M= Cr, Mo, W) and M (CO)3L (M= Ni, Pd, Pt; L= CO, SiO, CS, N2, NO+, CN-, NC-, HCCH, CCH2, CH2, CF2, H2)".* Organometallics, 15.1 (**1996**) 105-117.

CHAPTER IV

Bonding and electronic structures in Nickel alkyne complexes

I. Introduction

The discovery of the first synthetic organometallic compound, Zeise's salt in 1827 [1], and the determination of their structure with the advent of X-ray crystallography [2] (Scheme 1), has played a major role in the studies of metal−olefin bonding interaction [3,4]. In addition, the synthesis of cyclooctatetraene discovered in 1940 by Reppe [5], who proposed that the formation of the cyclooctatetraene take place within nickel-acetylene complexes (Scheme 2), has contributed in the development of effective methods for the production of functionalized ring systems which has been always a crucial subject in synthetic chemistry [6-9].

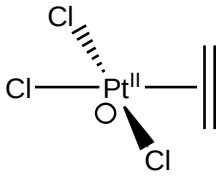

Scheme 1. Zeise's salt [2]

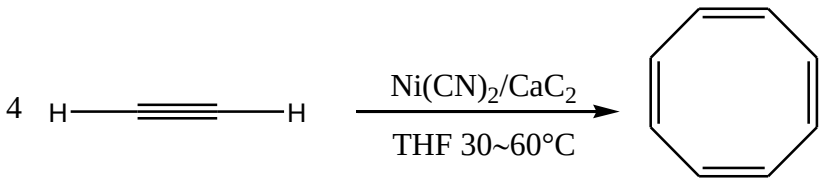

Scheme 2. Reppe's cyclooctatraene synthesis [5]

Transition metal alkyne complexes are essential intermediates in a diversity of homogeneous catalytic processes, such as the oxidation, the hydrogenation, the cyclotrimerisation, and the oligomerization or the polymerization of alkynes [6, 7-10]. For these reasons, extensive efforts in both experimental and theoretical aspects have been devoted to the development of the transition metal alkyne complexes since more than 60 years ago [11-20].

The scheme 3 represent a general mechanistic pathway proposed for cyclotrimerisation of alkynes [6]. These reactions occur more easily in the case of complexes in which the metals have d^8-d^{10} electron configurations such as Fe, Co, Ni, Ru, Pd, and Ir

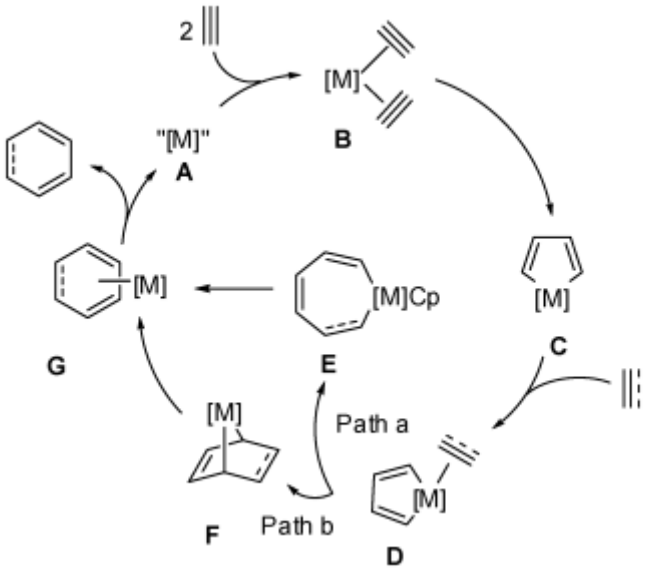

Scheme 3. A general mechanistic pathway proposed for cyclotrimerisation of alkynes into Benzene [6]

The nickel-alkyne complexes have been studied, since Chatt and his collaborators [11] synthesized various platinum- alkyne compounds. One of the most interesting aspects of these compounds is the capacity of NiL_2 (L = PPh_3, CO) to stabilize the alkynes during the formation of the complex. $Ni(CO)_2C_2H_2$, $Ni(PH_3)_2C_2H_2$ and $Ni(CNH)_2C_2H_2$ are the simplest complexes that have been modeled by theoretical calculations [17,19,21].

In this work, we undertook a detailed theoretical study on a series of compounds of general formula $NiL_2(RC{\equiv}CR)$ / (L = CO or t-BuNC) and (R = H, CH_3, Phenyl, CF_3, Cl, F or CN) where $Ni(CO)_2(CF_3C{\equiv}CCF_3)$ [16] , Ni(tBuNC)2($CF_3C{\equiv}CCF_3$) [16] and Ni(tBuNC)2(C2(Ph)2) [13, 14] are characterized experimentally. The aim of this study is to examine the electronic structure of these complexes as well as the strength of the bond between NiL_2 and RC≡CR the symmetrical substituted alkynes. Note that the $Ni(CO)_2C_2H_2$ complex has been the subject of a detailed preliminary theoretical study [19].

Before presenting the results obtained for the NiL_2 (RC≡CR) / (L = CO or t-BuNC) and (R = H, CH_3, Phenyl, CF3, Cl, F or CN) complexes, it is useful to study the electronic structure of the ligands CO, t-BuNC and RC≡CR to understand their coordination mode and to identify its donor and acceptor MOs.

I.1. Acetylene ligand

It is well known that the acetylene C_2H_2, was discovered in 1836 by the English chemist Edmund Davy [22,23], and prepared in 1860 by M. Berthelot [24], who gives it its name. It is characterized by the presence of a C≡C triple bond in its molecule.

Besides the important role it plays as fuel in the oxyacetylene torch, Acetylene - in the presence of metal catalysts - can react as a raw material to give a wide range of chemicals of industrial importance. Alkyne substituents are among the more widely studied ligands in organometallic complexes [12,13]

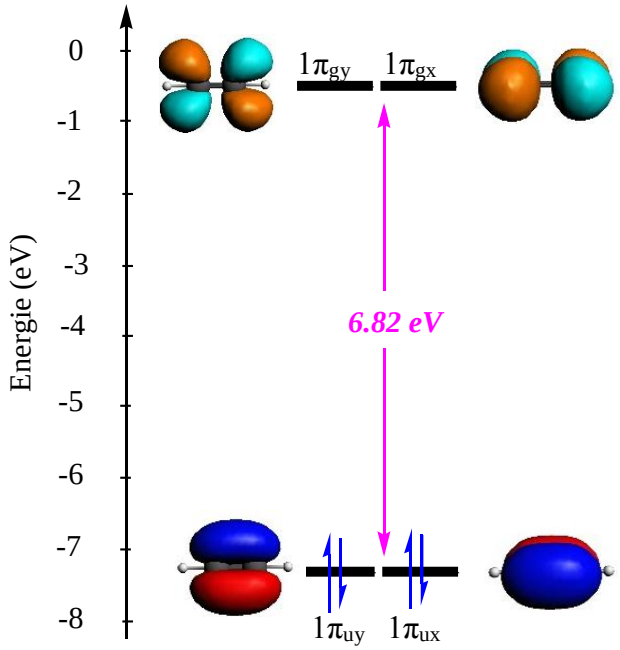

Figure 1. Frontier Molecular orbital energy diagram for acetylene

We have determined the electronic structure of the acetylene to understand its mode of coordination and to identify the donor and acceptor MOs. Figure 1 represents the diagram of the orthogonal FMO π and π* of acetylene, obtained by the DFT calculation, where a large energy gap (6.82 eV) separates the molecular orbitals occupied from the unoccupied ones.

I.2. Metal - alkyne bonding

By using the DCD model [3,4], the bonding interaction between alkyne and transition metals consists of σ-donation from π orbital occupied of alkyne to an empty orbital on the metal and π back-donation from occupied d-orbitals of the metal to a vacant π * orbital

of alkyne. Due to the presence of a double π-system in alkyne ligands, two donor and two acceptor interactions are possible (Figure 2). The alkyne act as a 2 or 4 electrons donor ligand by means of its two π orbitals, or acceptor of the electrons of the metal (π back-donation) . On the other hand, the perpendicular acceptor orbital (π⊥*) can only form a δ-type bond with the metal d orbitals, and therefore it does not significantly contribute to the bonding

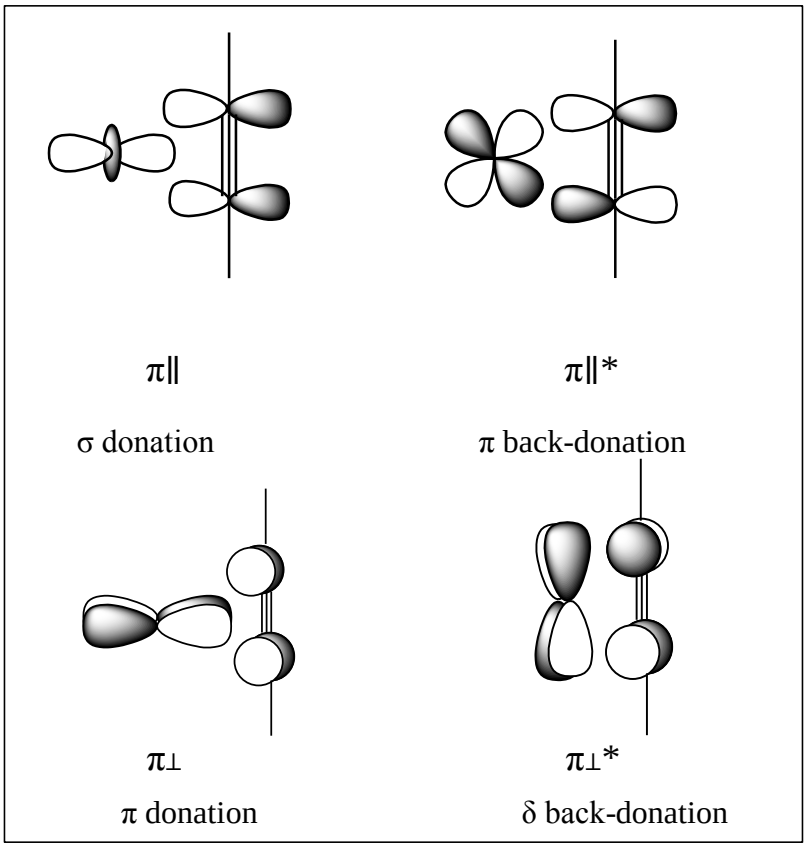

Figure 2: schematic representations of donor-acceptor interactions of alkyne complexes

When the alkyne is sufficiently good π acceptor, π metal-alkyne complex can be considered as a metallacyclopropene.

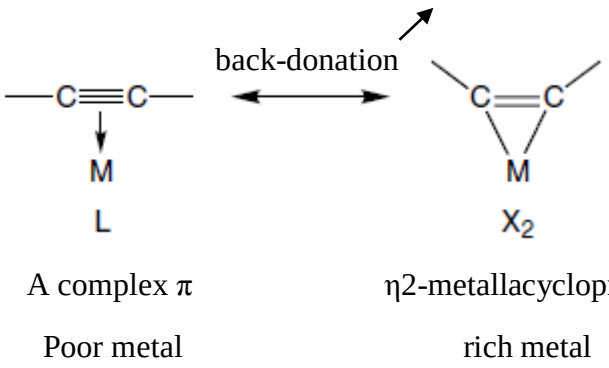

Figure 3. Mesomeric forms limits for the coordination of alkyne [25]

I.3. Tert-butyl isocyanide ligand

Tert-butyl isocyanide is an organic compound of formula $(CH_3)_3CNC$. Like most alkyl isocyanides, is a toxic and reactive colorless liquid with an extremely disagreeable odor. [26]

Figure 4 represents frontier molecular orbital energy diagram for t-butyl isocyanide, obtained by the DFT calculation, where a large energy gap (6.69 eV) separates $10a_1$ the non bonding molecular orbital from the π* anti-bonding molecular orbitals ($7e_1$). This neutral ligand has a σ-donor character by donation due to the non-bonding orbital $10a_1$ located on the C atom of CN. On the other hand, it is a π-acceptor ligand and its interaction with metal depends largely on π back-donation M → $CNC(CH_3)_3$,

I.4. Carbon monoxide ligand

Since the discovery of the first metal carbonyl $Ni(CO)_4$ in 1890 [27], the carbon monoxide has become one of the most studied ligands in organometallic chemistry. It is a versatile ligand toward transition metals. It has several bonding modes, and its small size means that a relatively large number can surround a metal cluster [28].

A comparison between the two ligands (t-BuNC) and (CO), shows that the t-BuNC has a higher- energy π * acceptor orbitals (-0.29 eV) and higher-energy σ-donor orbitals (-6.98 eV), revealing its strong donor effect and weak acceptor effect; as result the Tert-butyl isocyanide ca stabilize higher oxidation states [28]

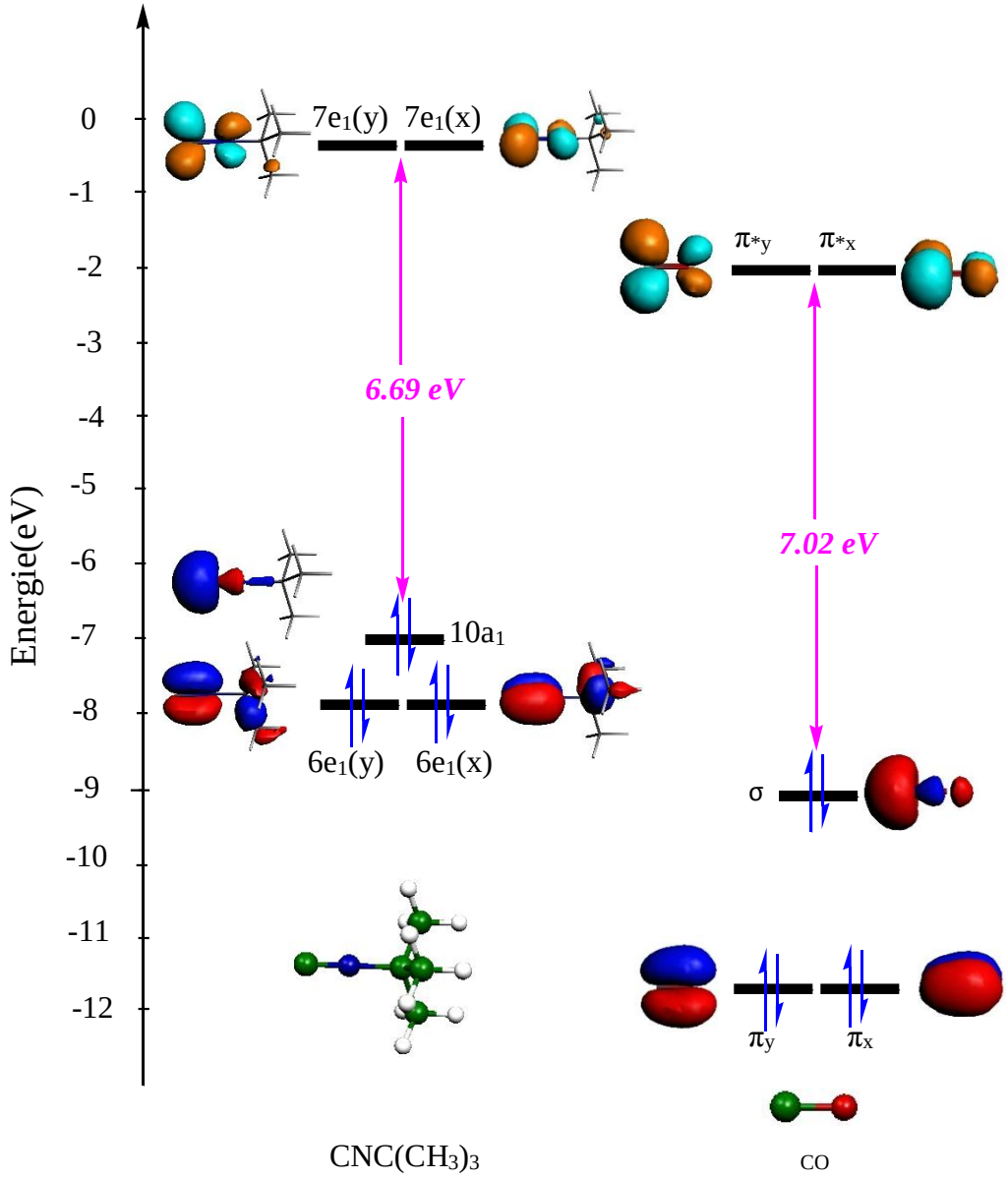

.

Figure 4. Frontier molecular orbital energy diagram for t-butyl isocyanide and carbon monoxide

II. Results and Discussion

II.1. Structural study

The full geometry optimizations of the complexes $NiL_2(C_2R_2)$ / (L = t-BuNC, CO), (R = H, CH_3, F, Cl, CN, CF_3, Ph) without symmetry constraints, leads to trigonal planar complexes in their singlet and triplet spin states. The optimized geometries have been verified as minima by vibration frequencies calculation. It should be noted that the triplet

structures were found very high in energy (lying at 50 kcal/mol above the singlet structures) compared to the singlet structures; therefore, they are not discussed in the context of this study.

The experimental molecular structures of investigated complexes are not known and only that of **3a, 3b** and **5b** has been determined [13,14,16]. The neutral complex $[Ni(tBuNC)_2\{C_2(Ph)_2\}]$ (**3a**) has been isolated and characterized by X-ray diffraction [14]. It containing a single atom of Ni in a square planar environment, crystallizing in the monoclinic space group C2h5 -P2 / a. Its elementary cell contains eight molecules. In the optimized geometry (3a), the calculated bond lengths Ni-C_{ac} and C≡C of 1.914 Å, and 1.293 Å respectively, are in good agreement with the experimental values 1.902 and 1.924 Å (Ni-C_{ac}) and 1.291 Å (C≡C) present in the X-ray structure.

The results summarized in figures 5 and 6 reveal structural modifications that occur during the change of hydrogen at acetylene by the different symmetrical substituents (CH_3, F, Cl, CN, CF_3 and Ph). The influence appears clearly in the values of the Ni-C_{ac}, and C≡C bonds and of the R-C≡C bond angle. The distances of the C≡C bonds calculated in the complexes $NiL_2(C_2R_2)$ / (R = H, CH_3) are shorter than in the other investigated compounds. Note that these C≡C distances between 1,266 Å and 1,302 Å are significantly longer than those calculated for free acetylene (1,201 Å with the same method).

Moreover, the calculated Ni-C_{ac} bonds decreased from 1,912 and 1,933 Å for 2a and 2b to (1,897 and 1,918 Å), (1,894 and 1,914 Å), (1,887 and 1,901 Å) and (1,874 and 1, 881 Å) for (4a and 4b), (5a and 5b), (6a and 6b) and (7a and 7b) and increased to (1.914 and 1.937 Å) and (1.925 and 1.952 Å) for (3a and 3b) and (1a and 1b) respectively.

The interaction between the ligand RC≡CR and the metal fragment Ni(t-BuNC)$_2$ is also reflected by the angle R-C≡C in different geometries, which strongly deviates from the linear arrangement of free alkyne on going from 150.7 ° (R = CH_3), 148.8 ° (R = H) to 144.7° (R = F) and 143.9 ° (R = Cl). Similar trends were observed for the $Ni(CO)_2(C_2R_2)$ complexes. For example the angles decrease from 153.3 ° in the $Ni(CO)_2(C_2(CH_3)_2)$ complex to 147.2 ° in the $Ni(CO)_2(C_2(Cl_2)$ complex. As, the complexes Ni(t-BuNC)$_2$(C_2F_2) and $Ni(CO)_2(C_2F_2)$ have the shortest Ni-C_1 bond lengths, and the smallest angles R-C≡C, we can say that the difluoroacetylene ligand (C_2F_2) is more strongly bound to nickel than acetylene and the other symmetrical substituted alkynes C_2R_2.

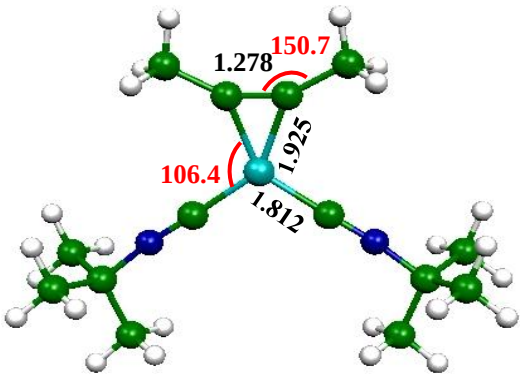

R= CH_3
1a

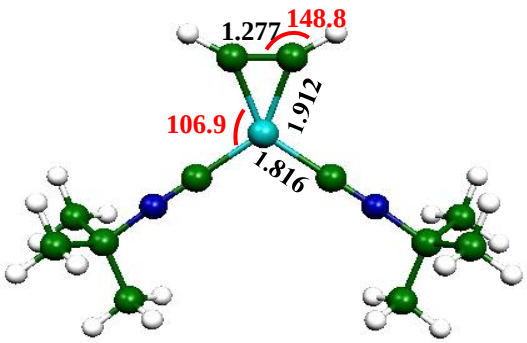

R = H
2a

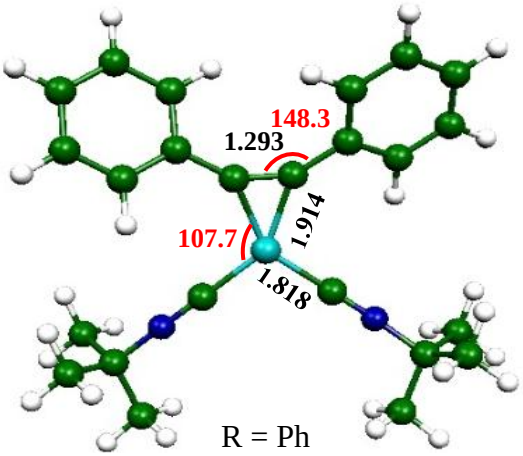

R = Ph
3a

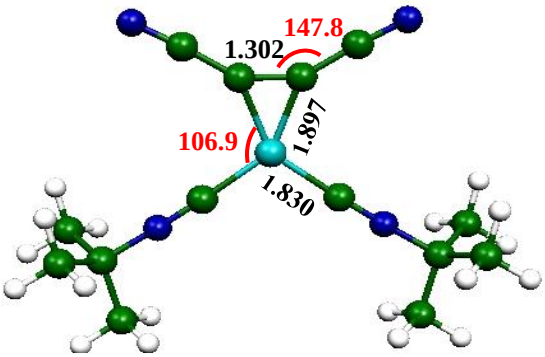

R = CN
4a

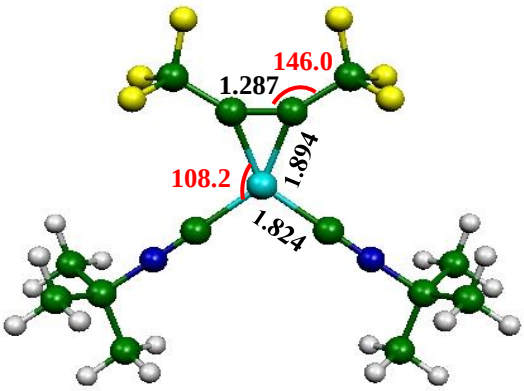

R = CF_3
5a

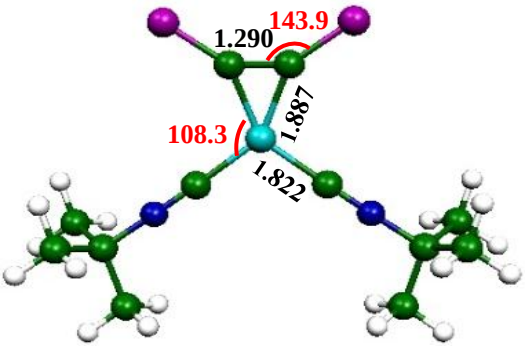

R = Cl
6a

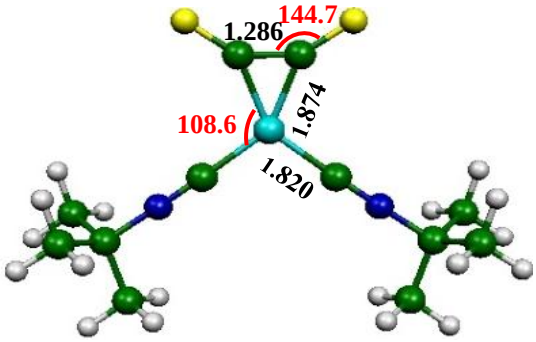

R = F
7a

Figure 5. Optimized structures obtained for Ni(t-BuNC)$_2$(C_2R_2) complexes

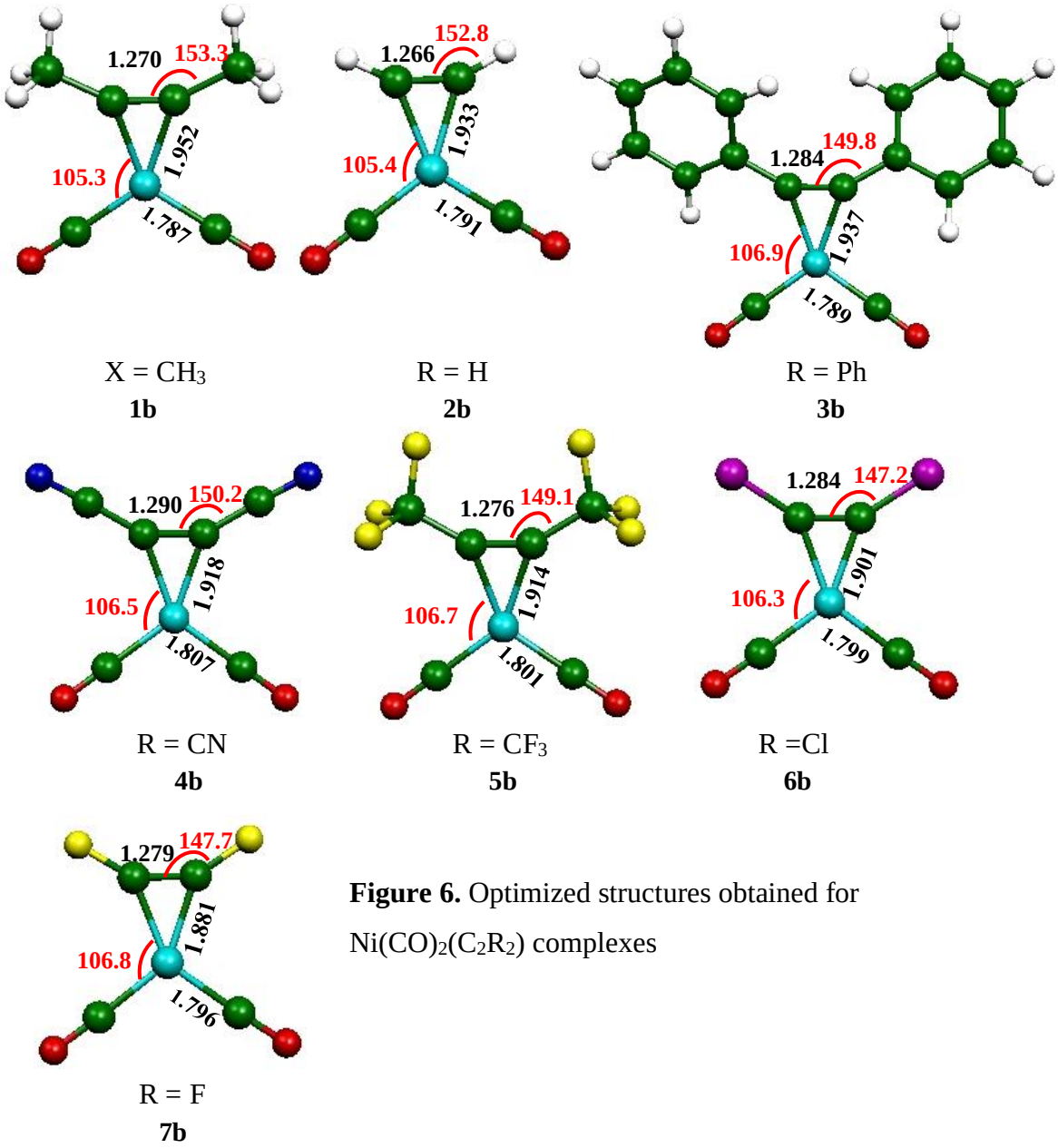

X = CH_3 **1b**

R = H **2b**

R = Ph **3b**

R = CN **4b**

R = CF_3 **5b**

R =Cl **6b**

R = F **7b**

Figure 6. Optimized structures obtained for $Ni(CO)_2(C_2R_2)$ complexes

II.2. Molecular Orbital Analysis

MO diagrams obtained for the complexes $NiL_2(RC{\equiv}CR)$ / R = F, Cl, CF_3, CN, Ph, H and CH_3 are shown in Figures 7 and 8. The contribution (d / L_2 / C_2R_2) represent, respectively, percentage weights of the d orbitals and the ligands $(t\text{-ButNC})_2$ or $(CO)_2$ and C_2R_2 .

A large HOMO-LUMO energy gap implies good thermodynamic stability for all the studied complexes. The HOMOs of $NiL_2C_2F_2$, $NiL_2C_2Cl_2$, $NiL_2C_2Ph_2$ and $NiL_2C_2(CH_3)_2$, and the HOMO-1 of $NiL_2C_2(CF_3)_2$, $NiL_2C_2(CN)_2$ and $NiL_2C_2H_2$ which located on nickel

atom and the ligand C_2R_2, are combinations of the d_{xz} orbital of Nickel and the out-of-plane MO $\pi\perp$ of alkyne, and clearly show the Ni-C_2R_2 anti-bonding character. This means that the bonding contribution of HOMO-5 is essentially compensated by the anti-bonding nature of HOMO (or HOMO-1) as shown above, which leaves alkyne act as 2 electron donor ligand via HOMO-4 in all of the cases studied and leading to an 16 electron complex (MVE = 16)

The HOMO-4, HOMO-5 and HOMO-6 show the occupied MOs of $NiL_2(C_2R_2)$ complexes that contribute to Ni-C_2R_2 interactions. As shown in figure 9, the shapes of these MOs illustrate well the model of synergistic donor-acceptor interactions. The HOMO-5 indicates the σ donation of $C_2R_2 \rightarrow$ Ni from MO $\pi\|$ in the plane of the alkyne ligand. The HOMO-4 displays the Ni $\rightarrow C_2R_2$ back-donation to the MO $\pi\|$ * in the plane of the alkyne ligand. In addition, the HOMO-6 shows that there is significant contribution of the out-of-plane OM $\pi\perp$ of the alkyne ligand in the $C_2R_2 \rightarrow$ Ni donation.

All LUMOs of the complexes studied are mainly located on the t-butyl isocyanide ligand or the carbon monoxide. This result was expected due to the strong acceptor character of these ligands, except for $NiL_2(C_2(CN_2))$ (see 4a Fig. 7 and 4b Fig. 8), which located on $C_2(CN)_2$ ligand.

The destabilization of the MOs for each type of complexes studied depends on the C_2R_2 ligand, the more it is donor, the more the MOs will be destabilized and vice versa. Indeed, the MOs of the CN complexes (4a and 4b) are the most stabilized because the ligand $C_2(CN)_2$, the weakest electron donor, stabilizes the Ni d orbitals. Whereas CH_3 is the most donor, its MOs are the most destabilized.

If we compare the energy level of MO diagrams (see Fig 7, 8), we find that HOMOs and LUMOs of $Ni(t\text{-}BuNC)_2(C_2R_2)$ are less stabilized than those of $Ni(CO)_2(C_2R_2)$. The results summarized in the Table 1, clearly point that the auxiliary ligand t-BuNC is a weak electron acceptor as compared to carbonyl ligand. Consequently, the CO ligand stabilize the Nickel orbitals and largely responsible for low energy of MOs of $Ni(CO)_2(C_2R_2)$.

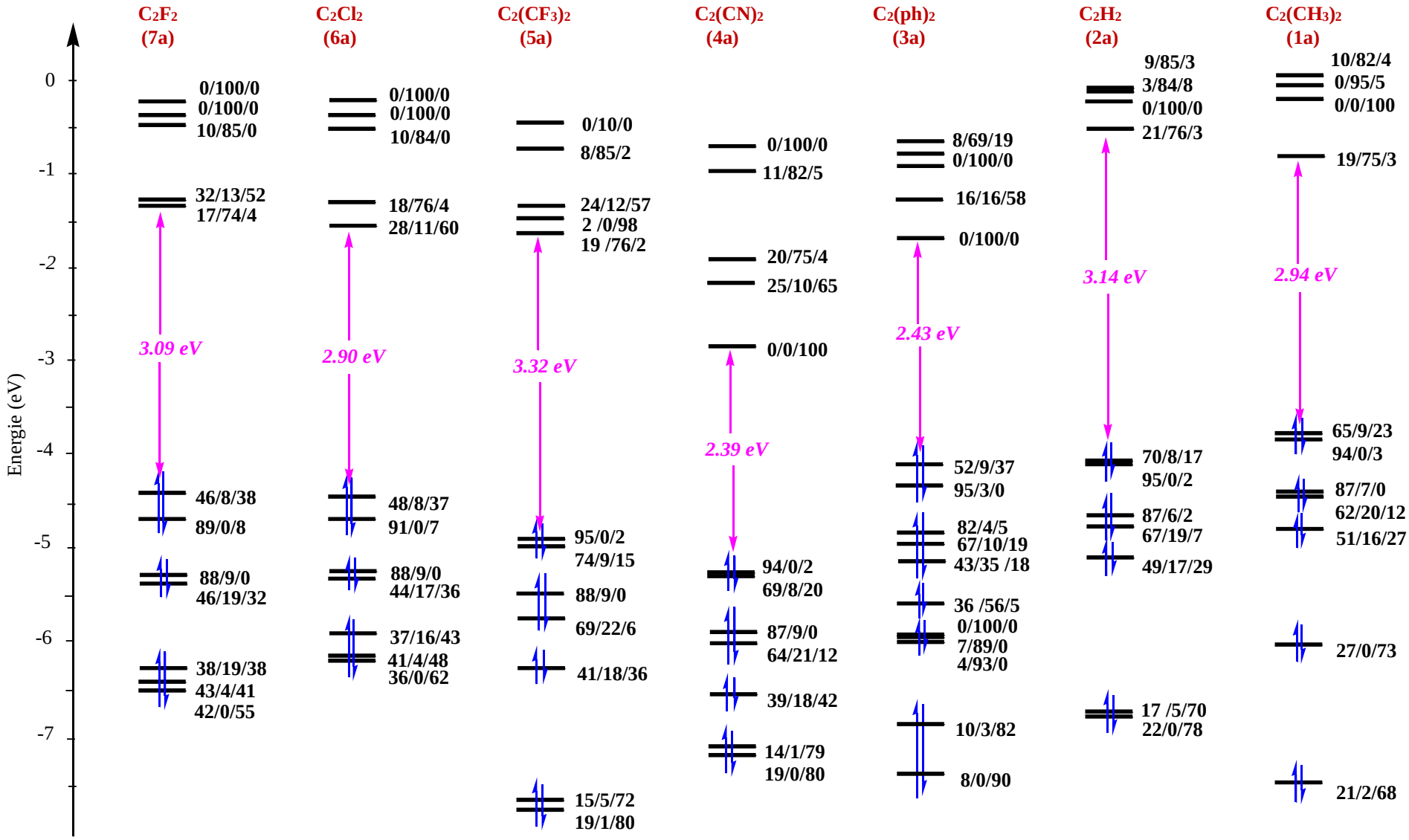

Figure 7. MO diagrams of Ni(t-BuNC)$_2$(C_2R_2) complexes / (R = F, Cl, CF_3, CN, Ph, H, CH_3) . The nickel and ligands contributions are given as Ni /(t-BuNC)$_2$ /C_2R_2 %

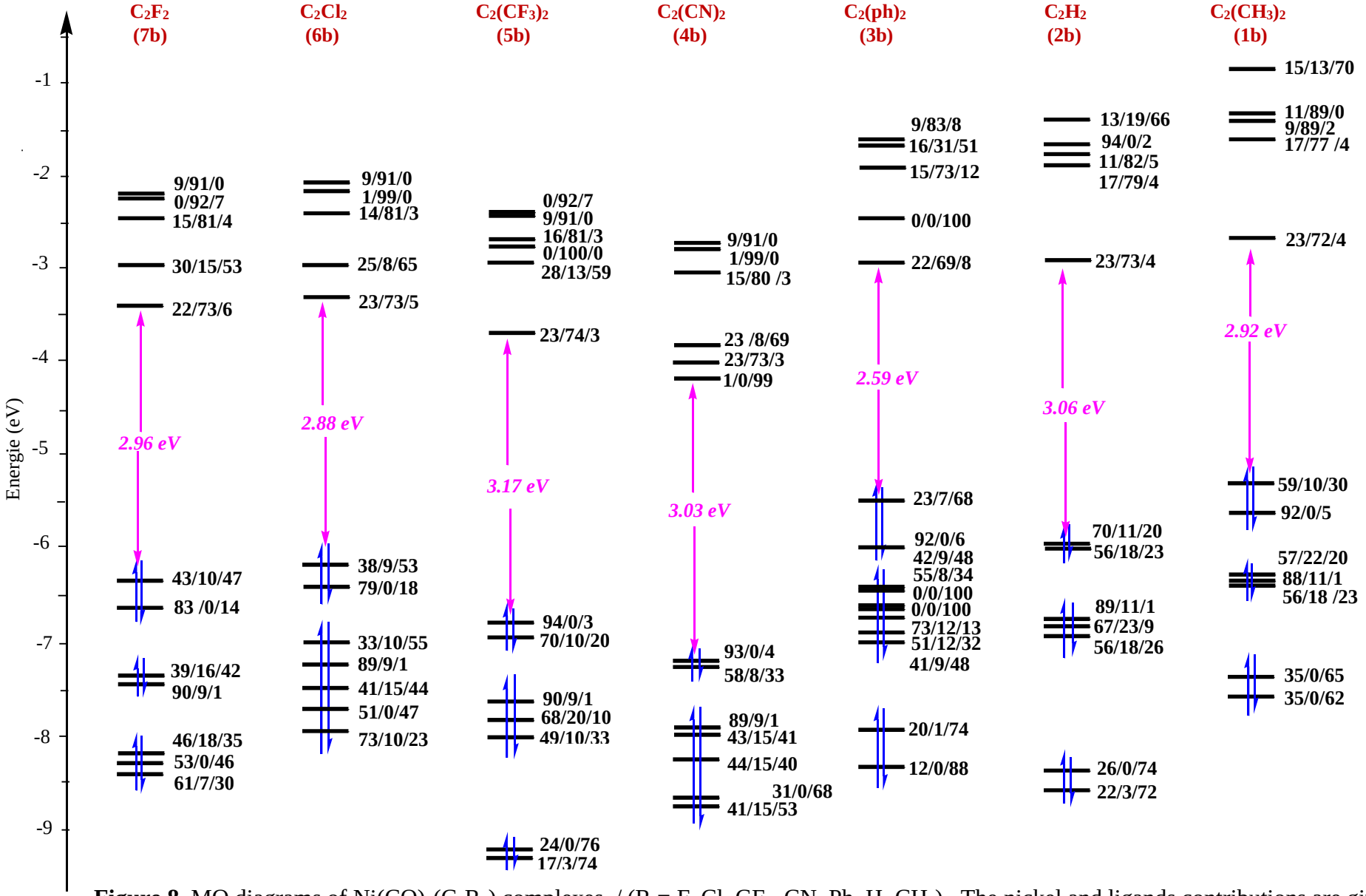

Figure 8. MO diagrams of $Ni(CO)_2(C_2R_2)$ complexes / (R = F, Cl, CF_3, CN, Ph, H, CH_3) . The nickel and ligands contributions are given as Ni /$(CO)_2$ /C_2R_2 %

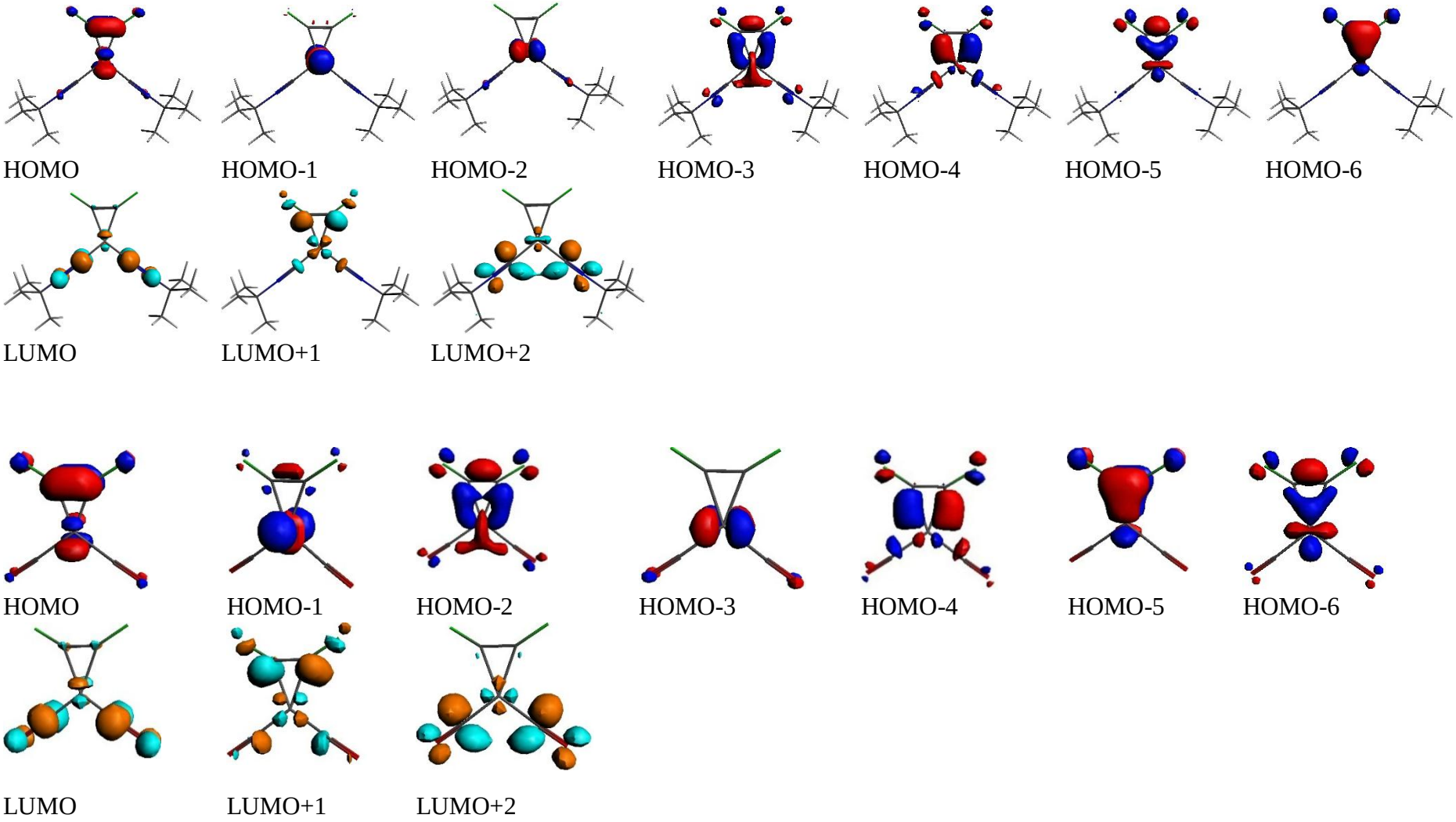

Figure 9. Selected molecular orbital of the $NiL_2(C_2F_2)$ complexes (isovalue = 0.067) showing the nature of the bonding in the structure of $Ni(t\text{-}BuNC)_2(C_2F_2)$ (7a) and $Ni(CO)_2(C_2F_2)$ (7b)

II.3. Bonding Analysis

In this part, we are interested in a comparative study of the order of stability of $NiL_2(C_2R_2)$/ L = t-BuNC or CO complexes, to get a deeper understanding based on the different interactions that took place between the $Ni(t\text{- }BuNC)_2$ or $Ni(CO)_2$ and different symmetrical substituted alkynes. .

The natural populations of the frontier molecular orbitals C_2R_2 $\pi\perp$ indicate that occupations in the interval from [1.83 - 1.94] have negligible participations in the Ni-C_{ac} bond, as displayed in Table 1. While the natural populations of the C_2R_2 $\pi\parallel$ frontier molecular orbitals in the $Ni(t\text{-}ButNC)_2(C_2R_2)$ and $Ni(CO)_2C_2R_2$ / (R = F, Cl, CF_3, H, CH_3) complexes, respectively indicate occupations of (1.66 - 1.69), (1.79-1.76), (1.76-1.71), (1.72-1.67) and (1.74-1.70), have significant participations and contribute to the bond HOMO- 5 for $Ni(t\text{-}BuNC)_2(C_2F_2)$ and HOMO-6 for $Ni(CO)_2(C_2F_2)$ (see Figure 9)

The Ni-C_{ac} bond is also associated with the back-donation from the occupied orbitals of the metal fragment NiL_2 to the lowest vacant orbitals of the C_2R_2 fragment. As expected, this MO is responsible for Ni- C_{ac} bonding.

The lowest vacant alkyne orbital C_2F_2 ($\pi \parallel$ *) receives 0.79 and 0.66 electrons, respectively, from the metal fragments [Ni $(t\text{-}ButNC)_2$] and $[Ni(CO)_2]$, also justified by the net charges of C_2F_2 and nickel as collected in Table 2.

The Ni-C_{ac} distances calculated for the $Ni(CO)_2(C_2R_2)$ complexes, accompanied by a shortening of the C≡C bonds are longer than those in their $Ni(t\text{-}BuNC)_2(C_2R_2)$ counterparts. (See the figures 1 and 2). This is explained by the fact that carbonyl is a strong acceptor π and weak donor σ compared to teriobutyl isocyanide as shown in table 1. It participates in reducing the value of the electrons which contribute to the bak-donation towards alkyne while teriobutyl isocyanide the weak acceptor π and strong donor σ contributes to increasing the value of the back-donation. .

The ligand $C_2(CH_3)_2$ in the 1a and 1b complexes has the lowest charge compared to the other ligands, which is respectively -0.130 and -0.232, which confirms that the back-donation of the metallic orbitals towards the C≡C bond is quite weak. It should be noted that the positive charges on nickel in carbonyl complexes are higher than those obtained for tertiobutyl isocyanide complexes. This charge deficit confirm that tBuNC is a good donor for stabilizing nickel in the presence of a strong acceptor $C_2(CF_3)_2$, $C_2(Cl)_2$ and $C_2(CN)_2$

Table 1: Relevant computed data for the $NiL_2(C_2R_2)$ complexes / R = F, Cl, CF_3, CN, Ph, H, CH_3 and L = t-BuNC, CO

Substituant R	$Ni(t\text{-}BuNC)_2(C_2R_2)$							$Ni(CO)_2(C_2R_2)$						
	C_2R_2 Frontier orbital occupations [a]				$(t\text{-}BuNC)_2$[b]		Electronic confguration of Ni	C_2R_2 Frontier orbital occupations [a]				$(CO)_2$[b]		Electronic confguration of Ni
	π⊥	π∥	π*∥	π*⊥	d	b		π⊥	π∥	π*∥	π*⊥	d	b	
CH_3	1.90	1.74	0.56	0.01	0.74	0.65	$4s^{0.47}\ 3d^{8.73}\ 4p^{0.68}$	1.88	1.70	0.43	0.00	0.71	0.79	$4s^{0.44}\ 3d^{8.73}\ 4p^{0.75}$
H	1.89	1.72	0.60	0.03	0.75	0.55	$4s^{0.46}\ 3d^{8.72}\ 4p^{0.71}$	1.88	1.67	0.48	0.02	0.74	0.74	$4s^{0.43}\ 3d^{8.72}\ 4p^{0.76}$
Ph	1.93	1.80	0.57	0.02	0.74	0.58	$4s^{0.48}\ 3d^{8.72}\ 4p^{0.71}$	1.90	1.77	0.43	0.01	0.72	0.77	$4s^{0.45}\ 3d^{8.73}\ 4p^{076}$
CN	1.94	1.85	0.73	0.04	0.82	0.42	$4s^{0.43}\ 3d^{8.73}\ 4p^{0.66}$	1.83	1.93	0.57	0.02	0.74	0.61	$4s^{0.43}\ 3d^{8.74}\ 4p^{0.67}$
CF_3	1.92	1.76	0.75	0.03	0.81	0.46	$4s^{0.46}\ 3d^{8.73}\ 4p^{0.68}$	1.90	1.71	0.60	0.02	0.74	0.64	$4s^{0.42}\ 3d^{8.73}4p^{0.73}$
Cl	1.90	1.79	0.76	0.03	0.81	0.49	$4s^{0.47}\ 3d^{8.69}\ 4p^{0.73}$	1.83	1.66	0.66	0.02	0.74	0.68	$4s^{0.42}\ 3d^{8.68}\ 4p^{0.73}$
F	1.85	1.69	0.79	0.00	0.82	0.52	$4s^{0.50}\ 3d^{8.68}\ 4p^{0.78}$	1.83	1.66	0.66	0.02	0.76	0.69	$4s^{0.46}\ 3d^{8.67}\ 4p^{0.82}$

[a] Calculated Frontier orbital occupations of the C_2R_2 ligand after interaction with NiL_2 fragment.

[b] The σ-donation (d), π-back-donation (b), are obtained from interaction between NiC_2R_2 and L_2 ligand.

Table 2. Hirschfeld charges and Ni-C_{ac} Mayer bond order for $NiL_2(C_2R_2)$ complexes / R = F, Cl, CF_3, CN, Ph, H, CH_3 and L = t-BuNC, CO

Substituant R	$Ni(t\text{-}BuNC)_2(C_2R_2)$			$Ni(CO)_2(C_2R_2)$		
	Ni-C_{ac} Mayer bond order	Ni	R_2C_2	Ni-C_{ac} Mayer bond order	Ni	R_2C_2
CH_3	0.71	0.134	-0.232	0.67	0.185	-0.130
H	0.74	0.135	-0.279	0.70	0.194	-0.184
Ph	0.73	0.146	-0.287	0.71	0.222	-0.158
CN	0.67	0.184	-0.468	0.65	0.234	-0.330
CF_3	0.75	0.173	-0.429	0.73	0.224	-0.303
Cl	0.74	0.158	-0.437	0.71	0.204	-0.296
F	0.85	0.151	-0.420	0.83	0.205	-0.307

II.4. Energy decomposition analysis

To achieve a better understanding of the bonding between the symmetrical substituted alkynes ligands C_2R_2 / (R = CH_3, H, F, Cl, CN, CHO, CF_3 and Ph) and $Ni(t\text{-}BuNC)_2$ or $Ni(CO)_2$ fragments, an energy decomposition analysis (EDA) of Ziegler-Rauk [30-31] was carried out using the ADF program [32]. The results are given in Tables 3 and 4, where the total interaction energy (ΔE_{int}) between the fragments is divided into three terms, namely (1) the electrostatic energy ΔE_{elstat} between the fragments, calculated using the frozen electron density distribution of the fragments; (2) the interaction of repulsive exchange ΔE_{Pauli} between the fragments due to the fact that two electrons of the same spin cannot occupy the same region in space; (3) the orbital interaction (covalent) ΔE_{orb}, which represents the charge transfer bound to the interactions between the occupied and vacant orbitals of the fragments. This last term can be broken down into orbital contributions of different symmetry, which makes it possible to distinguish the bonds σ, π and δ

For all complexes studied, from whatever the ligand L (CO or t-BuNC), the total interaction energy follows the sequence: $NiL_2(C_2F_2)$ < $NiL_2(C_2Cl_2)$ < $NiL_2(C_2(CF_3)_2)$ < $NiL_2(C_2(CN)_2)$ < $NiL_2(C_2(Ph)_2)$ < $NiL_2(C_2H_2)$ < $NiL_2(C_2(CH_3)_2)$, which nicely agree with the corresponding Ni-C_{ac} bond strength discussed above.

It should also be noted that for the same ligand C_2R_2, the total interaction energies ΔE_{int} (including the orbital interaction ΔE_{orb}) of the complexes $Ni(t\text{-}BuNC)_2(C_2R_2)$, are smaller than those of the $Ni(CO)_2(C_2R_2)$ complexes, which indicates that the bonding is

stronger in the t-butyl isocyanide complexes than in those of carbonyl, and therefore are the most stable.

Tables 3 and 4 show that all the interactions present almost equilibrium between both electrostatic and covalent contributions. The electrostatic contribution ΔE_{elstat} increases for Ph, H and CH_3 substituents, reaching 55.90 %, 54.25 % and 58.31 % respectively, while for the $Ni(CO)_2C_2R_2$ complexes, reaching 57.44 %, 56.18 % and 60.06 % for the same substituents Ph, H and CH_3 respectively.

The energy contributions corresponding to σ donation and π back-donation for $Ni(CO)_2(C_2R_2)$ complexes of the C_{2v} point group are ΔE_{A1} and ΔE_{B2} respectively .
From the table 4, it follows that the electronic effect ΔE_{B2} has a significant contribution to ΔE_{orb} than ΔE_{A1} and plays a major role in relative stability. The most stable $Ni(CO)_2(C_2F_2)$ complex has the lowest values of ΔE_{A1} (-24.06 kcal / mol) and ΔE_{B2} (-93.05 kcal / mol), while the complexes $Ni(CO)_2(C_2(CN)_2)$ and $Ni(CO)_2(C_2(CH_3)_2)$ respectively have the large values of ΔE_{A1} (-20.91 kcal / mol) of ΔE_{B2} (-51.80 kcal /mol). These results are in agreement with the values of σ donation and π back-donation. We find that the $Ni(CO)_2(C_2F_2)$ complex has the greatest value of b = 0.66 and d = 0.68. Also, $Ni(CO)_2(C_2(CN)_2)$ has the smallest value of d = 0.33 and the least stable complex among the studied compounds $Ni(CO)_2(C_2(CH_3)_2)$ has the lowest value b = 0.45

Table 3. Energy decomposition in (kcal/mol) obtained by the interactions between C_2R_2 (R = F, Cl, CF_3, CN, Ph, H, CH_3) and Ni(t-ButNC)$_2$.

complexes	ΔEelstat	ΔEpauli	ΔEorb	*ΔEint*
Ni(t-ButNC)$_2${C_2F_2}	-138.54 (48.63 %)[(a)]	173.98	-146.35 (51.37 %)[(a)]	-110.91
Ni(t-ButNC)$_2${C_2Cl_2}	-130.74 (49.11 %)	170.23	-135.46 (50.89 %)	-95.97
Ni(t-ButNC)$_2${$C_2(CF_3)_2$}	-117.33 (47.15 %)	156.77	-131.53 (52.85 %)	-92.09
Ni(t-ButNC)$_2${$C_2(CN)_2$}	-113.65 (45.85 %)	157.27	-134.24 (54.15 %)	-90.62
Ni(t-ButNC)$_2${$C_2(ph)_2$}	-134.89 (55.90 %)	169.93	-106.44 (44.10 %)	-71.40
Ni(t-ButNC)$_2${C_2H_2}	-125.22 (54.25 %)	160.54	-105.60 (45.75 %)	-70.28
Ni(t-ButNC)$_2${$C_2(CH_3)_2$}	-135.20 (58.31 %)	164.27	-96.68 (41.69 %)	-64.61

[a] Values between parentheses are the percentage of the contributions into the total attractive energies.

Table 4. Energy decomposition in (kcal/mol) obtained by the interactions between C_2R_2 (R = F, Cl, CF_3, CN, Ph, H, CH_3) and $Ni(CO)_2$.

complexes	ΔE_{elstat}	ΔE_{pauli}	ΔE_{orb}	Ea_1	E_{a2}	E_{b1}	E_{b2}	ΔE_{int}
$Ni(CO)_2C_2F_2$	-130.05 (50.67 %)[a]	164.98	-126.61 (49.33 %)[a]	-24.06 (19.00 %)[b]	-2.01 (1.59 %)[b]	-7.48 (5.91 %)[b]	-93.05 (73.50 %)[b]	-91.68
$Ni(CO)_2C_2Cl_2$	-120.97 (51.62 %)	157.05	-113.38 (48.38 %)	-22.48 (19.83 %)	-2.04 (1.80 %)	-6.35 (5.60 %)	-82.51 (72.77%)	-77.30
$Ni(CO)_2C_2(CF_3)_2$	-101.22 (48.31 %)	139.69	-108.30 (51.69 %)	-20.95 (19.35 %)	-2.55 (2.35 %)	-5.43 (5.00 %)	-79.38 (73.30 %)	-69.84
$Ni(CO)_2C_2(CN)_2$	-92.81 (45.76 %)	136.56	-109.99 (54.24 %)	-20.91 (19.01 %)	-3.18 (2.90 %)	-5.96 (5.42 %)	-79.93 (72.67 %)	-66.24
$Ni(CO)_2C_2(ph)_2$	-121.46 (57.44 %)	148.95	-90.00 (42.56 %)	-23.26 (25.85 %)		-66.74 (74.15 %)		-62.51
$Ni(CO)_2C_2H_2$	-114.01 (56.18 %)	142.48	-88.94 (43.82 %)	-21.63 (24.32 %)	-1.70 (1.91 %)	-6.10 (6.86 %)	-59.51 (66.91 %)	-60.47
$Ni(CO)_2C_2(CH_3)_2$	-123.03 (60.06 %)	145.88	-81.80 (39.94 %)	-22.14 (27.07 %)	-1.14 (1.39 %)	-6.64 (8.12 %)	-51.87 (63.42 %)	-58.95

[a] The percentage of the contributions into the total attractive energies.

[b] The contribution to the total orbital interactions ΔE_{or}

III. Conclusion

In this theoretical study, calculations were performed on $Ni(t\text{-}BuNC)_2(C_2R_2)$ and $Ni(CO)_2(C_2R_2)$ complexes by varying the symmetrical substituted alkynes C_2R_2. The electronic structure and the bonding strength analysis between the metal fragments NiL_2 (L = t-BuNC, CO) and symmetrical substituted C_2R_2 have been studied by density functional theory with the BP86 functional and TZP basis sets. The electronic structure was analysed in terms of the Chatt–Dewar–Duncanson model.

The electronegative substituents on acetylene increases the ability of the triple bond to coordinate with the Nickel where the strongest bonding energies are calculated.

The presence of electron withdrawing ligand reduces the importance of nickel-alkyne back-donation, in which we have found that tert-butyl isocyanide complexes are more stable than those of carbonyl.

The energy decomposition analysis indicates that all symmetrical substituted C_2R_2 / (R = F, Cl, CF_3, CN, Ph, H and CH_3) bonded to the Ni metal present almost equilibrium between both electrostatic and covalent contributions

Our results are supported by experimental studies which indicate that [Ni(CO)2(CF3C≡CCF3) complex is a colorless volatile liquid while Ni(tBuNC)2(CF3C≡CCF3) and Ni(tBuNC)2(Ph C≡ C Ph) are crystalline complexes

Bibliography

1. (a) Zeise, W. C. "*Eine besondere Platinverbindung*." Ann. Phys 85 (**1827**) 632.
   (b) Zeise, William C. "*Von der Wirkung zwischen Platinchlorid und Alkohol, und von den dabei entstehenden neuen Substanzen*." Annalen der Physik 97.4 (**1831**) 497-541.
2. (a) Black, M., R. H. B. Mais, and P. G. Owston. "*The crystal and molecular structure of Zeise's salt, $KPtCl_3$. C_2H_4. H_2O*." Acta Crystallographica Section B: Structural Crystallography and Crystal Chemistry 25.9 (**1969**) 1753-1759.
   (b) Jarvis, J. A. J., B. T. Kilbourn, and P. G. Owston. "*A re-determination of the crystal and molecular structure of Zeise's salt, $KPtCl_3$. C_2H_4. H_2O*." Acta crystallogr., B Struct. crystallogr. cryst. 27.2 (**1971**) 366-372.
3. Dewar, J. S. "*A review of the pi-complex theory*." Bull. Soc. Chim. Fr 18.3-4 (**1951**): C71-C79.
4. J. Chatt, L. A. Duncanson, '*586. Olefin co-ordination compounds. Part III. Infrared spectra and structure: attempted preparation of acetylene complexes.*' J. Chem. Soc. (**1953**) 2939-2947
5. Reppe, Walter, et al. *"Cyclisierende polymerisation von acetylen I über cyclooctatetraen." Justus Liebigs Annalen der Chemie* 560.1 (1**948**) 1-92.
6. Domínguez, Gema, and Javier Pérez-Castells. "*Recent advances in [2+ 2+ 2] cycloaddition reactions*." Chemical Society Reviews 40.7 (**2011**) 3430-3444.
7 (a) Chopade, Pramod R., and Janis Louie. *"[2+ 2+ 2] Cycloaddition reactions catalyzed by transition metal complexes."* Adv. Synth. Catal. 348.16-17 (**2006**) 2307-2327.
   (b) Iyori, Yasuaki, et al. "*Nickel-catalyzed C–O/N–H, C–S/N–H, and C–CN/N–H annulation of aromatic amides with alkynes C–O, C–S, and C–CN activation*." Chem. Sci. (**2021**).
8. Zhao, Wei-Cheng, et al. *"Palladium-catalyzed desymmetric [2+ 2+ 2] cycloaddition of 1, 6-enyne and alkyne."* Tetrahedron 79 (**2021**) 131862.
9. J. F. Hartwig, *'Organotransition Metal Chemistry: From Bonding to Catalysis.'* University Science Books: Sausalito, **2010**
10. Kumar, Ravindra, et al. *"Two-step synthesis of chiral fused tricyclic scaffolds from phenols via desymmetrization on nickel."* Nat. Commun. 8.1 (**2017**) 1-7.

11 Chatt, J., et al. *"990. Complexes of acetylenes with platinum (II). Part II. Hydroxy- and methoxy-alkylacetylenes."* J. Chem. Soc. (Resumed) (**1963**) 5170-5183.

12. (a) Allen, A. D., and C. D. Cook. *"The effect of substituents on the stabilities of complexes of platinum with aryl acetylenes and phosphines."* Can. J. Chem. 41.5 (**1963**): 1235-1238.

(b) Allen, A. D., and C. D. Cook. *"Complexes of platinum (0): I. Complexes with triphenylphosphine and substituted phenylacetylenes."* Can. J. Chem. 42.5 (**1964**) 1063-1068.

(c) Collman, James P., and Jung W. Kang. *"Acetylene complexes of iridium and rhodium.*" J. Am. Chem. Soc. 89.4 (**1967**) 844-851.

(d) Greaves, E. O., C. J. L. Lock, and P. M. Maitlis. *"Metal–acetylene complexes. II. Acetylene complexes of nickel, palladium, and platinum."* Can. J. Chem. 46.24 (**1968**) 3879-3891

(e) Nelson, John Henry, et al. "New bonding model for olefinic and acetylenic complexes of transition metals." J. Am. Chem. Soc 91.25 (**1969**) 7005-7008.

(f) McClure, G. L., and W-H_ Baddley. "*Metal complexes of cyanocarbons VIII. Dicyanoacetylene complexes of platinum.*" J. Organomet. Chem. 25.1 (**1970**): 261-272.

(g) Nelson, John H., and Hans B. Jonassen. *"Monoolefin and acetylene complexes of nickel, palladium and platinum."* Coord. Chem. Rev. 6.1 (**1971**) 27-63

12. Otsuka, Sei, T. Yoshida, and Y. Tatsuno. "Isocyanide-nickel (0) and-palladium (0) complexes involving unsaturated ligands." J. Am. Chem. Soc. 93.24 (**1971**) 6462-6469.

13. Dickson, Ron S., and James A. Ibers. *"The structure of bis (tert-butyl isocyanide)(diphenylacetylene) nickel(0), $Ni(C_6H_5C{\equiv}CC_6H_5)[(CH_3)_3C{-}N{\equiv}C]_2$."* J. Organomet. Chem. 36.1 (**1972**) 191-207.

14 (a) Davies, Brian William, and Nicholas C. Payne. *"Studies on metal-acetylene complexes: V. Crystal and molecular structure of bis (triphenylphosphine)(1-phenylpropyne)platinum(0),$[P(C_6H_5)_3]_2(C_6H_5C{\equiv}CCH_3)Pt0$.*" J. Organomet. Chem. 99.2 (**1975**) 315-328.

(b) Davies, Brian William, and Nicholas C. Payne. *"Studies on metal—acetylene complexes: VI. Crystal and molecular structure of [diethylbis (1-pyrazolyl) borato]*

methyl (1-phenylpropyne)-platinum (II),[$(C_2H_5)_2B$ ($N_2C_3H_3$) 2](CH3) Pt (C6H5C≡CCH3)." J. Organomet. Chem. 102.2 (**1975**) 245-257.

15. Davidson, John L., et al. *"Formation of tetra-and trinuclear cluster complexes from tetracarbonylnickel and hexafluorobut-2-yne. Molecular structures of tris (hexafluorobut-2-yne) tetracarbonyltetranickel and cyclooctatetraene (hexafluorobut-2-yne) tricarbonyltrinickel."* J. Am. Chem. Soc. 97.26 (**1975**) 7490-7492.
16. Tatsumi, Kazuyuki, et al. *"Semiempirical Molecular Orbital Considerations of the Electronic Structures of Transition Metal Complexes. II. Acetylene-and Azo-Nickel Complexes."* Bull. Chem. Soc. Jpn. 49.8 (**1976**) 2170-2177.
17. Upton, Thomas H., and William A. Goddard III. *"Interaction of acetylene and ethylene with nickel atom."* J. Am. Chem. Soc. 100.1 (**1978**) 321-323.
18. Geurts, Petro, Hans Burgers, and Ad van der Avoird. *"Hartree—Fock—Slater-LCAO studies of the acetylene—transition metal interaction. III. Binding to mono-and dinuclear Ni complexes with carbonyl and isocyanide ligands."* Chem. Phys. 54.3 (**1981**) 397-409.
19. (a) Farrar, David H., and Nicholas C. Payne. "Studies of metal-acetylene complexes. 8. Syntheses and molecular structures of two platinum complexes containing bulky phosphine ligands." Inorg. Chem. 20.3 (**1981**) 821-828.

    (b) Pörschke, Klaus R., Yi-Hung Tsay, and Carl Krüger. *"Ethynebis (triphenylphosphane) nickel (0)."* Angewandte Chemie International Edition in English 24.4 (**1985**) 323-324.

    (c) Ziegler, Tom. *"Theoretical study on the stability of M (PH3) 2 (O2), M (PH3) 2 (C2H2), and M ($PH_3)_2$ (C_2H_4)(M= Ni, Pd, Pt) and M (PH3) 4 (O2)+, M (PH3) 4 (C2H2)+, and M (PH3) 4 (C2H4)+(M= Co, Rh, Ir) by the HFS-transition-state method."* Inorg. Chem. 24.10 (**1985** 1547-1552.

    (d) Burns, C. J., and R. A. Andersen. *"preparation of the first molecular^-acetylene complex of a 4f-transition metal,(me5c5) 2yb (2-mec cme)."* (**1986**).

    e) Rosenthal, U., W. Schulz, and H. Görls. *"[(C6H5) 3P] 2Ni (Me3Si-C≡C-SiMe3). Darstellung, Eigenschaften und Struktur des ersten stabilen Nickel (0)-Komplexes von Bis-trimethylsilylacetylen."* Zeitschrift für anorganische und allgemeine Chemie 550.7 (**1987**) 169-176.

f) Bartik, Tamas, et al. *"Synthesis and characterization of bis (phosphine) nickel (0) complexes containing nonsymmetrically substituted acetylenes."* Organometallics 11.3 (**1992**) 1235-1241.

(g) Li, Jian, Georg Schreckenbach, and Tom Ziegler. *"Relativistic Effects on Metal-Ligand Bond Strengths in. pi.-Complexes: Quasi-Relativistic Density Functional Study of M(PH3)2X2 (M= Ni, Pd, Pt; X2= O2, C2H2, C2H4) and M (CO) 4 (C2H4)(M= Fe, Ru, Os)."* Inorg.Chem.34.12 (**1995**) 3245-3252.

20 Hyla-Kryspin, Isabella, et al. *"Reassessment of the electronic and molecular structure, bonding, and stability of zerovalent nickel acetylene complexes by the density functional method."* Organometallics 17.21 (**1998**) 4724-4733.

21. Davy, E. *"Notice of a new gaseous bicarburet of hydrogen."* Report of the Sixth Meeting of the British Association for the Advancement of Science. Vol. 5. **1836.**

22. Miller, Samuel Aaron. "*Acetylene: its properties, manufacture, and uses*." Vol. 2. Academic Press, **1966.**

23. Berthelot, M. "*Sur une nouvelle série de composés organiques, le quadricarbure d'hydrogène et ses dérivés*." CR Acad Sci Paris 50 (**1860**) 805-808.

24. Astruc, Didier. '' *Chimie organométallique et catalyse''* EDP sciences, **2013.**

25. Bergsträsser, U. Science of Synthesis: Houben-Weyl "*Methods of Molecular Transformations*" Vol. 19. Thieme Chemistry, **2004.**

26. Mond, Ludwig, Carl Langer, and Friedrich Quincke. *" Action of carbon monoxide on nickel."* J. Chem. Soc. Trans 57 (1890): 749-753.

27. Dyson, Paul J., and J. Scott McIndoe. *Transition metal carbonyl cluster chemistry*. Vol. 2. CRC Press, **2000**.

28. Malatesta, L.; Bonati, F. Isocyanide Complexes of Transition Metals; Wiley: New York, NY, USA, **1969**

29 Morokuma K. "Molecular orbital studies of hydrogen bonds. III. C=O···H–O hydrogen bond in H2CO···H2O and H2CO···2H2O". J. Chem. Phys. 55 (**1971**) 1236–1244

30 Ziegler T, Rauk A. *" Carbon monoxide, carbon monosulfide, molecular nitrogen, phosphorus trifluoride, and methyl isocyanide as. sigma. donors and. pi. acceptors. A theoretical study by the Hartree–Fock–Slater transition-state method"*. Inorg. Chem. 18 **(1979)** 1755–1759

31. ADF, SCM. Theoretical Chemistry, VrijeUniversiteit, Amsterdam, The Netherlands

General conclusions and perspectives

The work described in this thesis reports a DFT method study of the geometrical and electronic properties of variety of mixed clusters of IIIa and Va groups such as Ga_mIn_{n-m} clusters (n = 4, 6, 8 and m < n) and Al_3N-nH_2 clusters.

During the second Chapter, a detailed study has been provided of structural parameters, relative stabilities and electronic properties of gallium–indium Ga_mIn_{n-m} clusters (n = 4, 6, 8 and m < n). The obtained clusters prefer to adopt three-dimensional (3D) structures, the trigonal prism and rhombic prism configurations are favored energetically when n = 6 and 8 respectively. The study of electronic properties show that the Ga-rich clusters are more stable than those of In-rich ones with the same number of the total atoms. Therefore, Ga_7In cluster is relatively, the most stable structure.

Density functional calculations were performed at the BP86-D and PW91 functionals for the interaction of molecular hydrogen on Al_3N cluster. A detailed study has been provided of structural parameters and electronic properties of Al_3N-nH_2. The results show that the hydrogen molecules can bond strongly to the Al_3N and form a covalent bond Al-H The values bonding energy of H_2 for all Al_3N-nH_2 (n =1-6) calculated by BP86-D nearly lie in the ideal range of 0.1 - 0.4 eV which are an advantage for hydrogen storage under ambient conditions. The fragment analysis was shown that the electron-donation interaction tends to weaken the H-H bond and enhances the attraction Al_3N- H_2.

In the last chapter, calculations were performed on $Ni(t\text{-}BuNC)_2(C_2R_2)$ and $Ni(CO)_2(C_2R_2)$ complexes by varying the symmetrical substituted alkynes C_2R_2. The electronic structure was analysed in terms of the Chatt–Dewar–Duncanson model and show that the contribution of π- back-donation from the metallic fragment to the π^* orbitals of C_2R_2 ligands is more dominant than that from σ donation for all Ni(t-BuNC)2(C2R2) complexes.

There are still many properties for gallium indium clusters to be addressed. In the coming times, I hope to studying and modifying optical properties of gallium indium clusters by adding organic compounds

ANNEXES

ANNEX I

Computational Methods

I. Introduction

ADF (Amsterdam Density Functional) is a Fortran program for calculations on atoms and molecules (in gas phase or solution). It can be used for the study of such diverse fields as molecular spectroscopy, organic and inorganic chemistry, crystallography and pharmacochemistry. It was developed at the university from Vrije in Amsterdam to Baerends and co-workers [1, 2], its particularity is the calculation of the total binding energy of the molecule. A separate program BAND is available for the study of periodic systems: crystals, surfaces, and polymers. The calculation method used is the theory of the DFT density functional which is based on the Kohn-Sham approach (see chapter I)

II-Computational methods

DFT calculations were carried out on the studied clusters using the Amsterdam density functional (ADF) program developed by Baerends and co-workers [1-5].
All geometries discussed in the chapter II have been optimized with the hybrid-type B3LYP functional (Becke′s three parameter hybrid exchange functional [6] coupled with the Lee–Yang–Parr nonlocal correlation functional) [7]
The generalized gradient approximation BP86 and PW91 [8-10] functional have been used for calculations in both chapter III and Chapter IV. The numerical integration procedure applied for the calculations was developed by te Velde et al [6].

The atomic electronic configurations were described by a triple-ζ Slater-type orbital (STO) basis set for H 1s, C 2s and 2p, O 2s and 2p , F 2s and 2p, Cl 3s and 3p Al 2s and 2p, N 2s and 2p, Ga 3d, 4s, and 4p, In 4d, 5s, and 5p augmented with a 3d single-ζ polarization for C, N, O, F , Al, N and Cl atoms and with a 2p single-ζ polarization for H atoms, augmented with a 4d single-ζ and 5d single-ζ polarization for Ga and In atoms, respectively

Full geometry optimizations were carried out using the analytical gradient method implemented by Versluis and Ziegler [11]. Frequency calculations [12] were performed for all the studied compounds to check that the optimized structures are at the local minima. The representation of the molecular structures was made using MOLEKEL4.1 [13].

The bonding interactions in both Al_3N-nH_2 and $NiL_2(RC{\equiv}CR)$ systems have been analysed by means of Morokuma-type energy decomposition analysis (decomposition of the bonding energy into the Pauli(exchange) repulsion, total steric interaction, and orbital interaction terms) developed by Zieglerand Rauk [14] for DFT methods and incorporated in ADF

Bibliography

[1] Baerends, E. J., Ellis, D. E., & Ros, P. J. C. P." *Self-consistent molecular Hartree—Fock—Slater calculations I. The computational procedure"* Chem. Phys. 2.1 (**1973)** 41-51.

[2] te Velde, G., & Baerends, E. J. *"Numerical integration for polyatomic systems".* J. Comput. Phys. 99.1 (**1992**) 84-98

[3] Guerra, C. F., Snijders, J. G., te Velde, G. T., & Baerends, E. J." *Towards an order-N DFT method"*. Theor. Chem. Acc. (**1998**) 391-403

[4] (a) Bickelhaupt, F. M., & Baerends, E. J. *"Kohn-Sham density functional theory: predicting and understanding chemistry"* Rev. Comput. Chem. 15(**2000)** 1-86. (b) Te Velde, G. T., Bickelhaupt, F. M., Baerends, E. J., Fonseca Guerra, C., van Gisbergen, S. J., Snijders, J. G., & Ziegler, T. *"Chemistry with ADF"* J. Comput. Chem. 22.9 **(2001**) 931-967.

[5] Becke, A. D. "*Becke's three parameter hybrid method using the LYP correlation functional."* J. Chem. Phys. 98.492 (**1993**) 5648-5652.

[6] Lee, C., Yang, W., & Parr, R. G. *" Development of the Colle-Salvetti correlation-energy formula into a functional of the electron density"* J. Phys. Rev. B 37.2 (**1998)** 785-789

[8] Becke, A. D. "*Density functional calculations of molecular bond energies*" J. Chem. Phys 84.8 (**1986)** 4524-4529.

[9] Becke, A.D. "Density-functional exchange-energy approximation with correct asymptotic behavior" Phys. Rev. A 38.6 **(1988)** 3098-3100

[10] Perdew, J.P *"Density-functional approximation for the correlation energy of the inhomogeneous electron gas"* Phys. Rev. B 33.12 (**1986)** 8822-8824

[11] Versluis, L., & Ziegler, T. *"The determination of molecular structures by density functional theory. The evaluation of analytical energy gradients by numerical integration"* J. Chem. Phys. 88.1 (**1988)** 322-328.

[12] (a) Fan, L., & Ziegler, T. "*Application of density functional theory to infrared absorption intensity calculations on main group molecules*" J. Chem. Phys. 96.1 (**1992)** 9005-9012

(b) Fan, L., & Ziegler, T. *" Application of density functional theory to infrared absorption intensity calculations on transition-metal carbonyls"* J. Phys. Chem., 96.17 (**1992**) 6937-6941

[13] P. Flükiger, H. P. Lüthi, S. Portmann, and J. Weber. MOLEKEL. Version 4.3.win32. Switzerland: Swiss Center for Scientific Computing (CSCS), **2000/2001.**

[14] (a) Kitaura, K., & Morokuma, K. *"A new energy decomposition scheme for molecular interactions within the Hartree-Fock approximation."* International Journal of Quantum Chemistry, 10.2 (**1976**) 325-340.

(b) Ziegler, T., & Rauk, A. "On the calculation of bonding energies by the Hartree Fock Slater method". Theoret. Chim. Acta 46.1 (**1977**) 1-10.

ANNEX II

Figures

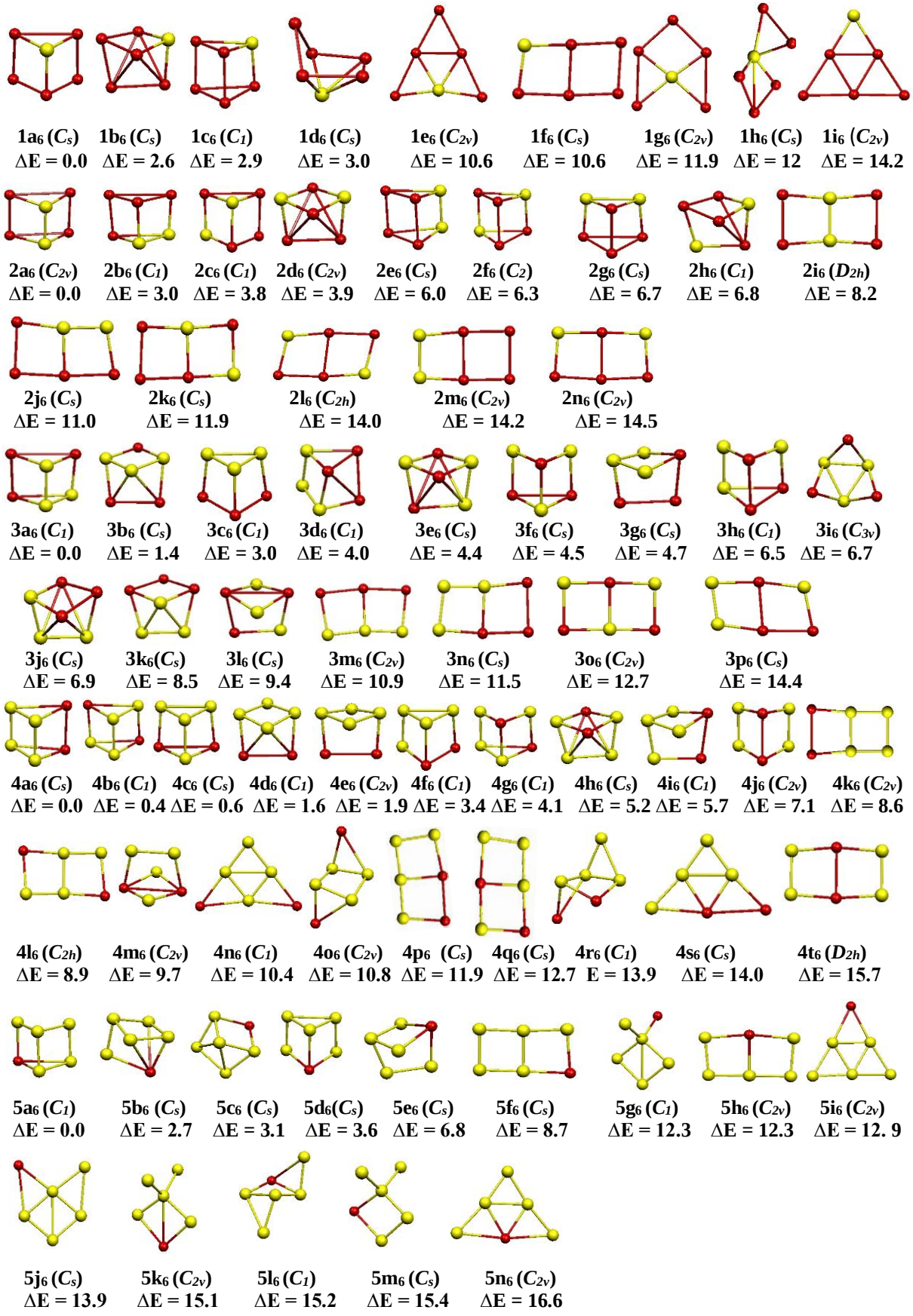

Figure 1A. Ground state structures of Ga_mIn_{6-m} (m < 6) clusters. Relative energies ΔE between the isomers are given in kcal/mol.

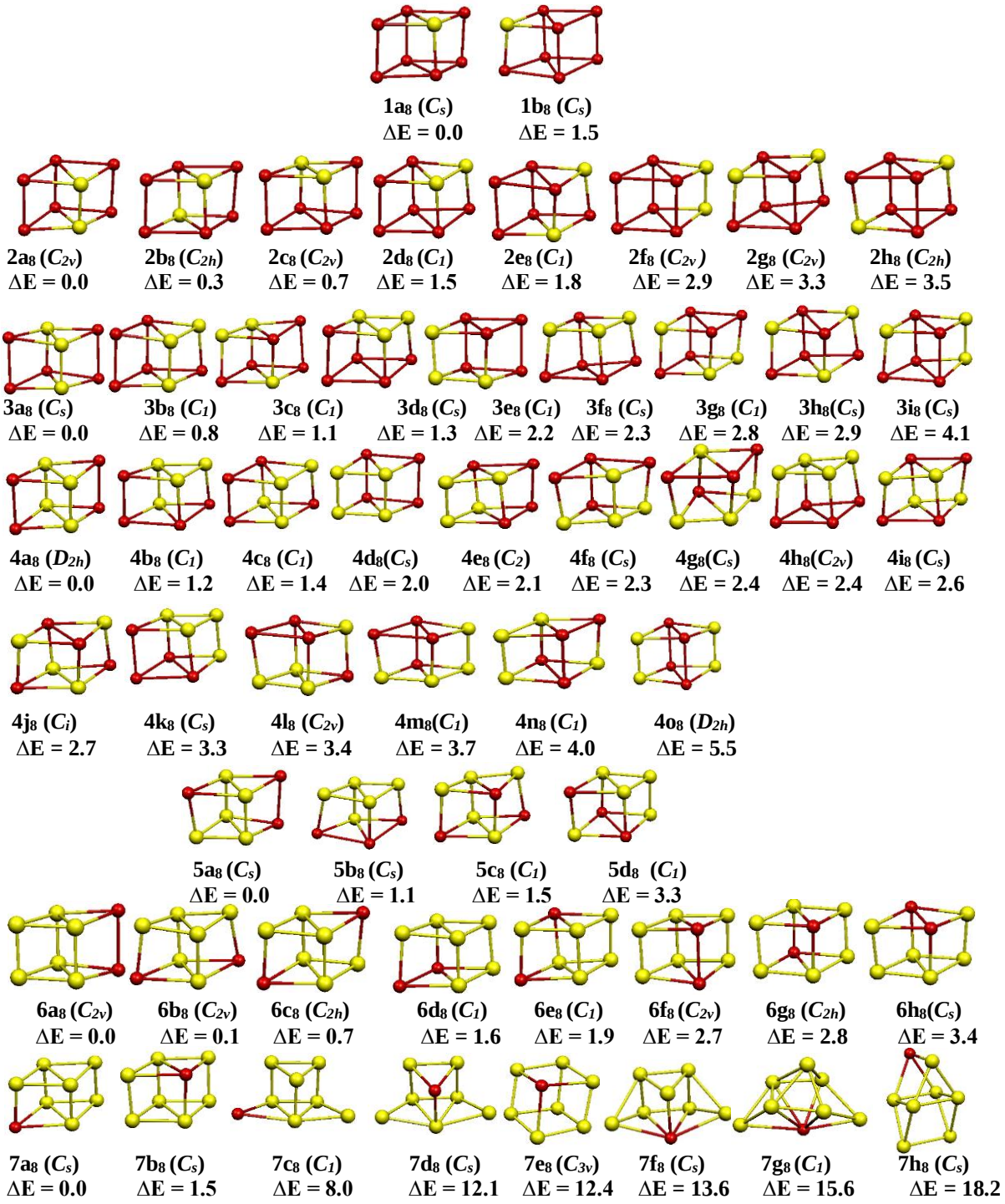

Figure 2A. Ground state structures of Ga_mIn_{6-m} ($m < 8$) clusters. Relative energies ΔE between the isomers are given in kcal/mol.

ANNEX III

Tables

Table 1A. Relative Energies (kcal / mol), HOMO-LUMO Gaps (eV), Ga–Ga, In-In, and Ga–In Bond Lengths (Å) for Ga_mIn_{6-m} (m < 6) Clusters

Cluster	Isomer	Sym	Relative energy	HOMO-LUMO gap	Ga-Ga	In-In	Ga-In
$GaIn_5$	$1a_6$	C_s	0.0	1.52	-	2.976	2.762
	$1b_6$	C_s	2.6	1.35	-	2.966	2.766
	$1c_6$	C_1	2.9	1.35	-	2.955	2.755
	$1d_6$	C_s	3.0	1.49	-	3.021	2.703
	$1e_6$	C_{2v}	10.6	1.27	-	2.971	2.825
	$1f_6$	C_s	10.6	1.32	-	2.879	2.697
	$1g_6$	C_{2v}	11.9	1.36	-	2.927	2.670
	$1h_6$	C_s	12.0	1.40	-	2.955	2.722
	$1i_6$	C_{2v}	14.2	1.25	-	2.979	2.890
Ga_2In_4	$2a_6$	C_{2v}	0.0	1.65	2.547	3.002	2.771
	$2b_6$	C_1	3.0	1.50	2.541	2.966	2.773
	$2c_6$	C_1	3.8	1.47	-	2.978	2.761
	$2d_6$	C_{2v}	3.9	1.40	-	3.128	2.770
	$2e_6$	C_s	6.0	1.36	2.550	2.970	2.776
	$2f_6$	C_2	6.3	1.34	-	2.998	2.749
	$2g_6$	C_s	6.7	1.35	-	2.982	2.767
	$2h_6$	C_1	6.8	1.32	-	2.971	2.769
	$2i_6$	D_{2h}	8.2	1.45	2.526	3.033	2.753
	$2j_6$	C_s	11.0	1.42	2.508	2.937	2.753
	$2k_6$	C_s	11.9	1.38	-	2.759	2.739
	$2l_6$	C_{2h}	14.0	1.47	-	2.968	2.704
	$2m_6$	C_{2v}	14.2	1.33	2.593	2.939	2.73
	$2n_6$	C_{2v}	14.5	1.32	-	2.949	2.740
Ga_3In_3	$3a_6$	C_1	0.0	1.66	2.550	3.091	2.766
	$3b_6$	C_s	1.4	1.63	2.514	3.129	2.822
	$3c_6$	C_1	3.0	1.55	2.546	3.000	2.792
	$3d_6$	C_1	4.0	1.46	2.552	3.088	2.739
	$3e_6$	C_s	4.4	1.38	2.567	3.608	2.771
	$3f_6$	C_s	4.5	1.47	-	3.565	2.778
	$3g_6$	C_s	4.7	1.48	2.566	2.997	2.767
	$3h_6$	C_1	6.5	1.34	2.557	2.994	2.759
	$3i_6$	C_{3v}	6.7	1.57	2.813	-	2.792
	$3j_6$	C_s	6.9	1.28	2.557	2.972	2.787
	$3k_6$	C_s	8.5	1.43	2.664	3.040	2.699
	$3l_6$	C_s	9.4	1.35	-	3.008	2.774
	$3m_6$	C_{2v}	10.9	1.43	2.527	2.964	2.767
	$3n_6$	C_s	11.5	1.44	2.509	2.943	2.760
	$3o_6$	C_{2v}	12.7	1.41	-	-	2.747
	$3p_6$	C_s	14.4	1.58	2.590	2.997	2.685

Table 1A. (Continued)

Cluster	Isomer	Sym	Relative energy	HOMO-LUMO gap	Ga-Ga	In-In	Ga-In
Ga_4In_2	$4a_6$	C_s	0.0	1.68	2.570	3.025	2.771
	$4b_6$	C_1	0.4	1.65	2.546	-	2.794
	$4c_6$	C_s	0.6	1.67	2.559	3.758	2.789
	$4d_6$	C_1	1.6	1.63	2.530	3.150	2.811
	$4e_6$	C_{2v}	1.9	1.56	2.758	3.139	2.791
	$4f_6$	C_1	3.4	1.52	2.541	2.992	2.778
	$4g_6$	C_1	4.1	1.46	2.567	-	2.779
	$4h_6$	C_s	5.2	1.33	2.609	-	2.789
	$4i_6$	C_1	5.7	1,48	2.541	3.040	2.775
	$4j_6$	C_{2v}	7.1	1.38	2.574	3.067	2.775
	$4k_6$	C_{2v}	8.6	1.57	2.535	3.071	2.760
	$4l_6$	C_{2h}	8.9	1.59	2.529	-	2.770
	$4m_6$	C_{2v}	9.8	1.69	2.490	-	2.913
	$4n_6$	C_1	10.4	1.75	2.504	-	2.811
	$4o_6$	C_{2v}	10.8	1.31	2.705	3.785	2.789
	$4p_6$	C_s	11.9	1.49	2.531	-	2.525
	$4q_6$	C_s	12.7	1.50	2.510	-	2.738
	$4r_6$	C_1	13.9	1.58	2.492	-	2.784
	$4s_6$	C_s	14.0	1.67	2.528	3.486	2.705
	$4t_6$	D_{2h}	15.7	1.38	2.637	3.020	2.751
Ga_5In	$5a_6$	C_1	0.0	1.69	2.551	-	2.792
	$5b_6$	C_s	2.7	1.56	2.566	-	2.815
	$5c_6$	C_s	3.1	1.59	2.504	-	2.840
	$5d_6$	C_s	3.6	1.56	2.553	-	2.790
	$5e_6$	C_s	6.8	1.42	2.559	-	2.785
	$5f_6$	C_s	8.7	1.61	2.533	-	2.774
	$5g_6$	C_1	12.3	2.13	2.501	-	2.747
	$5h_6$	C_{2v}	12.3	1.51	2.532	-	2.765
	$5i_6$	C_{2v}	12.9	1.41	2.587	-	2.941
	$5j_6$	C_s	13.9	1.71	2.480	-	2.921
	$5k_6$	C_{2v}	15.1	2.14	2.501	-	2.804
	$5l_6$	C_1	15.2	1.67	2.548	-	2.771
	$5m_6$	C_s	15.4	2.09	2.493	-	2.704
	$5n_6$	C_{2v}	16.6	1.57	2.542	-	2.709

Table 2A. Relative Energies (kcal/mol), HOMO–LUMO Gaps (eV), Ga–Ga, In–In, and Ga–In Bond Lengths (Å) for Ga_mIn_{8-m} (m < 8) Clusters

Cluster	Isomer	Sym	relative energies	HOMO-LUMO gap	Ga-Ga	In-In	Ga-In
$GaIn_7$	$1a_8$	C_s	0.0	1.62	-	2.913	2.724
	$1b_8$	C_s	1.5	1.66	-	2.926	2.742
Ga_2In_6	$2a_8$	C_{2v}	0.0	1.66	2.517	2.940	2.907
	$2b_8$	C_{2h}	0.3	1.65	-	2.938	2.722
	$2c_8$	C_{2v}	0.7	1.68	2.730	2.945	2.715
	$2d_8$	C_1	1.5	1.63	2.671	2.918	2.730
	$2e_8$	C_1	1.8	1.64	-	2.949	2.729
	$2f_8$	C_{2v}	2.9	1.61	2.533	2.930	2.936
	$2g_8$	C_{2v}	3.3	1.66	-	2.926	2.745
	$2h_8$	C_{2h}	3.5	1.67	-	2.932	2.746
	$2i_8$	C_s	7.8	1.78	2.565	2.881	2.712
Ga_3In_5	$3a_8$	C_s	0.0	1.71	2.508	2.947	2.711
	$3b_8$	C_1	0.8	1.68	2.520	2.913	2.744
	$3c_8$	C_1	1.1	1.67	2.669	2.948	2.725
	$3d_8$	C_s	1.3	1.69	2.712	2.943	2.722
	$3e_8$	C_1	2.2	1.64	2.528	2.925	2.738
	$3f_8$	C_s	2.3	1.67	2.664	2.927	2.737
	$3g_8$	C_1	2.8	1.70	2.686	2.924	2.736
	$3h_8$	C_s	2.9	1.69	-	2.917	2.739
	$3i_8$	C_s	4.1	1.67	2.535	2.940	2.759
	$3j_8$	C_s	6.2	1.83	2.569	3.053	2.682
Ga_4In_4	$4a_8$	D_{2h}	0.0	1.79	2.505	2.944	2.934
	$4b_8$	C_1	1.2	1.73	2.514	2.955	2.718
	$4c_8$	C_1	1.4	1.72	2.522	2.963	2.727
	$4d_8$	C_s	2.0	1.69	2.526	2.918	2.922
	$4e_8$	C_2	2.1	1.68	2.524	2.950	2.734
	$4f_8$	C_s	2.3	1.72	2.529	2.914	2.752
	$4g_8$	C_s	2,4	1.70	2.655	3.201	2.728
	$4h_8$	C_{2v}	2.4	1.73	2.693	3.157	2.726
	$4i_8$	C_s	2.6	1.69	2.540	2.961	2.735
	$4j_8$	C_i	2.7	1.72	2.684	3.174	2.732
	$4k_8$	C_s	3.3	1.74	2.735	3.158	2.734
	$4l_8$	C_{2v}	3.4	1.75	2.722	3.247	2.726
	$4m_8$	C_1	3.7	1.70	2.540	2.923	2.743
	$4n_8$	C_1	4.0	1.71	2.532	2.927	2.750
	$4o_8$	D_{2h}	5.5	1.73	2.546	2.943	2.954

Table 2A (Continued)

Cluster	Isomer	Sym	relative energies	HOMO-LUMO gap	Ga-Ga	In-In	Ga-In
Ga_5In_3	$5a_8$	C_s	0.0	1.81	2.508	2.959	2.749
	$5b_8$	C_s	1.1	1.78	2.521	3.242	2.727
	$5c_8$	C_1	1.5	1.77	2.529	-	2.728
	$5d_8$	C_1	3.3	1.75	2.540	3.212	2.732
Ga_6In_2	$6a_8$	C_{2v}	0.0	1.81	2.530	2.959	2.955
	$6b_8$	C_{2v}	0.1	1.86	2.517	-	2.758
	$6c_8$	C_{2h}	0.7	1.87	2.513	-	2.756
	$6d_8$	C_1	1.6	1.81	2.527	3.219	2.727
	$6e_8$	C_1	1.9	1.80	2.524	-	2.759
	$6f_8$	C_{2v}	2.7	1.80	2.543	2.928	2.991
	$6g_8$	C_{2h}	2.8	1.78	2.543	-	2.750
	$6h_8$	C_s	3.4	1.80	2.555	3.181	2.750
Ga_7In	$7a_8$	C_s	0.0	1.88	2.523	-	2.757
	$7b_8$	C_s	1.5	1.85	2.539	-	2.733
	$7c_8$	C_1	8.0	1.72	2.514	-	2.852
	$7d_8$	C_s	12.1	1.99	2.513	-	2.689
	$7e_8$	C_{3v}	12.4	1.52	2.570	-	3.012
	$7f_8$	C_s	13.6	1.90	2.510	-	2.686
	$7g_8$	C_1	15.6	1.67	2.581	-	2.913
	$7h_8$	C_s	18.2	1.27	2.505	-	2.722
	$7i_8$	C_{2v}	21.4	1.47	2.572	-	3.095

Table 3A. Vibrational modes H-H stretching (in cm^{-1}) of Al_3N-nH_2 (n =1-6) clusters

	H-H stretching frequency (cm^{-1})	
Compounds	BP86-D	PW91
H_2	4291	4308
Al_3N-H_2 (1A)	4016	3995
Al_3N-$2H_2$ (2A)	4055, 4057	4084, 4082
Al_3N-$2H_2$ (2B)	4094, 4099	4211, 4213
Al_3N-$3H_2$ (3A)	4063, 2*4118	4090, 4190, 4187
Al_3N-$3H_2$ (3B)	2*4086, 4093	4151, 4149*2
Al_3N-$4H_2$ (4A)	4127, 4121, 4122, 4124	4211*2, 4212, 4214
Al_3N-$4H_2$ (4B)	4104, 4109, 4140, 4136	4283, 4170, 4162, 4160
Al_3N-$5H_2$ (5A)	4124, 4142, 4143*2, 4148	4232, 4172, 4229*2, 4230
Al_3N-$6H_2$ (6A)	4153*5,4158	4211*3,4212*2, 4214

Abstract

Abstract :

In this thesis, we have investigated the electronic and structural properties of variety of mixed clusters Ga_mIn_{n-m} , Al_3N-nH_2 and $NiL_2(RC{\equiv}CR)$. The calculations were carried out using DFT method with B3LYP, BP86-D, PW91 and BP86 functionals. Bonding energies, HOMO-LUMO gap, ionization potential (IP), electron affinity (EA) and chemical hardness (η) as well as Charge, Molecular Orbital and the energy decomposition have been calculated. The results suggest that the optimized geometries of Ga_mIn_{n-m} tend to prefer compact structures and indicate that the Ga-rich clusters are more stable than the In-rich ones with the same number of total atoms. For the interaction of Al_3N-H_2, the results indicate that the behavior of H_2 molecules in Al_3N system, may either be in dissociative form or remain in molecular form. It was shown that the donation and back-donation is the mechanism of bonding in Al_3N-nH_2. The calculations of Nickel alkyne complexes $NiL_2(RC{\equiv}CR)/(L = CO, t\text{-}BuNC)$ indicate that the Nickel–C_2R_2 bond distances are more affected by the substitution of auxiliary ligand L than the modification of C_2R_2 ones

Keywords: Mixed clusters, DFT, Bond Energy, Bonding, Ionization potential,

Résumé :

Cette thèse est consacré à l'étude théorique de divers agrégats mixtes Ga_mIn_{n-m} , Al_3N-nH_2 et $NiL_2(RC{\equiv}CR)$. Les calculs ont été effectués en utilisant la DFT et les fonctionnelles B3LYP, BP86-D, PW91 et BP86. Les résultats suggèrent que les géométries optimisées de Ga_mIn_{n-m} ont tendance à préférer les structures compactes et indiquent que les clusters riches en Ga sont plus stables que ceux riches en In avec le même nombre d'atomes totaux. Pour l'interaction du Al_3N et nH_2, les résultats indiquent que le comportement des molécules H_2 dans le système Al_3N, peut être soit sous forme dissociative, soit resté sous forme moléculaire. Il a été montré que la donation et le rétro-donation est le mécanisme de liaison qui se produit dans Al_3N-nH_2. Les calculs des complexes Nickel-alcyne $NiL2(RC{\equiv}CR)$ / $(L = CO, t\text{-}BuNC)$ indiquent que les distances de liaison Nickel–C_2R_2 sont plus affectées par la substitution du ligand auxiliaire L que par la modification de celles de C_2R_2.

Mots-clés : Clusters mixtes, DFT, énergie de liaison, potentiel d'ionisation,

الملخص:

نقدم في هده الرسالة دراسة نظرية للمجاميع المختلطة Ga_mIn_{n-m}، Al_3N-nH_2 و $NiL_2(RC{\equiv}CR)$. تم إجراء الحسابات باستخدام نظرية الدالة الوظيفية للكثافة DFT. تشير النتائج إلى أن الأشكال الهندسية المحسّنة لـ Ga_mIn_{n-m} تميل إلى تفضيل الهياكل المدمجة وتشير إلى أن المجاميع الغنية بالـ Ga أكثر استقرارًا من المجاميع الغنية بالعدد نفسه من إجمالي الذرات. بالنسبة لتفاعل Al_3N و nH_2 ، تشير النتائج إلى أن سلوك جزيئات H_2 في نظام Al_3N يمكن أن يكون إما في شكل انفصالي أو يظل في شكل جزيئي. لقد ثبت أن التبرع والتبرع الرجعي هما آليتا الربط التي تحدث في Al_3N-nH_2. تشير حسابات مجمعات $NiL_2(RC{\equiv}CR)$ / $(L = CO, t\text{-}BuNC)$ إلى أن مسافات الروابط Nickel-C_2R_2 تتأثر باستبدال الرابط المساعد L أكثر من استبدال R الموجودة في C_2R_2

الكلمات الدالة: نظرية دالة الكثافة، المجاميع المختلطة، طاقة الارتباط، كمون التأين، الترابط

Journal of Structural Chemistry. Vol. 59, No. 5, pp. 997-1009, 2018.

PREDICTED STRUCTURES AND ELECTRONIC PROPERTIES OF GALLIUM-INDIUM CLUSTERS Ga_mIn_{n-m} (n = 4, 6, 8 AND $m < n$): A DENSITY FUNCTIONAL STUDY*

F. Hakkar[1] and B. Zouchoune[2,3]**

Various structural possibilities for small gallium-indium Ga_mIn_{n-m} (n = 4, 6, 8 and $m < n$) clusters are investigated using the density functional theory (DFT) method at the B3LYP/TZP level. The optimized structures tend to prefer compact structures, wherein the trigonal prism and rhombic prism configurations are favoured for n = 6 and 8, respectively. The bonding energy per atom is calculated according to the cluster size. The HOMO-LUMO gaps, ionization potentials, electron affinities, and chemical hardness (η) are also computed for the most stable isomers of each cluster and used to predict their relative stabilities. The obtained results indicate that the Ga-rich clusters are more stable than the In-rich ones with the same total number of atoms. The Ga–Ga bond is stronger than the Ga–In bond and the latter is stronger than the In–In one. Therefore, the Ga_7In cluster is relatively the most stable structure. The relative reactivity of Ga_mIn_{n-m} (n = 4, 6, 8 and $m < n$) clusters could be predicted based on the chemical hardness. The computed large HOMO-LUMO gap energies could be used as an index of the kinetic stability for the studied clusters.

DOI: 10.1134/S0022476618050013

Keywords: relative stabilities, bonding interactions, ionization potential, electron affinity, chemical hardness.

INTRODUCTION

The determination of the geometric and electronic structures of metal clusters and their chemical and physical properties has become an interesting field of research and grows significantly in importance [1]. Experimental and theoretical studies of small clusters formed by 13 group elements have been carried out during the past several decades because of their fundamental interest and potential application in nano-science.

Gallium and indium as 13 group elements are of great importance in physics and chemistry of nanoclusters and thin-film deposition. Small gallium clusters have been extensively studied in order to provide an in-depth look into these clusters.

[1]Université Abbes Laghrour de Khenchela, Algeria. [2]Laboratoire de Chimie appliquée et Technologie des Matériaux, Université Larbi Ben M′Hidi, El Bouaghi, Algeria; **b.zouchoune@univ-oeb.dz. [3]Unité de Recherche de Chimie de l′Environnement et Moléculaire Structurale, Université de Constantine (Mentouri), Constantine, Algeria. The text was submitted by the authors in English. *Zhurnal Strukturnoi Khimii*, Vol. 59, No. 5, pp. 1043-1055, June-July, 2018. Original article submitted November 9, 2017.

***** Supplementary materials are available for this article at doi 10.1134/S0022476618050013 and are accessible for authorized users.

There are several studies performed in both theoretical [2-16] and experimental [17-19] fields. Song and Cao [6] have theoretically investigated the geometrical parameters and electronic structures of Ga_n (n = 2-26) clusters, using the generalized gradient approximation for the exchange correlation potential to the DFT. It turned out that gallium clusters tend to adopt compact structures with increasing cluster size. Likewise, indium clusters have been studied experimentally [20-25], as well as theoretically [2, 27-30]. Zhang et al. [30] have systematically investigated the lowest-energy structures and electronic properties of indium In_n (n = 1-16) ones using DFT, showing the tendency towards compact structures with increasing cluster size.

Lill et al. have investigated the neutral and positively charged mixed gallium and indium Ga–In clusters [30, 31]. During the last two decades an important number of deltahedral clusters of Ga and In has been widely investigated, such as $Ga_9(CMe)_9$ [32], $In_8[Si(CMe_3)_3]_6$ [33], $Ga_{10}[Si(SiMe_3)_3]_6$ [34], $1n_{12}[Si(CMe_3)_3]_8$ [35], $[Ga_8(C_{13}H_9)]^{2-}$ [36] and the largest supraicosahedral structures [37, 39].

To gain a deep understanding of gallium-indium clusters, calculations have been carried out of small gallium-indium Ga_mIn_{n-m} (n = 4, 6, 8 and $m < n$) clusters, based on the DFT method at the B3LYP/TZP level. To our knowledge, a complete rationalization of stable geometries of Ga_mIn_{n-m} (n = 4, 6, 8 and $m < n$) clusters has not been achieved so far.

We have explored the lowest-energy structures of the mixed gallium-indium clusters and their electronic properties based on the MO analysis, HOMO-LUMO gaps, ionisation potential (IP), electron affinity (EA), and chemical hardness η in order to analyse their bonding and provide a detailed scheme of their electronic structures. The focus of this study is the investigation of the relative ordering of bare Ga_mIn_{n-m} structures with increasing number of gallium atoms.

We will endeavour to provide within the framework of this study the prediction of new structures by means of DFT calculations using the B3LYP functional. The reliability of the DFT method using B3LYP is already established to be valuable in determining the electronic structures, geometrical parameters, the bonding, and other properties from the previous works on cluster systems [40].

COMPUTATIONAL METHODS

DFT calculations were carried out on the studied clusters using the Amsterdam density functional (ADF) program [41] developed by Baerends and co-workers [42-46].

All geometries discussed in this paper have been optimized with the hybrid-type B3LYP functional (Becke′s three parameter hybrid exchange functional [47] coupled with the Lee–Yang–Parr nonlocal correlation functional) [48].

The numerical integration procedure applied for the calculations was developed by te Velde et al. [47]. The atomic electronic configurations were described by a triple-ζ Slater-type orbital (STO) basis set for H 1*s*, Ga 3*d*, 4*s*, and 4*p*, In 4*d*, 5*s*, and 5*p* augmented with a 4*d* single-ζ and 5*d* single-ζ polarization for Ga and In atoms, respectively, and with a 2*p* single-ζ polarization for H atoms. Full geometry optimizations were carried out using the analytical gradient method implemented by Versluis and Ziegler [49]. Frequency calculations [50, 51] were performed for all the studied compounds to check that the optimized structures are at the local minima. The representation of the molecular structures was made using MOLEKEL4.1 [52].

EXPERIMENTAL

Geometries and stability of isomers. We have explored the Ga_mIn_{n-m} (n = 4, 6, 8 and $m < n$) clusters in order to find their lowest-energy structures. Indeed, full geometry optimizations of Ga_mIn_{4-m} ($m < 4$), Ga_mIn_{6-m} ($m < 6$), and Ga_mIn_{8-m} ($m < 8$) showed a variety of singlet spin state structures found as the energy minimum much lower in energy than those of triplet state structures (Figs. 1-3). The different isomers are designated as ma_n, mb_n, mc_n, where m and ($n - m$) are the gallium and iridium atom numbers, respectively. For the studied structures, the calculated values of relative energies between isomers, HOMO-LUMO energy gaps, and Ga–In, In–In, and Ga–Ga bond distances are gathered in Table 1 and Tables S1, S2. In order to predict the relative stabilities and electronic properties of gallium-indium Ga_mIn_{n-m} (n = 4, 6, 8 and $m < n$) clusters, we have calculated the binding energy per atom, IPs, EAs, and the chemical hardness (η).

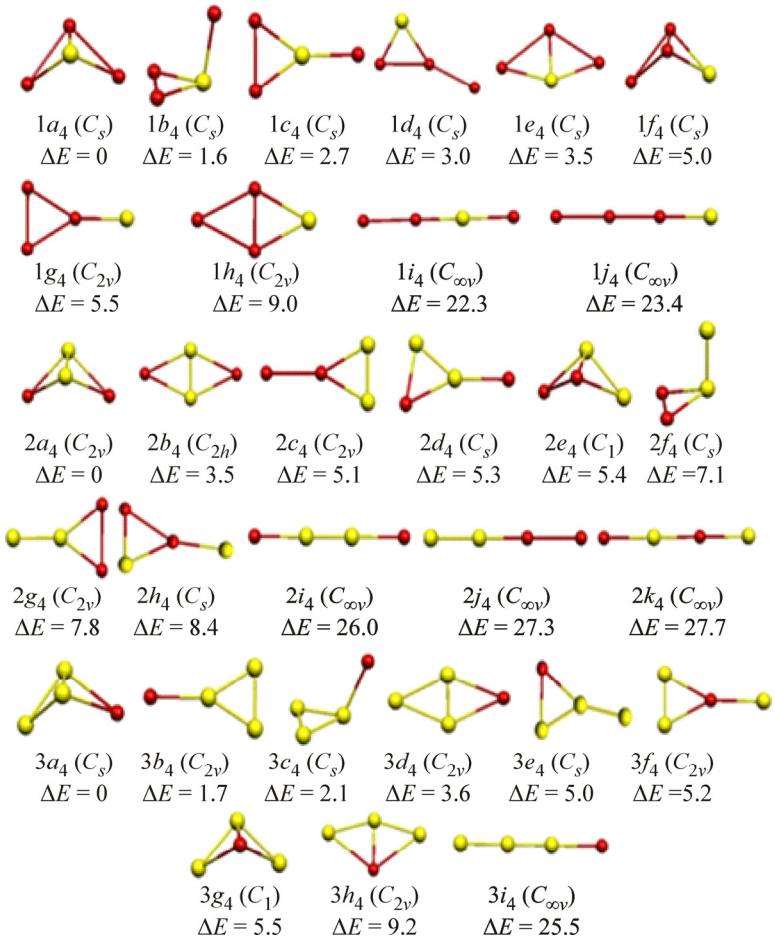

Fig. 1. Ground state structures of Ga_mIn_{4-m} ($m < 4$) clusters. Relative energies ΔE between the isomers are given in kcal/mol.

Four-vertex Ga_mIn_{4-m} ($m < 4$) clusters. The most stable structure for the $GaIn_3$ clusters corresponds to the bent 1a_4 isomer of the C_s structure (Fig. 1). Two other 1b_4 and 1c_4 isomers keeping the gallium atom between indium ones are higher in energy than the most stable one by 1.6 kcal/mol and 2.7 kcal/mol, respectively. The Ga atom binds to In ones with bond lengths of 2.553 Å, while the In–In bond distances are 3.369 Å, in accordance with the Ga and In radii. The global minimum 1a_4 structure exhibits a significant HOMO-LUMO gap of 1.15 eV, suggesting good kinetic stability, where the HOMO-LUMO energy separation serves as a simple measure of the kinetic stability [53-59]. A molecule with a small or zero HOMO-LUMO gap is chemically reactive, whereas a large HOMO-LUMO gap of 1.15 eV indicates an extraordinarily high stability of this cluster. The HOMO-LUMO energy separation could be used as an index of the kinetic stability for the studied clusters.

The *Y*-shaped 1g_4 isomer of the C_{2v} symmetry, in which the gallium atom is at the apex position, is the seventh low-lying isomer. It is important to note that the less stable isomers correspond to linear geometries featuring a maximum of In–In bonds.

For the Ga_2In_2 clusters, the bent 2a_4 structure characterized by the dihedral geometry of the C_{2v} symmetry is found as the global minimum presenting only Ga–Ga and Ga–In bonds, in which the gallium atoms are adjacent. This global minimum possesses one Ga–Ga bond with a length of 2.346 Å and four Ga–In bonds with an average bond distance of 3.085 Å. The computed HOMO- LUMO gap of 1.32 eV is large and predicts the possibility of the existence of this cluster. Energetically, the second 2b_4 isomer corresponds to a planar geometry of the D_{2h} symmetry, which lies 3.5 kcal/mol above the global minimum isomer and exhibits a large HOMO-LUMO gap of 1.35 eV with comparable Ga–Ga and Ga–In bond lengths, unlike those obtained for the 2a_4 structure. These results emphasize that the Ga–Ga bond acts as a stabilizing agent,

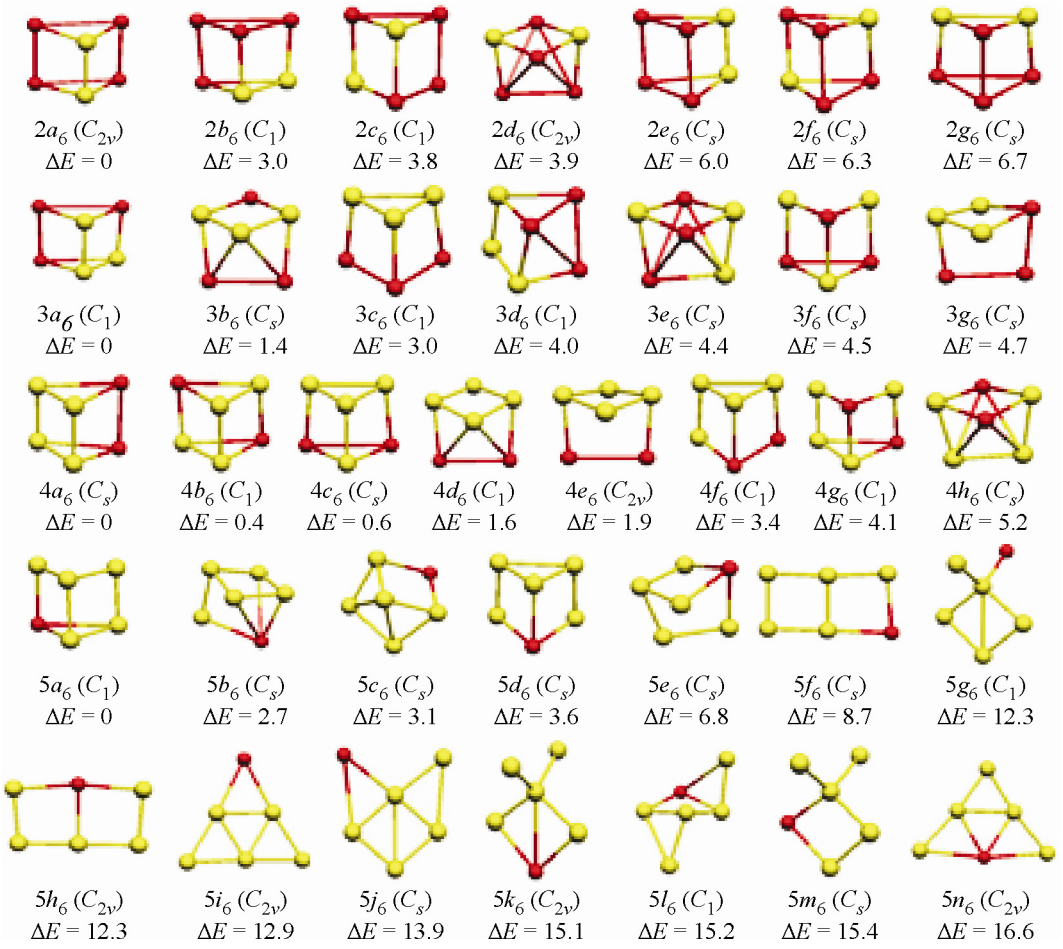

Fig. 2. Ground state structures of Ga_mIn_{6-m} ($m < 6$) clusters. Relative energies ΔE are given in kcal/mol.

contrarily to the In–In one. The different $2i_4$, $2j_4$, and $2k_4$ linear structures lie higher in energy than the global minimum (Fig. 1 and Table 1).

Three energetically close structures are found for Ga_3In species. The most stable one corresponds to the bent $3a_4$ C_s structure with the indium atom occupying a peripheral position, while the three Ga atoms occupy the three vertices of the same triangle. The Ga–Ga and Ga–In bond distances are 2.339 Å and 3.107 Å, in agreement with short and long lengths, respectively. The $3a_4$ global minimum structure displays a significant HOMO-LUMO gap of 1.35 eV, suggesting a kinetically stable species. The planar $3b_4$ structure, where the indium atom is connected to one Ga atom of triangular Ga_3, giving a *Y*-like structure, lies only 1.7 kcal/mol above the most stable $3a_4$ isomer. The three-dimensional $3c_4$ structure of the C_s symmetry is among the low-lying isomers found 2.1 kcal/mol above the global minimum, keeping the indium atom between the gallium ones, and does not provide Ga_3In clusters as more stable structures. It is clear that Ga_3In clusters prefer structures containing the Ga_3 triangle with a maximum of Ga–Ga bonds.

Six-vertex Ga_mIn_{6-m} ($m < 6$) clusters. The lowest-energy structure for $GaIn_5$ clusters corresponds to the $1a_6$ trigonal prismatic one having the C_s symmetry (Fig. S1 of Supplementary Materials), in which the In–Ga–In bond angle is 82°. The $1b_6$ isomer lies only 2.6 kcal/mol above the lowest energy structure. The third $1c_6$ isomer also corresponds to a distorted trigonal prismatic geometry in which the gallium atoms form an angle of 56° within the Ga_3 triangle, lying 2.9 kcal/mol above the global minimum (Table S1 of Supplementary Materials).

For Ga_2In_4 clusters, twelve structures were found as the energy minimum (Fig. 2, Fig. S1 and Table S1 of the Supplementary Information). The $2a_6$ structure of the C_{2v} symmetry (Fig. 2) is obtained by inserting gallium in the apex position of one triangular base of $GaIn_5$, forming a direct Ga–Ga bond. Other positions of gallium atoms of the trigonal

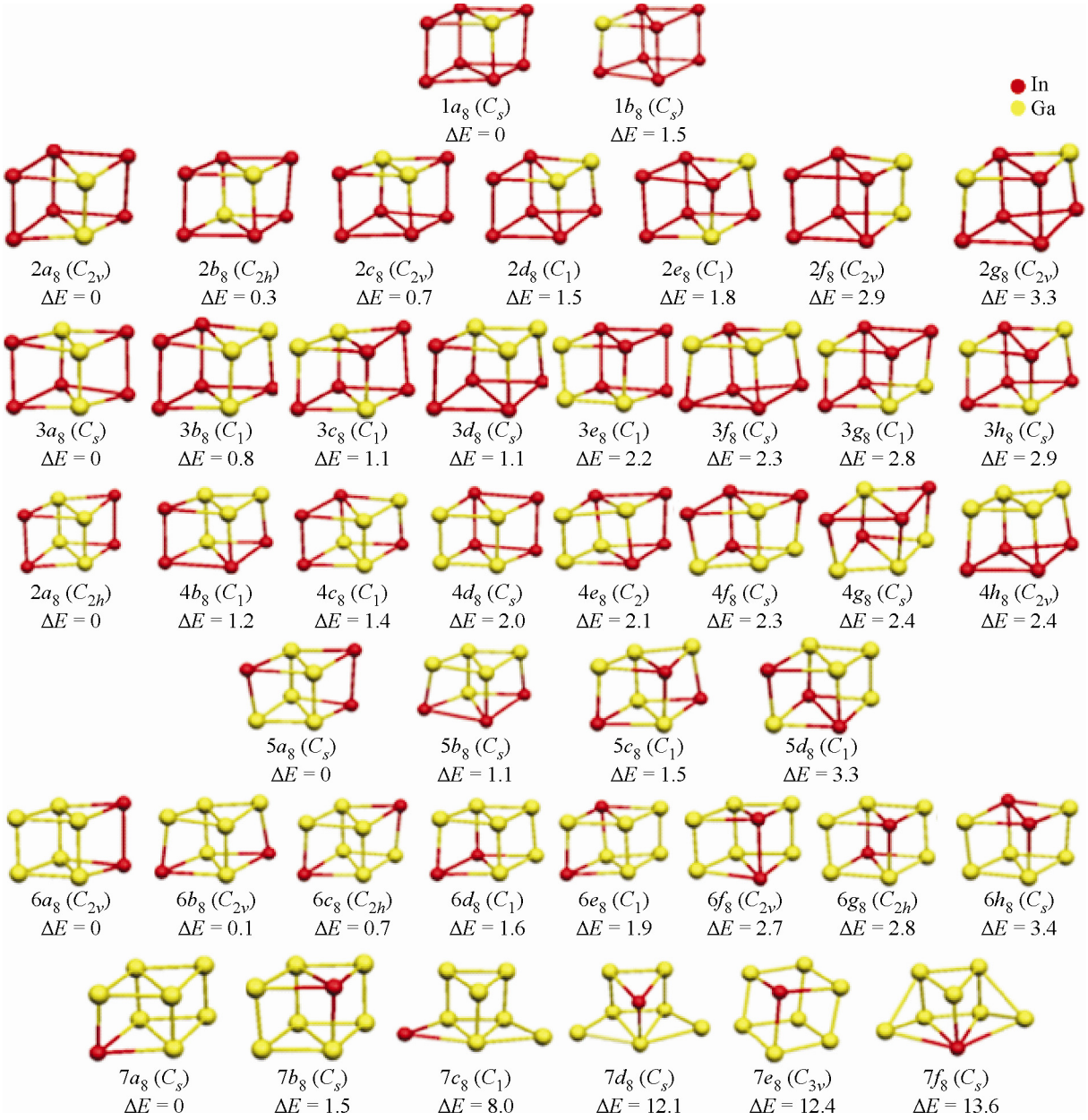

Fig. 3. Ground state structures of Ga_mIn_{8-m} ($m < 8$) clusters. Relative energies ΔE between the isomers are given in kcal/mol.

prismatic structure corresponding to $2b_6$, $2c_6$, $2e_6$, $2f_6$ and $2g_6$ isomers are less stable than the $2a_6$ global minimum by 3.0 kcal/mol, 3.8 kcal/mol, 3.9 kcal/mol, 6.0 kcal/mol, and 6.3 kcal/mol, respectively. It is obvious that the planar geometry gives rise to less stable isomers, thus, the absence of the Ga–Ga bond induces energy loss.

As shown in Fig. S1, ten isomers are found as the energy minimum of Ga_3In_3 clusters within the range of 14.4 kcal/mol. The most stable $3a_6$ structure corresponds to a distorted triangle prism obtained without symmetry constraints (Fig 2), which can be obtained by substituting one gallium atom for one indium atom from most stable Ga_2In_4.

The replacement of In by Ga atoms in the same lateral face of the trigonal prismatic structure of Ga_3In_3 gives rise to Ga_4In_2 clusters, where the $4a_6$ isomer is obtained as the lowest-energy structure and is slightly more stable than the $4b_6$ and $4c_6$ ones only by 0.4 kcal/mol and 0.6 kcal/mol, respectively, which is not significant at the considered level of calculations.

In the case of Ga_5In, the most stable structure of a trigonal prismatic geometry with one Ga–Ga bond broken is obtained without any symmetry constraints (Fig. 2). Another low-lying $5d_6$ structure with the lower C_s symmetry also

TABLE 1. Relative Energies Between the Isomers (kcal/mol), HOMO-LUMO Gap (eV), Ga–Ga, In–In, and Ga–In Bond Lengths (Å) for Ga_mIn_{4-m} ($m < 4$) Clusters of Different Symmetries (Sym)

Cluster	Isomer	Sym	Relative energy	HOMO-LUMO gap	Ga–Ga	In–In	Ga–In
$GaIn_3$	$1a_4$	C_s	0.0	1.15	–	3.369	2.553
	$1b_4$	C_s	1.6	0.99	–	3.107	2.746
	$1c_4$	C_{2v}	2.7	1.11	–	2.922	2.780
	$1d_4$	C_s	3.0	1.13	–	3.000	2.652
	$1e_4$	C_{2v}	3.5	1.14	–	3.404	2.523
	$1f_4$	C_s	5.0	1.11	–	2.743	3.117
	$1g_4$	C_{2v}	5.5	1.11	–	2.871	2.907
	$1h_4$	C_{2v}	9.0	1.07	–	2.703	3.127
	$1i_4$	$C_{\infty v}$	22.3	0.89	–	306.1	2.707
	$1j_4$	$C_{\infty v}$	23.4	0.84	–	2.877	2.885
Ga_2In_2	$2a_4$	C_{2v}	0.0	1.32	2.346	–	3.085
	$2b_4$	D_{2h}	3.5	1.35	2.333	–	3.093
	$2c_4$	C_{2v}	5.1	1.27	2.434	3.093	2.801
	$2d_4$	C_s	5.3	1.81	2.559	–	2.685
	$2e_4$	C_1	5.4	1.15	2.816	3.416	2.545
	$2f_4$	C_s	7.1	1.04	2.702	3.058	2.751
	$2g_4$	C_{2v}	7.8	1.14	2.703	2.904	2.782
	$2h_4$	C_s	8.4	1.15	–	2.992	2.657
	$2i_4$	$D_{\infty h}$	26.0	0.8	2.517	–	2.884
	$2j_4$	$C_{\infty v}$	27.3	0.91	2.687	3.060	2.696
	$2k_4$	$C_{\infty v}$	27.7	0.90	–	–	2.701
Ga_3In	$3a_4$	C_s	0.0	1.35	2.339	–	3.107
	$3b_4$	C_{2v}	1.7	1.38	2.459	–	2.908
	$3c_4$	C_s	2.1	1.33	2.501	–	2.869
	$3d_4$	C_{2v}	3.6	1.37	2.322	–	3.107
	$3e_4$	C_s	5.0	1.20	2.560	–	2.685
	$3f_4$	C_{2v}	5.2	1.31	2.434	–	2.802
	$3g_4$	C_1	5.5	1.17	2.849	–	2.540
	$3h_4$	C_{2v}	9.2	1.13	2.810	–	2.512
	$3i_4$	$C_{\infty v}$	25.5	0.98	2.511	–	2.889

displays a distorted trigonal prismatic geometry, in which the indium atoms form an angle of 56.2° and lie only 2.7 kcal/mol higher in energy than the $5a_6$ global minimum. Twelve other isomers exhibiting various geometries are sketched in Fig. S2 of the Supplementary Information.

Eight Ga_mIn_{8-m} ($m < 8$) clusters. For the $GaIn_7$ clusters, two isomers are found as the energy minimum featured by a rhombic prismatic geometry of the C_s symmetry, differing by the symmetry plane disposition (Fig. 3 and Table S2 of Supplementary Materials). The lowest $1a_8$ structure presenting four Ga–In bonds exhibits a large HOMO-LUMO gap of 1.62 eV and is characterized by In–In and Ga–In bond distances of 2.913 Å and 2.724 Å (Table S2), respectively. The second $1b_8$ isomer lies 1.5 kcal/mol above the lowest one, in which the gallium atom occupying a peripheral position forms three bonds with indium ones. We can see that the number of In–In bonds of the $1a_8$ structure as the most stable isomer is smaller than that of the $1b_8$ one. The $1a_8$ global minimum structure lies only 1.6 kcal/mol below the $1b_8$ structure, where this weak difference arises mainly from the difference concerning the number of Ga–In contacts, which are four in the latter and three in the former.

Five energetically close structures are found as the energy minimum for the Ga_2In_6 clusters (Fig. 3), which can be generated by substituting one indium atom by equivalent gallium one from the most stable $GaIn_7$ structure adopting the rhombic prismatic geometry. The lowest-energy $2a_8$ C_{2v} structure is computed to be slightly more stable than the $2b_8$ isomer (by 0.8 kcal/mol), which is not significant at the considered level of theory.

For the Ga_3In_5 clusters, the most stable $3a_8$ structure corresponds to a distorted rhombic prismatic geometry of the C_s symmetry. The Ga atoms are bound to each other forming two short Ga–Ga bonds of 2.565 Å, while there are seven Ga–In bonds with an average length of 2.711 Å, thus reducing the In–In direct contact to only two bonds of 2.947 Å. The computed HOMO-LUMO gap is 1.71 eV. Note that the reduction of Ga–Ga and Ga–In contacts induces energy loss. The other isomers can be generated by substituting one gallium atom for one indium atom at the equatorial position stemming the most stable Ga_2In_6.

In the case of Ga_4In_4 clusters, most stable $4a_8$ adopts the rhombic prismatic geometry with the D_{2h} symmetry, where gallium atoms occupy the equatorial positions, forming a Ga_4 rhombus. Fourteen distorted rhombic prisms with gallium atoms substituting different positions of a rhombic prism are obtained within the range of 5.5 kcal/mol (Fig. S2 and Table S2 in Supplementary Information). For the $4o_8$ D_{2h} structure, indium atoms occupy the equatorial positions of a rhombic prism and form a In_4 rhombus, unlike most stable $4a_8$ forming a Ga_4 rhombus. These results mean that the Ga–Ga bond is stronger than the In–In one and produces a stabilizing effect.

For the Ga_5In_3 clusters, the most stable $5a_8$ structure is also a distorted rhombic prism of the C_s symmetry, which can be obtained by substituting one indium atom by one gallium atom from the most stable Ga_4In_4 isomer. The remaining low-lying isomers are within the range of 3.3 kcal/mol.

In the case of Ga_6In_2 clusters, eight structures were found as the energy minimum (Fig. S2, Supplementary Information). The global minimum $3a_8$ structure adopts a distorted rhombic prism having the C_s symmetry, in which the indium atoms occupy peripheral positions and is lower in energy than $6b_8$, $6c_8$, and $6d_8$ by 0.1 kcal/mol, 0.7 kcal/mol, and 1.6 kcal/mol, respectively. It displays a large HOMO-LUMO gap of 1.81 eV and short Ga–Ga, Ga–In and In–In bond distances of 2.530 Å, 2.955 Å, and 2.959 Å.

Nine lowest-energy structures are found for the Ga_7In clusters with various geometries (Fig. S2 and Table S2). As presented in Fig. 3, the $7a_8$ isomer exhibiting rhombus prismatic or *cubane*-like structures is computed as the global minimum displaying a large HOMO-LUMO gap of 1.88 eV and short Ga–Ga and Ga–In bond distances of 2.523 Å and 2.757 Å, respectively. The second most stable isomer corresponds to the $7b_8$ one with the same rhombus prismatic geometry and lies only 1.5 kcal/mol above the global minimum, while the less stable $7i_8$ one with a planar geometry is found to be 21.4 kcal/mol above the global minimum.

Due to the existence of the $Ga_8(C_{13}H_9)_8^{2-}$ cluster [36], it seemed appropriate to us to investigate the substituted and bare Ga_8 and In_8 cages in order to gain a deeper understanding of the substitution effects on the cluster cage (Fig. 4). For the substituted Ga_8H_8 species, each gallium atom engages one of its three electrons to form a Ga–H bond, thus, requires more connections with its neighbouring gallium atoms to counter in this electronic deficiency. According to this electron consideration, it turned out that the square antiprismatic structure was obtained as the energy minimum, whereas the rhombic prismatic Ga_8H_8 structure was not obtained as the energy minimum exhibiting large imaginary frequencies. Similarly to Ga_mIn_{8-n} clusters, bare Ga_8 adopts a *cubane*-like geometry with tri-connected Ga atoms involving three electrons in the cluster cage rather than the substituted species adopting the square antiprismatic one with tetra-connected Ga atoms engaging only two electrons in the cluster cage. The calculations carried out for bare Ga_8^{2-} and the substituted $Ga_8H_8^{2-}$ prismatic species show the existence of large imaginary frequencies for the latter, thus, these dianionic rhombic prismatic clusters were not found as the energy minimum, while the $Ga_8H_8^{2-}$ square antiprismatic structure is authenticated as the energy minimum describing the experimental one with short Ga–Ga bond distances in the range 2.561-2.723 Å compared to those of the neutral G_8H_8 one ranging from 2.654 Å to 2.877 Å.

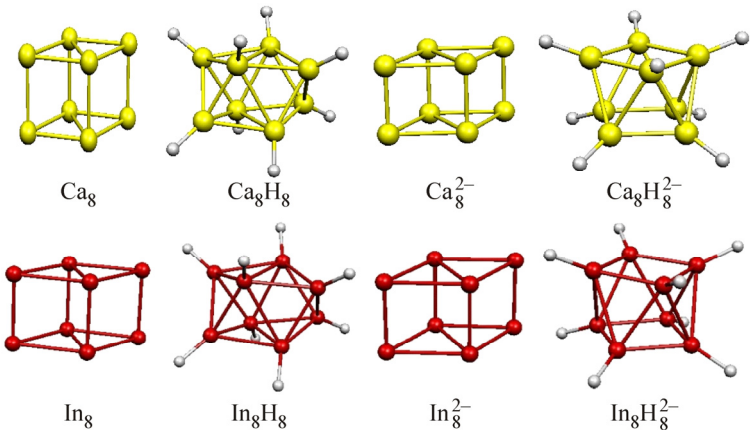

Fig. 4. Optimized molecular structures of the M_8, M_8H_8, M_8^{2-}, and $M_8H_8^{2-}$ (M = Ga, In) isomers with the lowest energy.

The Ga–Ga bond distances obtained for the dianionic $Ga_8H_8^{2-}$ species are comparable to those found in the recent theoretical work for protonated G_8H_{10} [61]. It is worthwhile noting that rhombic prismatic structures display comparable bond distances ranging from 2.534 Å to 2.810 Å. The same tendencies are obtained for In_8H_8 and In_8, where the bare cluster adopts the rhombic prismatic structure exhibiting short In–In bond distances within the large range 2.153-3.092 Å. However, the substituted species adopt the square antiprismatic one, with In–In bond distances being within the narrow range 2.993-3.262 Å. It is important to note that the In–In bond distances in the dianionic $In_8H_8^{2-}$ and In_8^{2-} species undergo somewhat lengthening as compared to those of the neutral $In_8H_8^{2-}$ and In_8^{2-} ones.

Bonding energy per atom. The bonding energies E(Ga) and E(In) per Ga or In atom of each of the most stable Ga_mIn_{n-m} ($n = 4$, 6, 8 and $m = 1$, 2.., n–1) clusters are calculated by the following expressions, respectively: $E(Ga) = [E(Ga_mIn_{n-m}) - (E(Ga_{m-1}In_{n-m}) + E(Ga))]$ and $E(In) = [E(Ga_mIn_{n-m}) - (E(Ga_mIn_{n-m-1}) + E(In))]$, where E(Ga) and E(In), $E(Ga_{m-1}In_{n-m})$ and $E(Ga_mIn_{n-m-1})$ are the energies of isolated gallium and indium atoms, respectively, while the $E(Ga_{m-1}In_{n-m})$ and Ga_mIn_{n-m-1} are the energies of fragments.

The values of bonding energies per atom calculated by the above formula are gathered in Table 2.

The relationship between E(Ga) and the m number of gallium atoms of the cluster is shown in Fig. 5. It is clear from the three curves that E(Ga) decreases gradually as m increases. Furthermore, one can observe that the cluster becomes more compact with enlarging cluster size, as found by the previous works on Al element clusters [62]. For Ga_mIn_{n-m} clusters with the same total number n, the bonding energies (E_B) of Ga_mIn_{n-m} ($m < 4$) are the smallest ones. This result indicates that Ga bonds are very important for the stability of Ga_mIn_{n-m} clusters. It further shows that the Ga-rich clusters are more stable than the In-rich ones with the same total number of atoms. Overall, according to the bonding energies per atom, it can be concluded that the most stable clusters correspond to those with the maximum of Ga atoms, while the less stable clusters correspond to those with the minimum of Ga atoms.

HOMO-LUMO energy gaps. The HOMO-LUMO gap is among the useful parameters evaluating the stability and chemical reaction of the clusters. A system with a large energy gap is chemically less reactive, therefore, could be more stable. From Table 1 and Tables S1, S2 of the Supplementary Information, it is interesting to mention that the calculated HOMO-LUMO gaps for the most stable Ga_mIn_{n-m} ($n = 4$, 6, 8 and $m < n$) clusters are in the range 1.15-1.88 eV (Fig. 6), suggesting a good kinetic stability of the studied clusters as aforementioned. Clearly from the curves displayed in Fig. 6, there is an apparent increase corresponding to the increase of the m number of gallium atoms. Moreover, one can see that the HOMO-LUMO gaps increase in the following order: $Ga_mIn_{4-m} < Ga_mIn_{6-m} < Ga_mIn_{8-m}$ and are consistent with the bonding energy results. The largest HOMO-LUMO gap of 1.88 eV corresponds to Ga_7In, indicating that this cluster is the less reactive system and relatively the most stable one mostly due to the stabilization of the HOMO, while the LUMO remains almost at the same energy as compared to those of Ga-rich clusters.

TABLE 2. Bonding Energies Per Atom E(Ga) and E(In), Vertical Ionization Potential (VIP), Adiabatic Ionization Potential (AIP), Vertical Electron Affinity (VEA), Adiabatic Electron Affinity (AEA), and Chemical Hardness (η) of the Most Stable Ga_mIn_{n-m} (n = 4, 6, 8 and $m < n$) Clusters (eV)

Cluster	E(Ga)	E(In)	VIP	AIP	VEA	AEA	η
$GaIn_3$	–3.08	–2.73	5.80	5.76	1.64	1.82	2.08
Ga_2In_2	–3.26	–2.85	5.94	5.89	1.53	1.65	2.21
Ga_3In	–3.24	–2.83	6.02	5.83	1.52	1.63	2.25
$GaIn_5$	–3.62	–3.02	6.03	5.90	1.77	2.04	2.13
Ga_2In_4	–3.86	–3.20	6.12	6.00	1.69	1.96	2.21
Ga_3In_3	–3.95	–3.12	6.18	6.04	1.70	1.98	2.24
Ga_4In_2	–3.87	–3.17	6.26	6.10	1.71	2.00	2.28
Ga_5In	–3.90	–3.24	6.35	6.18	1.71	2.01	2.32
In_8	–	–	6.35	6.18	1.71	2.01	2.32
$GaIn_7$	–4.00	–3.26	6.14	5.97	1.94	1.99	2.10
Ga_2In_6	–4.25	–3.27	6.16	6.01	1.90	1.91	2.13
Ga_3In_5	–4.28	–3.34	6.23	6.05	1.89	1.94	2.17
Ga_4In_4	–4.20	–3.40	6.30	6.12	1.86	1.86	2.22
Ga_5In_3	–4.25	–3.34	6.32	6.13	1.84	1.90	2.24
Ga_6In_2	–4.24	–3.39	6.37	6.22	1.90	1.87	2.26
Ga_7In	–4.31	–3.28	6.47	6.23	1.84	1.88	2.32
Ga_8	–	–	6.35	6.18	1.71	2.01	2.32

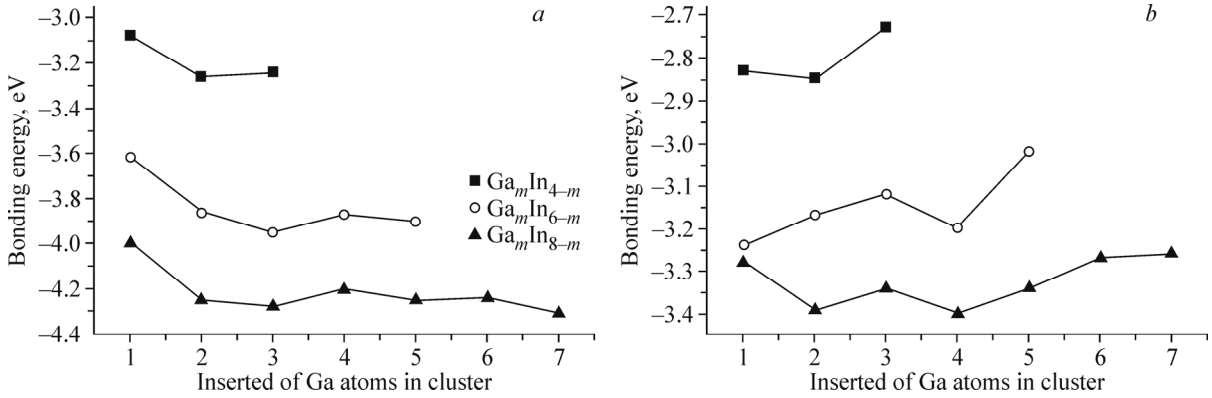

Fig. 5. Bonding energies as a function of inserted Ga (a) and In (b) atoms in various Ga_mIn_{n-m} (n = 4, 6, 8 and $m < n$) clusters.

Ionization potential and electron affinity. IP and EA are used as important characteristics to probe the electronic structure modifications with respect to the cluster size. Adiabatic IP (AIP), vertical IP (VIP) and adiabatic EA (AEA), vertical AE (VEA) were calculated for each of the most stable isomers related to the Ga_mIn_{n-m} (n = 4, 6, 8 and $m < n$) clusters (Fig. 7 and Table 2).

VIP is defined as the energy difference between the cationic and neutral clusters when both are in the optimized geometry of the neutral cluster. AIP is defined similarly, but with both clusters in their respective optimized geometries.

VEA is defined as the energy difference between the neutral and anionic clusters when both are in the optimized geometry of the neutral cluster. AEA is the energy difference between the neutral and anionic clusters when both are in their respective optimized geometries.

The calculated VIP and AIP values of the lowest-energy Ga_mIn_{n-m} (n = 4, 6, 8 and $m < n$) structures are summarized in Table 2 and plotted in Fig. 7, where the energy needed to remove an electron from the cluster yields valuable information on the electronic structure.

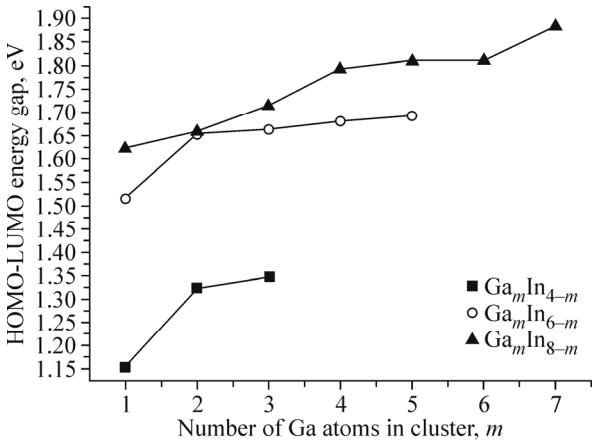

Fig. 6. Variation of HOMO-LUMO energy gaps as a function of m number of Ga atoms calculated for the most stable structures of Ga_mIn_{n-m} ($n = 4$, 6, 8 and $m < n$) clusters.

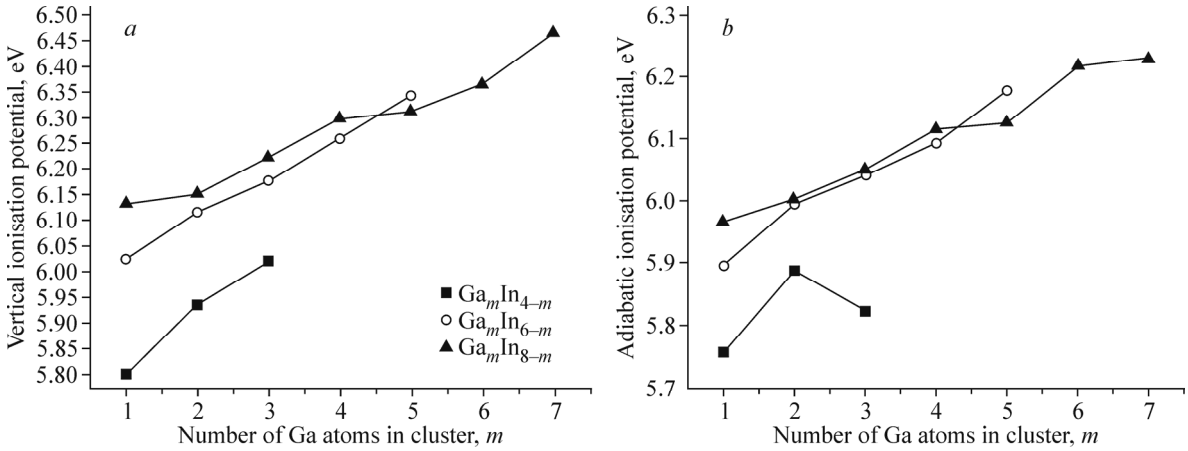

Fig. 7. VIPs (*a*) and AIPs (*b*) for the most stable structures of Ga_mIn_{n-m} ($n = 4$, 6, 8 and $m < n$) clusters as a function of the *m* number of Ga atoms.

The calculated VIP values are larger than the AIP ones and the energy difference between them is an indication of the energy gain due to structural relaxation. As can be seen from Fig. 7, the Ga_mIn_{n-m} clusters with the same total number n of atoms, VIP and AIP of Ga_mIn_{n-m} ($m = 1$) are the smallest ones. For all the three curves, Ga_mIn_{n-m} clusters with the same total number *n*, VIP, and AIP increase as a function of the m number of gallium atoms, showing the same behavior as compared to that of the bonding energy per atom *E*(Ga). Therefore, this result indicates that the Ga-rich clusters are more stable than the In-rich ones. The smallest VIP value (5.80 eV) shows that the $GaIn_3$ cluster is more readily ionized than the large and Ga-rich clusters.

The Ga_mIn_{3-m} clusters have the lowest VIPs (5.80-6.02 eV) and AIPs (5.76-5.89 eV), therefore, they are the most easily oxidizable species, contrarily to the Ga_mIn_{8-m} clusters with the highest VIPs (6.30-6.47 eV) and AIPs (6.12-6.23 eV). Thus, they are most difficult to oxidize, in accordance with their HOMO energies where the removal of one electron from a deep orbital requires more energy. This corresponds to the largest IP, unlike those related to the high HOMO energies. The AIP, VIP, and E_{HOMO} values summarized in Table 2 show clearly that the decrease in the HOMO energies correlates with the increase in AIP and VIP values. The comparison of Ga_mIn_{n-m} IPs shows a progressive rise in the presence of more Ga atoms and for a large cluster size, in accordance with the relatively high Ga electronegativity as compared to that of In. This upward trend of the IP as a function of the cluster size has been highlighted for the small Al–Al_7 clusters [63]. The reduction of IPs can be explained by an increase in the HOMO energies. Thus, Ga-rich species are more stable than the In-rich ones.

Contrarily to PI, the AEA values are larger than VEA ones (Fig. 8 and Table 2). For the same total number n, one can notice the downward energy trend led by an increase in the number of Ga atoms. The smallest VAE (1.52 eV) and AEA (1.63 eV) are obtained for the Ga_3In cluster, indicating its ease to be reduced, whereas the largest VAE (1.94 eV) and AEA (1.99 eV) are obtained for $GaIn_7$ containing the minimum of Ga, corresponding to the most difficult species to be reduced.

Chemical hardness. The chemical hardness (η) given below is an electronic quantity characterizing the relative stability of clusters. The chemical hardness (η) [64, 65] is a measure of the resistance of a chemical entity to change the number of electrons, which is given by the following formula: $\eta = 1/2(VIP - VEA)$. The computed chemical hardness (η) values for the studied lowest-energy clusters are summarized in Table 2 and plotted in Fig. 9. From the curves, one can observe that for the Ga_mIn_{n-m} clusters with the same total number n, the chemical hardness (η) increases as the number m of gallium atoms increases, showing the same behavior compared to those of the bonding energy per atom E_B, energy gaps, and IPs. The largest hardness values are obtained for the Ga_7In (2.34 eV) and Ga_8 (2.36 eV) isomers (Fig. 9), which have the largest HOMO-LUMO energy gap, and hence, the minimum tendency to exchange electrons (minimum reactivity), whereas the smallest hardness values are obtained for In_8 (2.06 eV) and GaI_3 (2.08 eV), predicting the maximum tendency to exchange electrons (maximum reactivity).

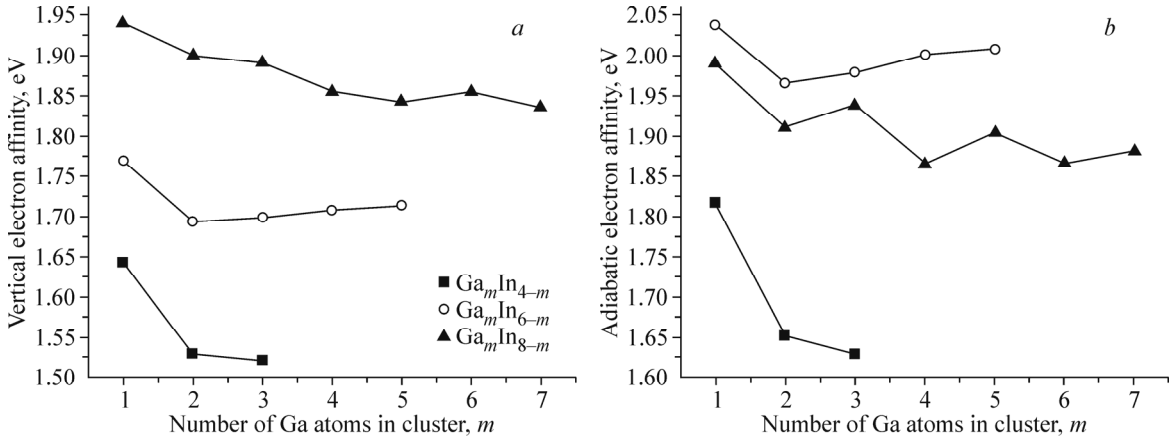

Fig. 8. VEA (*a*) and adiabatic electron affinity (*b*), calculated for the most stable structures of Ga_mIn_{n-m} (n = 4, 6, 8 and $m < n$) clusters as a function of the m number of Ga atoms.

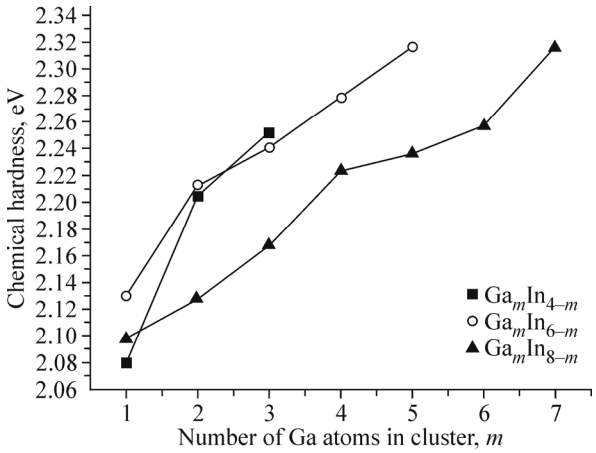

Fig. 9. Chemical hardness as a function of the m number of Ga atoms obtained for the most stable structures of Ga_mIn_{n-m} (n = 4, 6, 8 and $m < n$) clusters.

CONCLUSIONS

In this work, a detailed study has been provided of the structural parameters, relative stabilities, and electronic properties of gallium-indium Ga_mIn_{n-m} clusters ($n = 4$, 6, 8 and $m < n$). The obtained clusters prefer to adopt three-dimensional (3D) structures; the trigonal prismatic and rhombic prismatic configurations are favored energetically when $n = 6$ and 8, respectively.

The replacement of In atom(s) by Ga atom(s) keeps the geometry unchanged, but induces some important variations concerning the bonding energy per atom, the HOMO-LUMO gaps, IPs, EAs, and the chemical hardness. Indeed, the binding energy evolution and the electronic properties, including the HOMO-LUMO gap, IP, EA, and the chemical hardness (η) show that the Ga-rich clusters are more stable than In-rich ones with the same total number of atoms. It is found that the studied properties strongly depend on the cluster size as well as the Ga and In contributions. The Ga–Ga bond is stronger than the Ga–In bond and the latter is stronger than the In–In one. Therefore, the Ga_7In cluster is relatively the most stable structure. Thus, the stability increases with increasing number of the Ga–Ga bonds.

SUPPLEMENTARY INFORMATION

Bond distances (Å), relative energies of isomers, and HOMO-LUMO gaps (eV) for the optimized geometries of the computed Ga_mIn_{n-m} ($n = 6$, 8 and $m < n$) clusters with the lowest energy and various symmetries are given in Tables S1 and S2 of Supplementary Materials. Their corresponding molecular structures are given in Figs. S1 and S2 of Supplementary Materials.

The authors are grateful to the Algerian MESRS (Ministère de l′Enseignement Supérieur et de la Recherche Scientifique) and DGRS-DT (Direction Générale de la Recherche Scientifique et du Développement Technologique) for the financial support.

REFERENCES

1. R. L. Johnston. *Philos. Trans. R. Soc. London*, **1998**, *A356*, 211.
2. K. Balasubramanian and P. Y. Feng. *Chem. Phys. Lett*., **1988**, *146*, 155.
3. X. G. Gong and E. Tosatti. *Phys. Lett. A*, **1992**, *166*, 369.
4. R. O. Jones. *J. Chem. Phys*., **1993**, *99*, 1194.
5. J. Y. Yi. *Phys. Rev. B*, **2000**, *61*, 7277.
6. B. Song, P. L. Cao, and B. X. Li. *Phys. Lett. A*, **2003**, *315*, 308.
7. J. J. BelBruno. *Heteroat. Chem*., **2003**, *14*, 189.
8. Y. Zhao, W. G. Xu, Q. S. Li, Y. M. Xie, and H. F. Schaefer. *J. Phys. Chem. A*, **2004**, *108*, 7448.
9. S. Chacko, K. Joshi, D. G. Kanhereand, and S. A. Blundell. *Phys. Rev. Lett*., **2004**, *92*, 135506.
10. B. Song and P. L. Cao. *J. Chem. Phys*., **2005**, *123*, 144312.
11. S. Krishnamurty, K. Joshi, S. Zorriasatein, and D. G. Kanhere. *J. Chem. Phys*., **2007**, *127*, 054308.
12. N. Gaston and A. J. Parker. *Chem. Phys. Lett*., **2011**, *501*, 375.
13. N. Drebov, F. Weigend, and R. Ahlrichs. *J. Chem. Phys*., **2011**, *135*, 044314.
14. S. Nunez, J. M. Lopez, and A. Aguado. *Nanoscale*, **2012**, *4*, 6481.
15. K. G. Steenbergen and N. Gaston. *Phys. Chem. Chem. Phys*., **2013**, *15*, 15325.
16. C. Y. Cha, G. Ganteför, and W. Eberhardt. *J. Chem. Phys*., **1994**, *100*, 995.
17. A. Schnepf and H. Schnöckel. *Angew. Chem. Int. Ed*., **2002**, *41*, 3532
18. X. Ta and P. J. Dagdigian. *J. Phys. Chem. A*, **2003**, *107*, 2642.
19. H. J. Himmel and B. Gaertner. *Chem. Eur. J*., **2004**, *10*, 5936.
20. D. J. Van Harlingen, D. F. Heidel, and J. C. Garland. *Phys. Rev. B*, **1980**, *21*, 1842.
21. D. Rayane, P. Meliono, B. Cabaud, A. Hoareau, B. Tribollet, and M. Broyer. *J. Chem. Phys*., **1989**, *90*, 3295.

22. K. E. Schriver, J. L. Persson, E. C. Honea, and R. L. Whetten. *Phys. Rev. Lett*., **1990**, *64*, 2539.
23. L. Magaud, S. N. Khanna, and P. Jena. *Chem. Phys. Lett*., **1991**, *183*, 333.
24. A. Wucher, I. Z. Ma, W. F. Calaway, and M. J. Pellin. *Surf. Sci. Lett*., **1994**, *304*, 439.
25. C. Staudt and A. Wucher. *Phys. Rev. B*, **2002**, *66*, 075419.
26. B. N. Onwuagba. *Phys. Stat. Sol*., **1993**, *180*, 391.
27. G. V. Sin′ko and N. A. Smirnov. *Phys. Rev. B*, **2006**, *74*, 134113.
28. G. Lijing, S. Daning, Z. Jijun, W. Baolin, and J. Jianming. *J. Comput. Theor. Nanosci*., **2007**, *4*, 152.
29. W. Q. Zhang, G. F. Zhao, J. M. Sun, L. L. Zhi, and Y. Z. Gu. *Chem. Phys*., **2009**, *361*, 44.
30. T. B. Lill, W. F. Callaway, M. J. Pellin, and D. M. Gruen. *Phys. Rev. Lett*., **1994**, *73*, 1719.
31. T. B. Lill, W. F. Callaway, Z. Ma, and M. J. Pellin. *Surf. Sci*., **1995**, *322*, 361.
32. W. Uhl, L. Cuypers, K. Harms, W. Kaim, M. Wanner, R. Winter, R. Koch, and W. Saak. *Angew. Chem. Int. Ed. Engl*., **2001**, *40*, 566.
33. N. Wiberg, T. Blank, A. Purath, G. Stößer, and H. Schnöckel. *Angew. Chem. Int. Ed*., **1999**, *111*, 2754.
34. M. Kehrwald, W. Köstler, A. Rodig, G. Linti, T. Blank, and N. Wiberg. *Organometallics*, **2001**, *20*, 860.
35. N. Wiberg, T. Blank, H. Nöth, and W. Ponikwar. *Angew. Chem. Int. Ed. Engl*., **1999**, *38*, 839.
36. A. Schnepf, G. Stößer, and H. Schnöckel. *Z. Anorg. Allg. Chem*., **2000**, *626*, 1676.
37. A. Schnepf, G. Stößser, and H. Schnöckel. *J. Am. Chem. Soc*., **2000**, *122*, 9178.
38. A. Schnepf, E. Weckert, G. Linti, and H. Schnöckel. *Angew. Chem. Int. Ed. Engl*., **1999**, *38*, 3381.
39. A. Rodig and G. Linti. *Angew. Chem. Int. Ed. Engl*., **2000**, *39*, 2952.
40. S. Ababsa, F. Djamai, and B. Zouchoune. *J. Cluster Sci*., **2014**, *25*, 1665.
41. ADF2012.01, SCM, Theoretical Chemistry. Netherlands, Amsterdam: Vrije Universiteit. http//www.scm.com.
42. E. J. Baerends, D. E. Ellis, and P. Ros. *Chem. Phys*., **1973**, *2*, 41.
43. G. te Velde and E. J. Baerends. *J. Comput. Phys*., **1992**, *99*, 84.
44. C. Fonseca Guerra, J. G. Snijders, G. te Velde, and E. J. Baerends. *Theor. Chem. Acc*., **1998**, *99*, 391.
45. F. M. Bickelhaupt and E. J. Baerends. *Rev. Comput. Chem*., **2000**, *15*, 1.
46. G. te Velde, F. M. Bickelhaupt, C. Fonseca Guerra, S. J. A. van Gisbergen, E. J. Baerends, J. G. Snijders, and T. Ziegler. *J. Comput. Chem*., **2001**, *22*, 931.
47. A. D. Becke. *J. Chem. Phys*., **1993**, *98*, 5648.
48. C. Lee, W. Yang, and R. G. Parr. *Phys. Rev. B*, **1998**, *37*, 785.
49. L. Versluis and T. Ziegler. *J. Chem. Phys*., **1988**, *88*, 322.
50. L. Fan and T. Ziegler. *Chem. Phys*., **1992**, *96*, 9005.
51. L. Fan and T. Ziegler. *Phys. Chem*., **1992**, *96*, 6937.
52. P. Flükiger, H. P. Lüthi, S. Portmann, and J. Weber. MOLEKEL. Version 4.3.win32. Switzerland: Swiss Center for Scientific Computing (CSCS), **2000/2001**.
53. B. A. Hess Jr. and L. J. Schaad. *J. Am. Chem. Soc*., **1971**, *93*, 2413.
54. R. C. Haddon and T. Fukunaga. *Tetrahedron. Lett*., **1980**, *21*, 1191.
55. R. Pearson. *J. Am. Chem. Soc*., **1988**, *110*, 2092.
56. R. Pearson. *J. Org. Chem*., **1989**, *54*, 1423.
57. Z. Zhou and R. G. Parr. *J. Am. Chem. Soc*., **1990**, *112*, 5720.
58. D. E. Manolopoulos, J. C. May, and S. E. Down. *Chem. Phys. Lett*., **1991**, *181*, 105.
59. X. Liu, T. G. Schmalz, and D. J. Klein. *Chem. Phys. Lett*., **1992**, *188*, 550.
60. M. Maatallah, D. Cherqaoui, A. Jarid, and J. F. Liebman. *J. Mol. Model*., **2012**, *18*, 3321.
61. C. Majumder, and S. K. Kulshreshtha. *Phys. Rev. B*., **2004**, *69*, 115432.
62. J. Akola and M. Manninen. *Phys. Rev. B*, **1998**, *58*, 3601.
63. R. G. Pearson. *J. Chem. Ed*., **1987**, *64*, 561.
64. R. G. Parr and W. Yang. Oxford: Oxford Univ., **1989**.